

AD-A194 624



DTIC FILE COR

DTIC  
E  
JUN 23 1988  
S H D

PERFORMANCE OF GPS-AIDED INS DURING  
HIGH-DYNAMIC MANEUVERS

THESIS

Joseph R. Cunningham  
1Lt, USAF

AFIT/GE/ENG/87D-12

DEPARTMENT OF THE AIR FORCE  
AIR UNIVERSITY

**AIR FORCE INSTITUTE OF TECHNOLOGY**

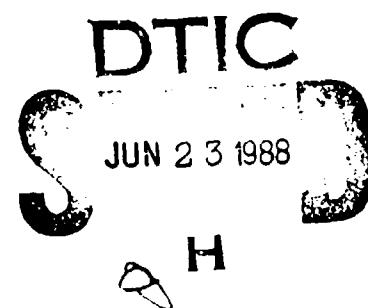
Wright-Patterson Air Force Base, Ohio

**DISTRIBUTION STATEMENT A**

Approved for public release;  
Distribution Unlimited

88 6 23 045

AFIT/GE/ENG/87D-12



PERFORMANCE OF GPS-AIDED INS DURING  
HIGH-DYNAMIC MANEUVERS

THESIS

Joseph R. Cunningham  
1Lt, USAF

AFIT/GE/ENG/87D-12

Approved for public release; distribution unlimited

AFIT/GE/ENG/87D-12

PERFORMANCE OF GPS-AIDED INS DURING  
HIGH-DYNAMIC MANEUVERS

THESIS

Presented to the Faculty of the School of Engineering  
of the Air Force Institute of Technology

Air University

In Partial Fulfillment of the  
Requirements for the Degree of  
Master of Science in Electrical Engineering

Joseph R. Cunningham, B.E.E.

First Lieutenant, USAF

December 1967

Approved for public release; distribution unlimited

## Acknowledgments

This thesis effort has been an evolutionary process which began upon my arrival at AFIT. Having had no prior knowledge of navigation systems or stochastic estimation, I hope this document reflects the phenomenal effort my professors put forth to educate me in such a short time frame.

I extend my deepest gratitude to my thesis advisor, Lt Col Z.H. Lewantowicz, whose bountiful knowledge, insight, and ideas kept me striving beyond what I thought my limits were. Now, I realize the only limitations are those you place upon yourself. Lt Col Lewantowicz served as a role model, and helped me overcome those artificial barriers. I would also like to thank my committee members, Dr. George Slouris and Dr. Peter Maybeck, for their expertise, experience, and feedback which was always available when requested. All three of these gentlemen deserve credit for their patience, understanding, and responsiveness which made this effort possible.

Special credit is due my loving wife, Barbara, and my energetic son, Bobby. Barbara assumed enormous responsibilities during my apparent absence. Though neglected at times, her understanding of the situation, willingness to help in any way possible, and optimistic view of the future gave me the encouragement and peace of

on For	
NAME	<input checked="checked" type="checkbox"/>
Grade	<input type="checkbox"/>
Date	
Distribution/	
Availability Code	
Dist	Acad and/or Special
A-1	

mind to achieve the goals I had sought. Bobby had accepted the disappointments associated with my rigorous schedule. But, his sparkling personality and endearing attitude towards me continued to prevail.

I must also thank my classmates and neighbors who contributed significantly through their support and loyalty to me and my family. Special thanks are deserving of Capt James Matthes, who sacrificed his time and energy, made everything come together in the end; Lt Philip Verret, the most perfect neighbor and friend anywhere, once again gave freely of himself to help someone in need; and, Lt Matthew Devitt and his wife, Anna, who not only provided timely support, but gave my family the companionship to ease the hardship during this interlude.

Last, but certainly not least, praise the Lord for giving me the strength, dedication, and ability to participate in, and complete, the course requirements.

Joseph R. Cunningham

## Table of Contents

	<u>Page</u>
Acknowledgments .....	ii
List of Figures .....	vii
Abstract .....	x
I. Introduction .....	1
1.1 Background .....	1
1.2 Problem .....	4
1.3 Scope .....	4
1.4 Assumptions .....	6
1.4.1 INS .....	6
1.4.2 GPS Receiver .....	6
1.4.3 Altimeter .....	7
1.4.4 Spherical Earth .....	7
1.4.5 Vehicle Dynamics .....	7
1.5 Current Knowledge .....	8
1.6 Approach .....	11
1.7 Outline .....	12
II. Theory .....	13
2.1 General .....	13
2.2 Reference Frames .....	14
2.2.1 Earth-Centered-Earth Fixed Coordinate Frame .....	14
2.2.2 North-East-Down Navigation Coordinate Frame .....	15
2.2.3 Line-of-Sight Coordinates .....	15
2.3 North-Slaved, Local-Level Inertial Navigation System .....	17
2.3.1 Platform .....	17
2.3.2 Single-Degree-of-Freedom Gyros .....	19
2.3.3 Accelerometers .....	22
2.3.4 System Integration .....	25
2.4 GPS Receiver .....	28
2.4.1 Satellite Signals .....	28
2.4.2 Receiver Operation .....	29

2.4.2.1	User Position Solution .....	29
2.4.2.2	Signal Acquisition and Tracking .....	32
2.5	Summary .....	34
III.	Analysis Tools and INS/GPS Receiver Modelling .....	35
3.1	Kalman Filter .....	35
3.1.1	Basic Kalman Filter Assumptions .....	36
3.2	Estimator Equations .....	41
3.3	INS Error Model .....	47
3.3.1	Basic Equations .....	47
3.3.2	Complete INS Error Model .....	50
3.3.2.1	Barometric Altimeter .....	50
3.3.2.2	Error Sources .....	52
3.4	GPS Receiver Error Model .....	57
3.4.1	Measurement Model .....	58
3.4.2	Code Tracking Loop .....	60
3.5	Truth Model .....	62
3.6	System Integration .....	64
3.7	Performance Analysis .....	67
3.7.1	General Description .....	67
3.7.2	Joint-Solution Kalman Filter .....	74
3.7.3	Two-Filter System .....	75
3.7.3.1	Full-State System .....	75
3.7.3.2	Baseline System .....	83
3.8	Closing Remarks .....	84
IV.	Results .....	85
4.1	Trajectory Candidates .....	85
4.1.1	Horizontal Turn Trajectory .....	86
4.1.2	Vertical Turn Trajectory .....	89
4.2	Eigenvalue Migration .....	91
4.3	Performance Analysis Results .....	97
4.3.1	24-State GPS Receiver Kalman Filter .	100
4.3.2	19-State INS Kalman Filter .....	103
4.3.3	Joint-Solution Kalman Filter .....	106
4.3.4	Two-Filter Systems .....	111
V.	Conclusions and Recommendations .....	112

Bibliography .....	115
Vita .....	117

## List of Figures

<u>Figure</u>		<u>Page</u>
2-1	ECEF Coordinate Frame .....	16
2-2	NED Navigation Coordinate Frame .....	16
2-3	Decomposition of a Vector Onto Three Nonorthogonal Axes .....	18
2-4	INS Platform Containing Three Accelerometers and Three Gyros .....	18
2-5	Single Degree-of-Freedom Gyro .....	20
2-6	NSLL INS Block Diagram .....	26
2-7	User Position Determination .....	31
3-1	Typical Kalman Filter Application .....	37
3-2	Random Constant Process .....	40
3-3	Exponentially Time-Correlated Process .....	40
3-4	Gaussian-Shaped Distribution .....	42
3-5	9-State INS Error Dynamics Model .....	51
3-6	INS Error Dynamics Model With Altimeter Readings .....	53
3-7	Complete (19-State) INS Error Dynamics Model ..	56
3-8	12-State GPS Receiver Error Dynamics Model ....	59
3-9	GPS Receiver Code Tracking Loop .....	61
3-10	Complete (24-State) GPS Receiver Error Dynamics Model .....	63

3-11	Truth Model Error Dynamics Model .....	65
3-12	Performance Evaluation of Kalman Filter Designs .....	68
3-13	Performance Evaluation of the Two-Filter Systems .....	79
4-1	Horizontal Turn Variables .....	88
4-2	Vertical Turn Variables .....	90
4-3	Horizontal Counter-Clockwise Turn Eigenvalues .....	92
4-4	Horizontal Clockwise Turn Eigenvalues .....	92
4-5	Initial East Heading, Vertical Turn Eigenvalues .....	94
4-6	Initial North Heading, Vertical Turn Eigenvalues .....	94
4-7	Eigenvalues, 7g Horizontal Counterclockwise Turn .....	95
4-8	Eigenvalues, 5g Horizontal Counterclockwise Turn .....	95
4-9	Eigenvalues, 3g Horizontal Counterclockwise Turn .....	96
4-10	GPS Receiver Position Errors (Constant East Velocity) .....	101
4-11	GPS Receiver Velocity Errors (Constant East Velocity) .....	101
4-12	GPS Receiver Position Errors (9g Turn) .....	102
4-13	GPS Receiver Velocity Errors (9g Turn) .....	102
4-14	INS North and East Position Errors (Constant East Velocity) .....	104

4-15	INS Vertical Position Errors (Constant East Velocity) .....	104
4-16	INS North and East Velocity Errors (Constant East Velocity) .....	105
4-17	INS Vertical Velocity Errors (Constant East Velocity) .....	105
4-18	INS North and East Position Errors (9g Turn) .....	107
4-19	INS Vertical Position Errors (9g Turn) .....	107
4-20	INS North and East Velocity Errors (9g Turn) .....	108
4-21	INS Vertical Velocity Errors (9g Turn) .....	108
4-22	Joint-Solution Position Errors (Constant East Velocity) .....	109
4-23	Joint-Solution Velocity Errors (Constant East Velocity) .....	109
4-24	Joint-Solution Position Errors (9g Turn) .....	110
4-25	Joint-Solution Velocity Errors (9g Turn) .....	110

Abstract

This thesis explores the unstable characteristic of an integrated inertial navigation system (INS) and Global Positioning System (GPS) receiver. During high-dynamic maneuvers, the INS Kalman filter provides velocity estimates to the GPS receiver code loop in an attempt to remove doppler-induced tracking errors. The GPS receiver Kalman filter, in turn, provides position and velocity estimates to correct INS errors. Due to the suboptimal nature of the two individual filters, this closed-loop process neglects key elements of information: time and spatial correlation. Therefore, this closed-loop system quickly becomes unstable during high-dynamic maneuvers, resulting in degraded navigational performance.

Truth models of the INS and GPS receiver are developed. Kalman filters based on these two models are combined to yield a joint-solution model Kalman filter which serves as an indication of the best structure of integration possible. The eigenvalues of the basic INS error dynamics model, when subjected to various dynamic scenarios, are examined. A candidate maneuver is selected to compare the performance of five systems: the INS truth model, the GPS receiver truth model, the joint-solution

model, a two-filter system containing the INS and GPS receiver truth models, and a two-filter system containing reduced-order models of the INS and GPS receiver indicative of current system configuration.

The performance of the individual Kalman filters and the joint-solution Kalman filter are demonstrated for three selected conditions: stationary with respect to the earth, a constant east velocity, and a constant acceleration turn in the horizontal plane. Results of the two-filter systems are incomplete at this time, and require follow-on efforts.

# PERFORMANCE OF GPS-AIDED INS DURING HIGH-DYNAMIC MANEUVERS

## I. Introduction

### 1.1 Background

The integration of an inertial navigation system (INS) with the Global Positioning System (GPS) allows users to realize capabilities of the main features of each independent system along with the additional advantages which can only be accomplished by integrating the two systems. However, under current integration schemes, vehicle dynamics prematurely restrict the incorporation of GPS information during all flight maneuver phases of a mission (Cox, 1978:144; Eller; Tanabe and others, 1985; Upadhyay and others, 1982:120).

Inertial navigation for aircraft was first demonstrated physically when a system named Spire, developed by the Massachusetts Institute of Technology Instrumentation Laboratory, was tested from 1953 to 1955 (Draper, 1981:457-458). The significance of this demonstration was the achievement of totally self-contained navigation. This meant the user could navigate without using electromagnetic signals which are susceptible to jamming and detection by hostile agents. The INS has

evolved to the point of being limited primarily by instrumentation errors (Upadhyay and others, 1982:122). The INS provides the user with position, velocity, and vehicle attitude information during all aircraft maneuvers. However, long-term drift errors arise due to instrumentation errors which degrade navigational accuracy (Britting, 1971:87-88).

GPS, when fully deployed in the early 1990's, will consist of 18 operational satellites equally spaced in six orbital planes (Sturza, 1983:117). By processing range and range-rate information from four satellites, either simultaneously or sequentially, a GPS receiver can solve for the vehicle's three-dimensional position and velocity vectors, and user clock bias. The attractiveness of this approach is the very high accuracy which the user can achieve. The accuracy of this information is not dependent on mission duration because the signal processing does not necessarily rely on past solutions. The receiver bandwidth is made as low as possible to reduce the susceptibility of signal jamming but, because of this low bandwidth, signal tracking is jeopardized during high frequency vehicle dynamics (Upadhyay and others, 1982:122-123).

Integration of INS and GPS allows the navigation performance to exceed that possible by either system operating independently (Cox, 1978:144). The INS exhibits the ability to perform well for short durations and under

severe vehicle dynamics, but is subject to long-term drifts. The GPS accuracy is not limited by mission duration, but the signals are susceptible to jamming, and signal tracking is limited by vehicle dynamics. These complementary features can aid each other in two major aspects:

- a. The GPS long-term accuracy can allow calibration of INS drifts such that the INS can operate autonomously for longer periods with greater accuracy,
- b. The INS can provide vehicle velocity data to the low bandwidth GPS receiver tracking loops, thus compensating for the doppler-induced errors.

This aiding results in improved signal tracking during high-dynamic vehicle maneuvers in addition to providing increased tolerance to signal jamming (Eller).

For these reasons, INS/GPS integrated systems are very attractive for aircraft navigation. An optimally integrated system would model both the INS and GPS receiver dynamics and any interaction between the two systems. However, three historical reasons limit the use of an optimal system for on-line applications:

- a. The computer requirement greatly stresses flight computer capabilities (Maybeck, 1979:403),
- b. INS models have been well-established without relying on GPS availability (Britting, 1971; Widnall and Grundy, 1973),

c. The GPS receiver must accommodate a wide class of users who may or may not have or need an INS (Brooks and others, 1982:4.1-1).

### 1.2 Problem

In the early integration efforts, separate INS and GPS receiver models are maintained, and only selected parameters are exchanged between the two systems. During high-dynamic maneuvers, the GPS receiver relies on the Kalman filter velocity estimate from the INS to aid in tracking the GPS signals. At the same time, the INS Kalman filter processes GPS-derived vehicle position and velocity information as measurements to estimate the navigation solution (Upadhyay and others, 1982:120). However, the statistical properties of the INS-estimated velocity information and the GPS-estimated navigation solution, which would be available in a filter which optimally combines all system information, are not modelled in a two-filter system. By not accounting for these statistical properties, a closed-loop instability is believed to exist under certain vehicle dynamic maneuvers.

### 1.3 Scope

This study examines and compares the stability and performance of the following systems:

a. A joint-solution, fully integrated INS/GPS system,

- b. A full-state two-filter system which accounts for all available spatial information passed between filters, but neglects the time-correlatedness of the measurements. In other words, each system does not attempt to simulate or model the other system. Therefore, the measurements are treated as though they are equally likely to be in error by a positive or negative amount at any instant of time.
- c. A full-state two-filter system which does not account for the cross-correlation between the passed information,
- d. A reduced order two-filter system which exchanges all available information,
- e. A reduced order two-filter system which typifies current integration schemes by not accounting for cross-correlation of the passed information, and
- f. Two-filter systems which exchange limited amounts of cross-correlation information.

From this analysis, a qualitative assessment of the performance differences is made. The ultimate goal is to achieve maximum performance benefit with a minimum amount of information exchange. As such, only the INS and GPS receiver are modelled. The satellite error dynamics, type and location of the receiver antenna, and methods for compensating deterministic errors are of no consequence to the fundamental closed-loop system.

#### 1.4 Assumptions

In order to study the stability and performance of the various closed-loop systems, some basic assumptions of the system configuration and vehicle maneuver are presented.

1.4.1 INS. For the purposes of this study, the INS is chosen to be a local-level, north-slaved system mechanized in a north, east, down orientation. Three gyros and three accelerometers are mounted on a platform with their sensitive axes perfectly aligned, forming a mutually orthogonal set. All measurements of specific force and angular velocity are referenced to the center of the platform which coincides with the mass center of the vehicle. Although this is not typical for actual systems, transformations of the actual inputs to the mass center of the vehicle are possible which would accomplish identical results.

1.4.2 GPS Receiver. The GPS receiver is a four-channel set capable of processing signals from four satellites simultaneously, producing range and range-rate data from the user to each of the satellites. Only the range measurements are modelled in this study because, under high dynamic conditions, the internally-derived range-rate information is unavailable. It is assumed that any computational delay has been established and the navigation solution is available at the required instant of time. It is also assumed that four satellite signals are available to the receiver throughout the vehicle maneuver.

1.4.3 Altimeter. A barometric altimeter is available for measurements to the INS and GPS receiver processing units. This measurement stabilizes the inherently unstable vertical channel of the INS.

1.4.4 Spherical Earth. The ellipticity of the earth is ignored. Reference ellipsoids are available for a more accurate representation, but this factor is considered inconsequential to the stability and performance characteristics of the closed-loop system.

1.4.5 Vehicle Dynamics. Since instability is believed to exist during high dynamic maneuvers, the system is considered to reside in a high performance aircraft. The maneuvers used in this study to excite the instability are subsonic, high acceleration turns in both horizontal and vertical planes. The maneuvers are short in duration such that the favorable satellite geometry chosen is considered to be fixed throughout. For longer flight scenarios, the changing satellite geometry would be properly modelled.

These are the basic assumptions established at the outset of the study. Further assumptions concerning the theory and analysis are presented as necessary in applicable sections of the text.

### 1.5 Current Knowledge

The complementary features, the short-term accuracy of an INS and long-term accuracy of the GPS system, allow integration in such a way that either the Kalman filter can estimate long-term INS drift given GPS measurements, or the INS can provide velocity aiding to the code tracking functions of the receiver. The latter benefit is analyzed in this study.

The INS-derived velocity is used to aid the GPS receiver tracking loops, thus reducing the bandwidth of the loops by eliminating the requirement to track aircraft dynamics. This reduction in bandwidth allows the GPS signal to be less susceptible to jamming interference (Widnall, 1978:1; Eller). This, in itself, is very beneficial and causes no stability problem if done correctly.

The GPS receiver uses its measurements periodically to correct for estimated errors in the INS position and velocity variables. This is also very beneficial and, in fact, necessary for extended navigation performance. By itself, no stability problem is created.

However, aircraft applications require both of the above processes to occur simultaneously, creating a closed-loop system. A potential instability of this closed-loop system exists because typical integration schemes omit modelling the tracking loop error, thus

ignoring the coupling of INS velocity error into the receiver dynamics (Eller; Dosh and Yakos; Carrol and Mickelson, 1977:311). Therefore, the receiver uses the INS-derived velocity as though it is from an independent source, while the receiver is directly providing corrections to the INS velocity channel.

Carrol and Mickelson (Carrol and Mickelson, 1977) analyzed the instability of this loop for the vertical channel. Their solution was to develop a compensation loop to improve the system stability. In the design, they used linearized system models and steady-state filter gains. The approach was to select a loop bandwidth, determine a compensation function, and optimize the system for best performance.

Widnall (Widnall, 1978) also performed a vertical channel analysis using a linearized error model. He discusses three possible design changes: a filter-feedback limiter, reduced INS error control gains, and decorrelation of tracking errors from the GPS measurement. He evaluated the latter two in his analysis. The reduced control gains of his analysis increase the system cut-off frequency by a factor of ten over his baseline system. The decorrelation approach results in a completely stable system. However, because of the method for estimating detector gain, this method is not practical in high jamming or highly dynamic environments.

Eller (Eller) concludes that adequate modelling and proper noise selection to account for unmodelled nonlinearities is essential for integrating INS and GPS systems. For his study, Eller models three types of process noise: dynamics-independent, nominal dynamics-dependent, and dynamics-dependent processes which are adjusted by using real-time measurements. Dynamics-independent noises are those which do not change as the vehicle undergoes motion. These include biases, and time-correlated and uncorrelated noises. Nominal dynamics-dependent noises arise during low dynamic scenarios in which steady-state conditions can be assumed. The dynamics-dependent noises are associated with acceleration-sensitive factors and instrument misalignments. The instability issue was not raised since the INS and GPS of Eller's system provided measurements to a single processor rather than to each other.

Dosh and Yakos (Dosh and Yakos) explored a decoupled error integration scheme. Their analysis, and subsequent test, showed the benefit of providing residual data as a raw measurement to a central computer which interfaces between the INS and GPS receiver. However, the performance of this scheme was not demonstrated in a high-dynamic environment.

Tanabe and others (Tanabe and others, 1985) suggest including a correlator control loop which directly uses INS

aiding information to extract tracking errors. This integration scheme demonstrates an increase in the operating region of the integrated system. However, stability of the system is not guaranteed.

Each of these articles evolve around the stability issue of the two-filter system. Of the studies, only Widnall's analysis of the decorrelation method exhibited a completely stable system. The other approaches indicate possible improvements for system stability, but complete stability is not demonstrated.

#### 1.6 Approach

To analyze the system dynamics associated with an INS/GPS integrated system, INS and GPS receiver models which represent the current systems are chosen. The INS model is augmented with additional error sources which are significant when subjected to high dynamics and short time duration to more closely represent a "truth" model. The GPS receiver model is augmented to include characteristics of a code-tracking loop for each of four channels in order to examine the closed-loop system dynamics. The two models are combined with respect to a common reference frame and a covariance analysis is performed for this joint-solution filter. Then the models are separated and analyzed to demonstrate the best possible performance of a two-filter system if the time-correlation of measurements is

neglected. Next the models are reduced to the current configuration to establish the baseline performance. Finally, varying levels of integration are studied and compared to the joint-solution and baseline systems.

### 1.7 Outline

Chapter 2 introduces the coordinate frames used for this study, the operation of an INS, and concepts of the GPS system.

Chapter 3 presents the system models used in this study. Also, Kalman filtering and a performance analysis method using covariance analysis is introduced.

Chapter 4 examines the stability and performance of the joint-solution, baseline, and the other levels of system integration modelled. The analysis results from examining the following areas:

- a. Eigenvalue migration of the INS model through various turns,
- b. Performance of the various filters under static and constant velocity conditions,
- c. Performance of the various filters during a dynamic maneuver.

Finally, Chapter 5 contains concluding comments and recommendations for future study.

## II. Theory

### 2.1 General

Navigation allows a user to determine his position and velocity expressed with respect to some reference. The reference can be at any location convenient to the user. The user's position and velocity can be expressed, among other ways, as components of an orthogonal or nonorthogonal coordinate frame. Therefore, the reference frames used in this study are first explained.

Position and velocity determination also implies some form of instrumentation which provides the user with information, either continuously or at discrete instants of time. Two types of instrumentation which provide the required information are the INS and the GPS.

An INS processes specific force and angular velocity measurements to extract vehicle motion from some initial location and velocity to another. In space-stabilized and local-level systems, gyroscopes, which measure angular velocity, send appropriate torquing commands to a platform in order to maintain accelerometers, which measure specific force, fixed with respect to a chosen reference frame. A strapdown system operates similarly, except the instruments are mounted directly to the vehicle and the "platform" is an appropriate transformation performed by the processing

unit (Britting, 1971:186). In this study, a north-slaved, local-level navigator is used. Its description and operating principles are explored in this chapter.

Unlike the INS, which relies on no externally transmitted or received signals, the GPS receiver requires transmission and reception. A receiver, carried by the user, receives and processes satellite-transmitted data to determine vehicle location and motion. Receiver operation is also explained in this chapter.

## 2.2 Reference Frames

Vehicle location and dynamics form the basis of any navigation problem. As such, expressing position, velocity, and acceleration as vector quantities allows the use of basic vector operations to express relationships between system variables. However, these vectors have no particular meaning unless expressed with respect to some chosen reference frame. Three specific reference frames are used in the ensuing study: earth-centered-earth-fixed (ECEF) coordinate frame, north-east-down (NED) navigation coordinate frame, and line-of-sight (LOS) coordinates.

### 2.2.1 Earth-Centered-Earth-Fixed Coordinate Frame.

The ECEF coordinate frame contains a set of three mutually orthogonal axes ( $x_e$ ,  $y_e$ ,  $z_e$ ) which originate at the mass center of the earth. The  $z_e$ -axis points in a direction which passes directly through the north pole. The  $x_e$ -axis

is directed to pass through the  $0^\circ$  Latitude,  $0^\circ$  Longitude intersection point. The  $0^\circ$  Latitude line represents the earth's equator, and the  $0^\circ$  Longitude line represents the Greenwich Meridian. The  $y_e$ -axis completes the orthogonal set in accordance with the right-hand-rule. The ECEF coordinate frame rotates about the  $z_e$ -axis at the same rate as the earth's rotation rate ( $w_{1e}$ ). This coordinate frame is shown graphically in Figure 2.1.

2.2.2 North-East-Down Navigation Coordinate Frame (Britting, 1971:33-34). The NED navigation coordinate frame also is composed of three mutually orthogonal axes (N, E, D). The origin of this set, however, is located at the system's location. The D-axis, for a spherical earth assumption, is directed toward the mass center of the earth. The N-axis points toward the north pole in the plane perpendicular to the D-axis. The E-axis completes the orthogonal set in accordance with the right-hand-rule. This axes set and its relationship with the user and the earth is shown graphically in Figure 2.2.

2.2.3 Line-of-Sight Coordinates. When considering GPS satellite positions with respect to the user, the ensemble LOS vectors do not, in general, form a set of orthogonal axes, as was the case with the ECEF and NED navigation coordinate frames. However, just as a

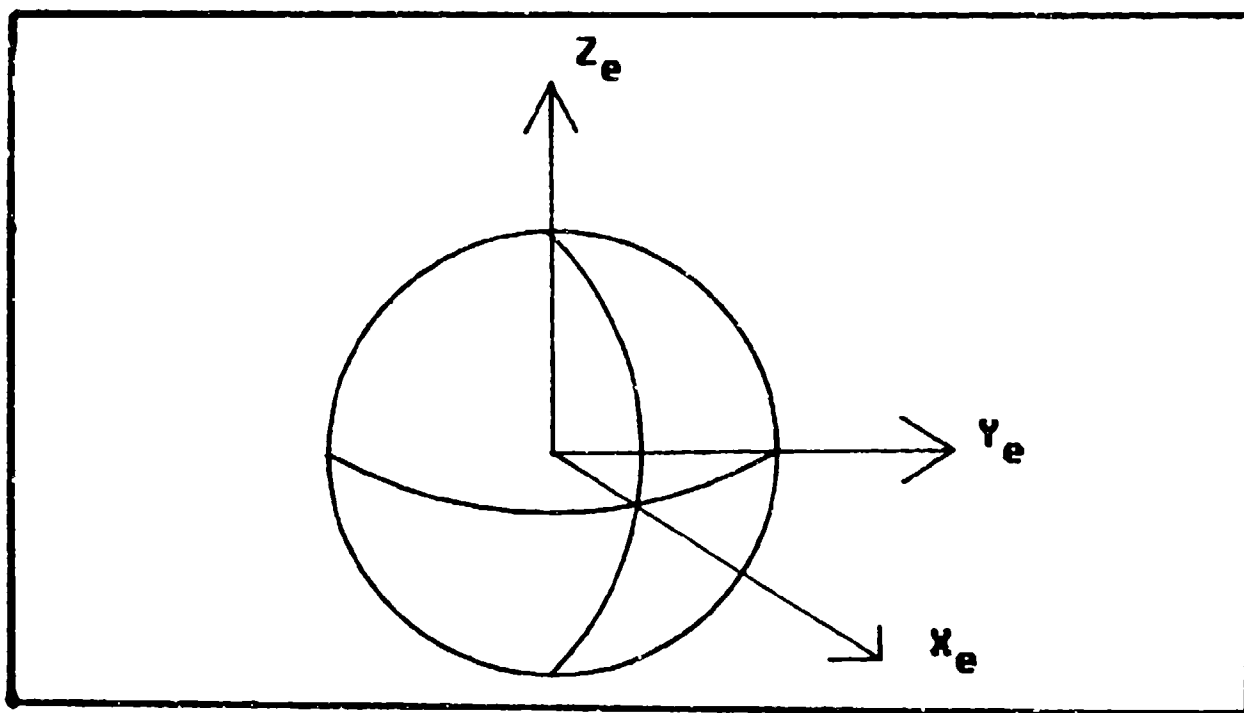


Figure 2.1. ECEF Coordinate Frame

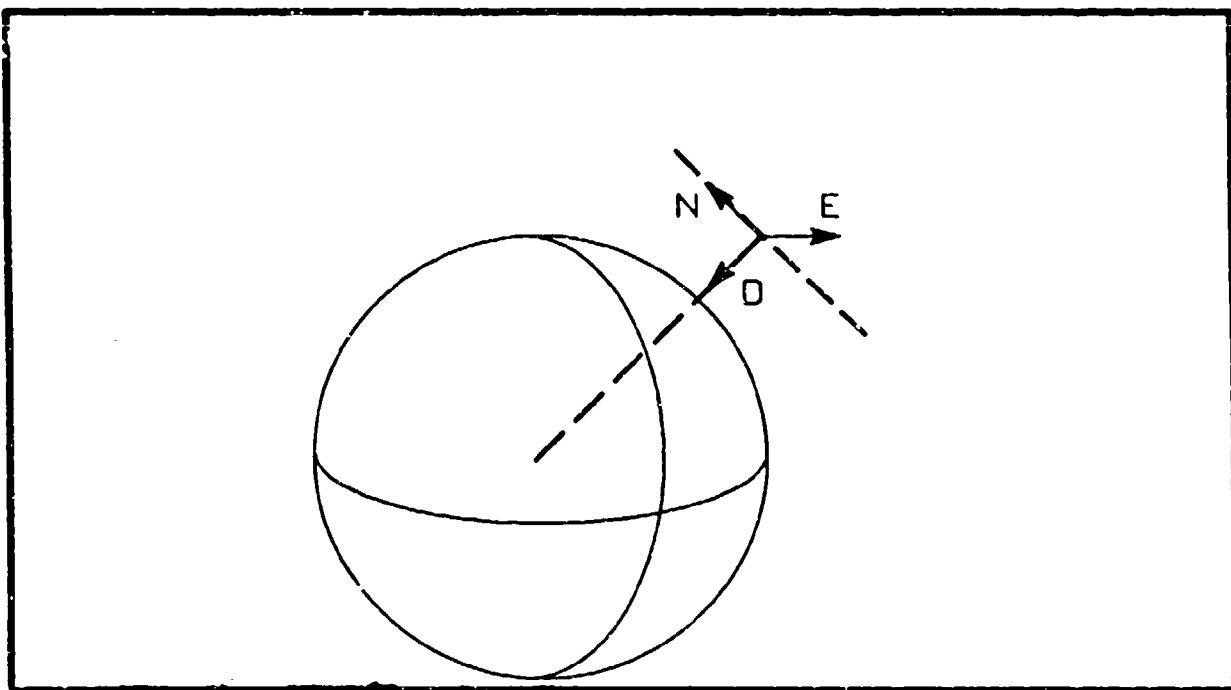


Figure 2.2. NED Navigation Coordinate Frame

three-dimensional vector,  $\underline{v}$ , can be thought of as components along each of the three axes of the previous frames, it can also be described as components along three nonorthogonal axes ( $u_1, u_2, u_3$ ) provided the axes are linearly independent. Figure 2.3 shows this relationship. The relevance of these coordinate systems becomes more apparent as the development of INS and GPS proceed.

## 2.3 North-Slaved, Local-Level Inertial Navigation System

2.3.1 Platform. The INS used for this study is a gimballed north-slaved, local-level (NSLL) INS. Three single-degree-of-freedom (SDOF) gyros and three accelerometers are mounted on a platform such that the six sensitive axes (three for the gyros and three for the accelerometers) form a right-handed orthogonal set. Figure 2.4 shows one possible arrangement of the instruments on the platform.

In typical applications, the measurements obtained by the gyros and accelerometers are referenced to the center of the platform, then transformed appropriately to the mass center of the vehicle. The equations to follow assume these transformations have already taken place such that the resulting measurements refer to the mass center of the vehicle.

Another feature of the NSLL INS is its orientation. The platform is torqued to maintain alignment of the

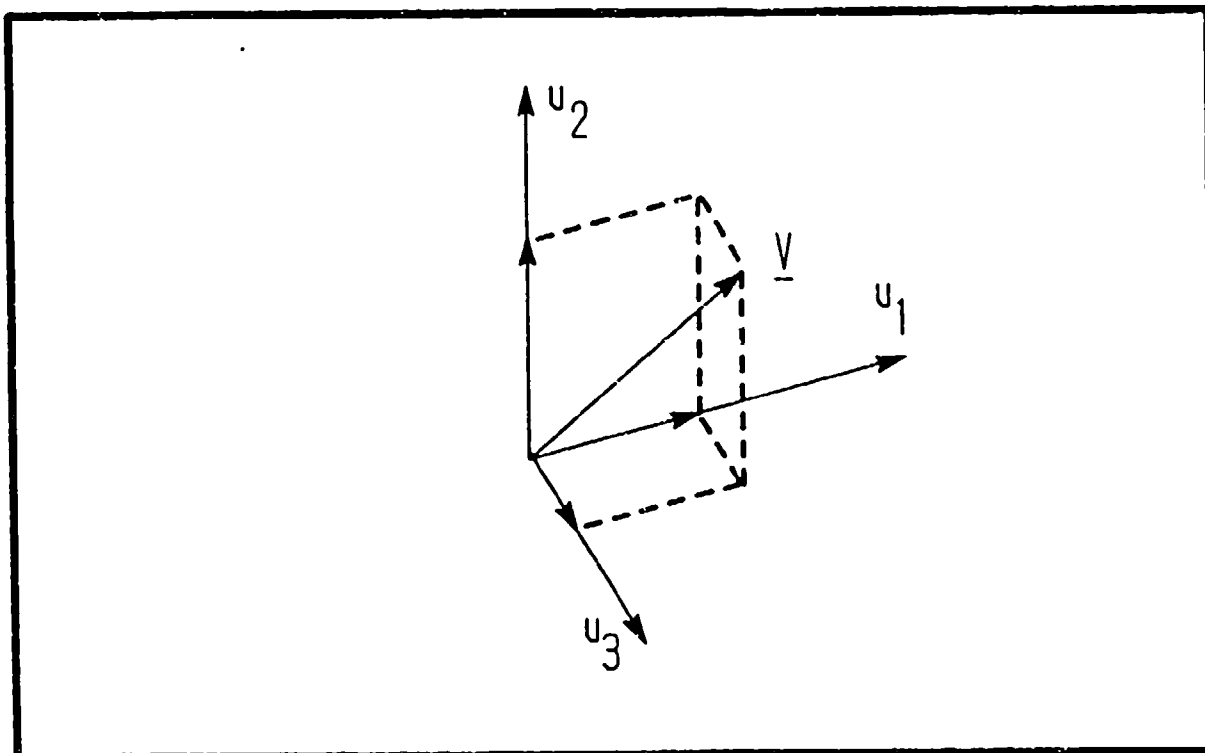


**Figure 2.3. Decomposition of a Vector onto  
Three Nonorthogonal Axes**

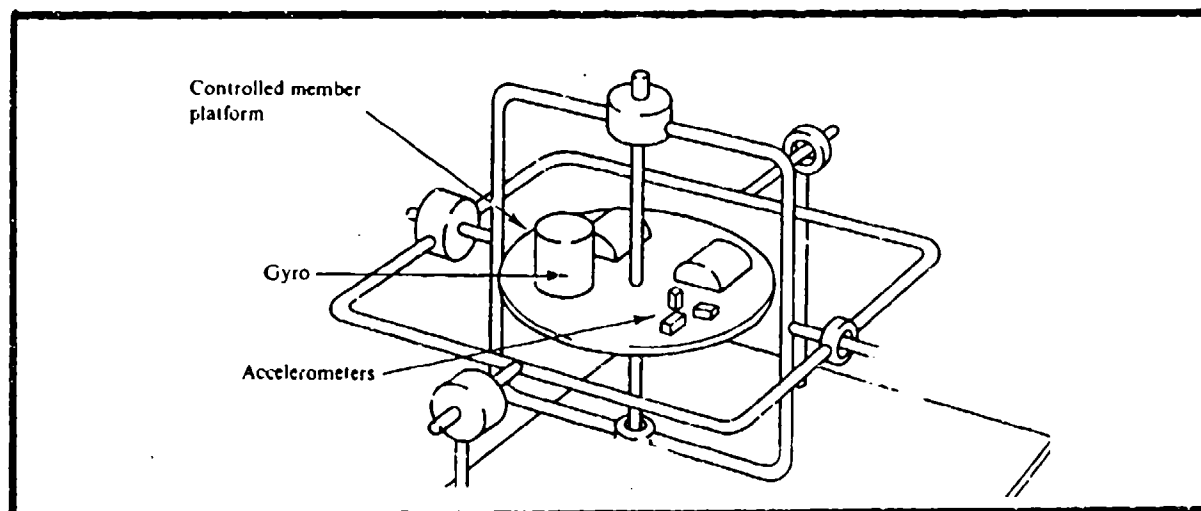


**Figure 2.4. Platform Containing Three  
Accelerometers and Three Gyros (Maybeck, 1979:292)**

sensitive axes with the NED navigation coordinate frame. Thus, the sensitive axes of the NSLL INS measure motion with respect to north, east, and down components. For the purposes of this study, the torquing command applied to the platform is assumed to be perfect. Also, the gyro and accelerometer sensitive axes are assumed to be perfectly mounted on the platform. Therefore, the INS dynamics are driven only by the vehicle dynamics and instrumentation errors. Platform and instrument misalignments cause an additional error in the torquing signal, but are considered secondary and not considered in this study.

2.3.2 Single-Degree-Of-Freedom Gyros. The purpose of the three SDOF gyros on a NSLL INS is to maintain the platform fixed with respect to the NED navigation coordinate frame. To do this, the platform is commanded to account for the earth's rotation as well as the motion of the vehicle on which it is mounted. Ideally, the resulting command to the platform indicates the angular velocity of the NED navigation coordinate frame with respect to inertial space (Britting, 1971:111). The SDOF gyros provide the commands necessary to torque the platform.

A representation of a SDOF gyro is shown in Figure 2.5. It contains a mass which is spun to attain a high angular momentum. The mass is suspended within a gimbal which is free to rotate in one direction. The entire assembly is mounted on a platform. In its nominal state,

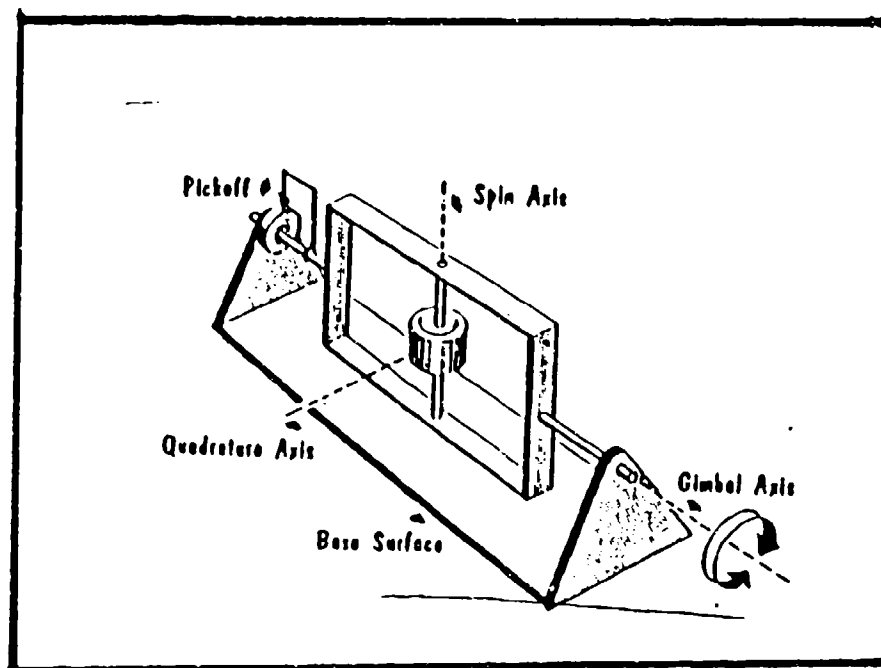


Figure 2.5. Single-Degree-of-Freedom Gyro  
(Lewantowicz, 1986)

the spin axis of the mass is aligned with a spin reference axis. Perpendicular to the spin reference axis is the output, or gimbal, axis. The input, or sensitive, axis completes the orthogonal set. An angular rate about the input axis produces a torque on the output axis. This torque causes the gimbal to precess about the output axis which causes the spin axis to be deflected from the spin reference axis (Lewantowicz, 1986). The precession rate,  $\omega_p$ , is related to the applied torque,  $T$ , and angular momentum of the mass,  $H$ , by the vector relationship

$$\underline{T} = \underline{H} \times \underline{\omega_p}$$

A signal proportional to the precession rate commands the platform to rotate until the torque is nulled, which again aligns the spin axis with the spin reference axis. For this study, the process is assumed to take place instantaneously and perfectly when forced by vehicle dynamics.

For a NSLL INS, an additional source commands the platform. The vehicle's angular velocity commands the platform in the previous case. The angular motion of the NED navigation coordinate frame with respect to inertial space is the additional source which commands the platform. The angular rate about the north axis,  $\omega_N$ , is given by

$$w_N = \dot{\lambda} \cos L \quad (2-1)$$

where  $L$  is the latitude at which the NED navigation coordinate frame is projected onto the surface of the earth, and  $\dot{\lambda}$  is the time rate of change of the celestial longitude which is computed from the time rate of change of the terrestrial longitude,  $\dot{l}$ , and the earth's rotation rate,  $w_{ie}$ , by the relationship

$$\dot{\lambda} = \dot{l} + w_{ie} \quad (2-2)$$

The angular rate about the east axis,  $w_E$ , is proportional to the time rate of change of the latitude, that is

$$w_E = -\dot{L} \quad (2-3)$$

Finally, the angular rate about the down axis,  $w_D$  is given by

$$w_D = -\dot{\lambda} \sin L \quad (2-4)$$

Since  $L$ ,  $\dot{L}$ , and  $\dot{l}$  are computed quantities, the commands to the platform can be in error depending on the accuracy of the computations (Britting, 1971:154).

2.3.3 Accelerometers. Accelerometers are used to measure the contact specific force of the vehicle. By

keeping the platform aligned with the NED navigation coordinate frame, the accelerometer outputs measure north, east, and down components of specific force. Vehicle acceleration is computed from the specific force by removing the gravitational force sensed by the accelerometers.

An accelerometer can conceptually be thought of as a proof mass suspended from a frame mounted on a platform. If the sensitive axis (SA) is aligned with gravity, the accelerometer measures 1g of specific force. An acceleration of the frame causes the mass to be displaced an additional amount proportional to, and opposite of the acceleration direction (Wrigley and others, 1969:49). The resulting specific force sensed by the accelerometer includes the effects of gravity and vehicle acceleration. Therefore, the vehicle acceleration is computed by removing gravity effects from the accelerometer measurement. This relationship is given vectorially as

$$\ddot{\underline{x}} = \underline{f} + \underline{g} \quad (2-5)$$

where

$\ddot{\underline{x}}$  is the vehicle acceleration relative to the inertial frame

$\underline{f}$  is the specific force sensed by the accelerometers

$\underline{g}$  is the gravity vector

This relationship is true in all applications. However, if the acceleration is expressed with respect to the NED navigation coordinate frame, an additional force caused by the rotation of the earth and the movement of the NED navigation coordinate frame about the earth must be calculated. This force is commonly referred to as the Coriolis effect. This results in the following relationships between specific force and vehicle motion:

$$f_N = \dot{v}_N + v_E(\dot{l} + 2w_{le})\sin L - \dot{L} v_D \quad (2-6)$$

$$f_E = \dot{v}_E - v_N(\dot{l} + 2w_{le})\sin L - v_D(\dot{l} + 2w_{le})\cos L \quad (2-7)$$

$$f_D = \dot{v}_D + v_E(\dot{l} + 2w_{le})\cos L + \dot{L} v_N - g \quad (2-8)$$

where

$f_N$ ,  $f_E$ , and  $f_D$  are the north, east, and down components of specific force as measured by the accelerometers

$\dot{v}_N$ ,  $\dot{v}_E$ , and  $\dot{v}_D$  are the time rates of change of the north, east, and down components of velocity ( $v_N$ ,  $v_E$ ,  $v_D$ )

and

$g$  is the acceleration due to the gravity magnitude. Errors in vehicle motion are introduced by such computations if the platform is not perfectly aligned with the NED navigation coordinate frame. For example, if the

platform were tilted such that the north sensing accelerometer was not precisely aligned in the vertical plane with the north axis, a component of gravity is sensed by the accelerometer. When vehicle motion is calculated from Equation (2-6), this gravity effect is not removed and apparent vehicle acceleration results.

2.3.4 System Interaction. The NSLL INS is functionally represented by the block diagram of Figure 2.6. In the figure,  $\underline{f}$  represents the specific force acting on the vehicle. The resulting vector of measurements from the accelerometers is symbolized by  $\tilde{\underline{f}}$ . This information, along with initial conditions, is provided to a navigation computer which calculates the position and velocity of the vehicle. These calculations also provide torquing commands to the platform to represent the motion of the NED navigation coordinate frame with respect to inertial space. Finally, the physical connection between the platform and the accelerometer triad represents the nonlinear relationship of how gravity is coupled through the platform misalignments. In other words, a platform or instrument misalignment causes the accelerometers to sense a specific force components due to gravity. The navigation computer uses linearized perturbation relationships, to be discussed in Chapter III, to obtain an accurate description of this information to determine the vehicle's position and velocity. This same information is used to provide

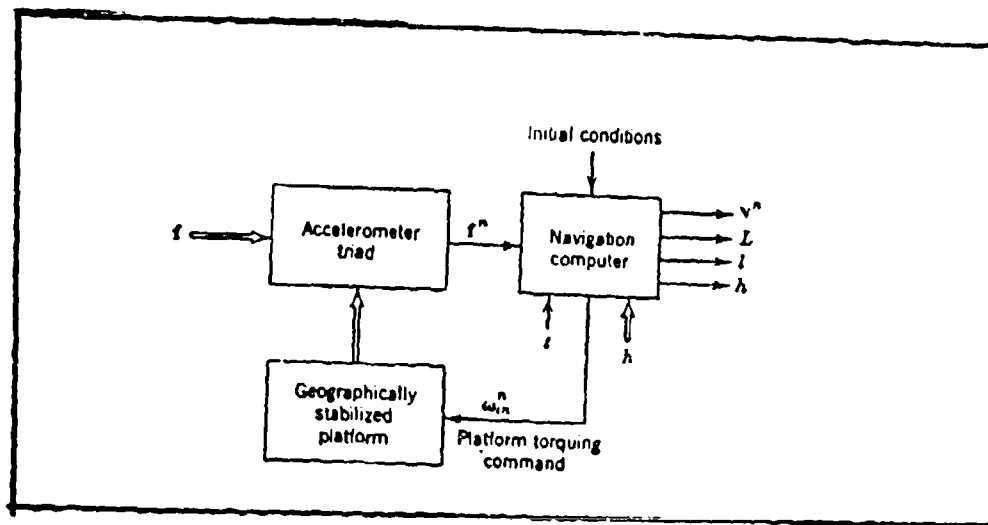


Figure 2.6. NSLL INS Block Diagram  
(Britting, 1971:110)

torquing commands to the platform. The platform, in its new orientation, is again in error and the cycle continues (Lewantowicz, 1986). The resulting motion of the platform is oscillatory and unstable in nature (Britting, 1971:Ch 7).

Two dominant frequencies appear in the oscillations: Schuler and Foucault. Schuler frequency,  $\omega_s$ , is given by

$$\omega_s = (g/R)^{1/2} \quad (2-9)$$

where  $g$  is the acceleration due to gravity, and  $R$  is the distance from the center of the earth to the system's location. This frequency represents the characteristic frequency of a hypothetical pendulum which has a radius arm equal to  $R$ . In an accelerometer, since the radius arm is less than  $R$ , any acceleration induced by changing speed or direction causes the pendulum to deviate from vertical. This deviation exhibits a natural frequency identical to the Schuler frequency (Wrigley and others, 1969:215).

Foucault frequency is related to the rotational motion of the NED Navigation Coordinate Frame with respect to inertial space. This frequency,  $\omega_F$ , is given by

$$\omega_F = \dot{\lambda} \sin L \quad (\text{Britting, 1971:128}) \quad (2-10)$$

The magnitudes of these oscillations depend upon

initial platform misalignment, as well as various forcing functions such as instrumentation errors and vehicle motion (Britting, 1971:Ch 7).

## 2.4 GPS Receiver

2.4.1 Satellite Signals. When the GPS is fully operational in the early 1990's, 18 satellites will provide highly accurate three-dimensional position and velocity information around the world. The satellites are placed in six orbital planes inclined at  $55^{\circ}$ . Each plane consists of three satellites in 12-hour orbits separated by  $120^{\circ}$ . Between planes, the satellites are phased  $40^{\circ}$  apart (Sturza, 1983:117).

A Master Control Station (MCS) has uplink capabilities to each satellite for correcting the satellites' clock offset, frequency, and other parameters (Milliken and Zoller, 1978:5). Four monitoring stations, under direct control of the MCS, collect data from each satellite. The MCS uses this data for its correcting operations (Russell and Schaibly, 1978:75). In this manner, very accurate knowledge of the satellites' position and motion exists.

The satellites continuously transmit a 50 bit per second data stream which contains this ephemeris data along with other data including system time, clock behavior, and satellite health (Van Dierdonck and others, 1978:55). This data is modulated by two pseudo-random codes (PRC): the

precision, or P-code and the clear/acquisition, or C/A-code. The C/A-code contains 1023 bits that repeat each millisecond. The P-code sequence is generated by multiplying two PRC's together. The first contains 15,345,000 binary data bits and has a period of 1.5 seconds. The second is 37 bits longer. This code then is divided among the 18 satellites and is regenerated on a weekly basis such that no two satellites ever transmit the same sequence. Each satellite transmits the P-code on two separate frequencies simultaneously: 1575.52 MHz and 1227.6 MHz. This gives the user capability to compensate for ionospheric-induced path delays during satellite signal transmission (Spilker, 1978:34).

#### 2.4.2 Receiver Operation.

2.4.2.1 User Position Solution (Milliken and Zoller, 1978:6-7). The four-channel GPS receiver receives the PRC from four separate satellites simultaneously. Each of these codes are compared to identical internally generated codes by means of an autocorrelation function. By performing the autocorrelation, the receiver calculates a time shift between the satellites' codes and the receiver's codes. This time shift, scaled by the speed of light, represents the pseudorange to each of the four satellites. It is called pseudorange because the calculated distance includes timing uncertainties between the receiver clock and the satellite clocks, path delays

through the troposphere and ionosphere, and other lesser effects in addition to the true range between the satellites and the user. The user removes the ionospheric-caused path delays by taking advantage of the two transmission frequencies, thus leaving clock errors as the major error source for calculating range between the user and the satellite.

If no clock errors existed, three satellites would be sufficient to calculate the user's position. However, receiving signals from four satellites, the user can also calculate his clock offset. The receiver processes signals from four satellites to obtain four equations in four unknowns. The four equations solve the vectorial relationship between user position in ECEF coordinates,  $\underline{R}_u$ , satellite position in ECEF coordinates,  $\underline{R}_i$ , and the vector from the user to the satellite,  $\underline{D}_i$ , as shown in Figure 2.7:

$$\underline{R}_u = \underline{R}_i - \underline{D}_i \quad i=1,2,3,4 \quad (2-11)$$

But, only the magnitude of  $\underline{D}_i$  ( $= D_i$ ) is known from the propagation time between the satellite and the user. Therefore, a unit LOS vector is needed to indicate the direction of the satellite from the user. The satellites' positions are known from the ephemeris data. The approximate unit LOS vector is found either by knowing the user's position from an independent source or by knowing

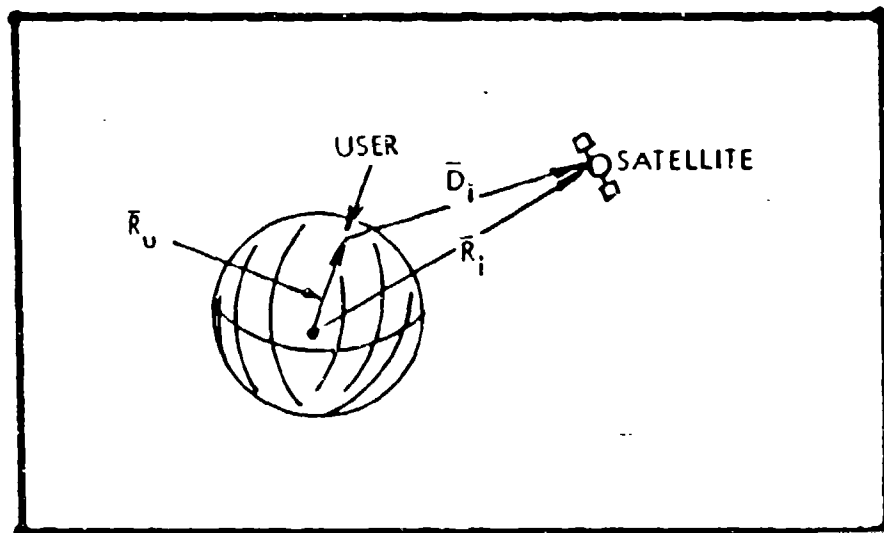


Figure 2.7. User Position Determination  
(Milliken and Zoller, 1978:13)

the direction the satellite signal arrives. Thus,

$$\underline{u}_1 \cdot \underline{D}_1 = D_1 = \rho_i - b \quad i=1,2,3,4 \quad (2-12)$$

where  $\rho_i$  is the measured pseudorange to the  $i^{\text{th}}$  satellite and  $b$  is the user clock offset. Equation (2-11) then becomes

$$\begin{aligned} \underline{u}_1 \cdot \underline{R}_u &= \underline{u}_1 \cdot \underline{R}_1 - D_1 \\ &= \underline{u}_1 \cdot \underline{R}_1 - \rho_i + b \quad i = 1,2,3,4 \end{aligned} \quad (2-13)$$

The four equations of Equation (2-13) are solved simultaneously resulting in a solution for user position and clock offset.

**2.4.2.2 Signal Acquisition and Tracking.** In order to determine signal propagation time, the receiver must first acquire and then track the signal. Two control loops within the receiver accomplish this task.

For high accuracy navigation, the GPS receiver must acquire and track the P-code signal. However, due to the length of this code, direct acquisition is not reasonable. Therefore, the receiver takes advantage of the slower, shorter length C/A-code which contains a handover word and directs the receiver to a specific message location to begin searching the P-code. Once the P-code acquisition is accomplished, continuous tracking is required to achieve the highly accurate navigation solution (Milliken and Zoller, 1978:7).

The tracking function consists of two interacting processes. Once the signal has been acquired, a relatively wide bandwidth phase-lock loop tracks the satellite signal carrier. By measuring the difference between the satellite-transmitted carrier frequency and the received frequency, the carrier loop determines a doppler shift. This shift indicates the apparent separation rate, or delta pseudorange, of the vehicle with respect to the satellites (Milliken and Zoller, 1978:11-12). At the same time, a low bandwidth delay-lock loop slews the phase of the receiver's internally generated code until it achieves maximum correlation with the received signal. This phase shift, scaled by the speed of light, generates the pseudorange measurement. The phase shift is returned to the phase-lock loop as an on-time estimate to allow extraction of the 50 Hz navigation data. In order to allow more accurate tracking of the code and, thus, the possibility of a lower bandwidth, the phase-lock loop supplies its doppler estimate as an aiding signal to the delay-lock loop (Upadhyay and others, 1982:121).

Since the phase-lock loop has a greater bandwidth than the delay-lock loop, loss of carrier tracking implies loss of code tracking and the corresponding failure to demodulate the navigation data. Flight tests at U.S. Army Yuma Proving Ground determined that aircraft maneuvers of about 4g causes a loss of signal tracking (Meyer, 1987:8).

But, in typical applications, external velocity aiding is provided to the delay-lock loop in the event that carrier tracking is lost. The transfer from the doppler aiding internal to the receiver to the external aiding source is transparent to the delay-lock loop, and continued operations under higher dynamic maneuvers is achieved (Cox, 1978:144; Upadhyay and others, 1982:122; Widnall, 1978:1).

## 2.5 Summary

This chapter presented the foundation for understanding the basic INS and GPS receiver operation. The next chapter develops the analysis tools and models necessary to analyze the systems individually, and as an integrated system.

### III. Analysis Tools and INS/GPS Receiver Modelling

Analysis of any system requires a set of tools which can display the characteristic behavior of the system. In this study, as with typical INS and GPS systems, the Kalman filter as an estimator provides the data processing structure to solve the navigation equations. The performance of these Kalman filters are judged by how well they represent the true world. Therefore, the basic assumptions of the Kalman filter are described in this chapter along with the processing algorithm which serves as an estimator.

Next, truth models of the INS, GPS receiver, and INS/GPS integrated systems are developed. These truth models exhibit the characteristics of the optimal system against which the reduced order models are compared.

Finally, the basic structure of a covariance performance analysis is presented along with extensions of this concept as applied to the systems under study.

#### 3.1 Kalman Filter (Maybeck, 1979:4-5)

A Kalman filter is an optimal data processing algorithm. It provides the best possible estimate of system variables by considering the system dynamics, any available measurements, and initial uncertainties of the

system states. As with any control system, the engineer attempts to establish relationships between observed outputs and deterministic inputs. To do this, he develops mathematical models which describe these relationships. By using a Kalman filter, however, the engineer goes a step further. He not only models deterministic relationships between system variables, he also models the uncertainties of his system, of the inputs to the system, and of the measurements from which he observes the system. This is the basis for the optimality of the Kalman filter. It uses knowledge of the system and measurements device dynamics, along with the modelled uncertainties, and processes all available measurements, weighed by their precision, to obtain a best estimate of the variables of interest. Figure 3.1 illustrates a typical application of the Kalman filter.

**3.1.1 Basic Kalman Filter Assumptions.** The Kalman filter can only be applied if three basic assumptions of the system can be made: the model of the system must be described by linear equations, any noises entering the system or measurements are white, and the amplitudes of the noises take the shape of a Gaussian or bell-shaped curve. If these assumptions are satisfied, then the mathematics involved become tractable, and only the first and second order statistics (mean and variance) are necessary to

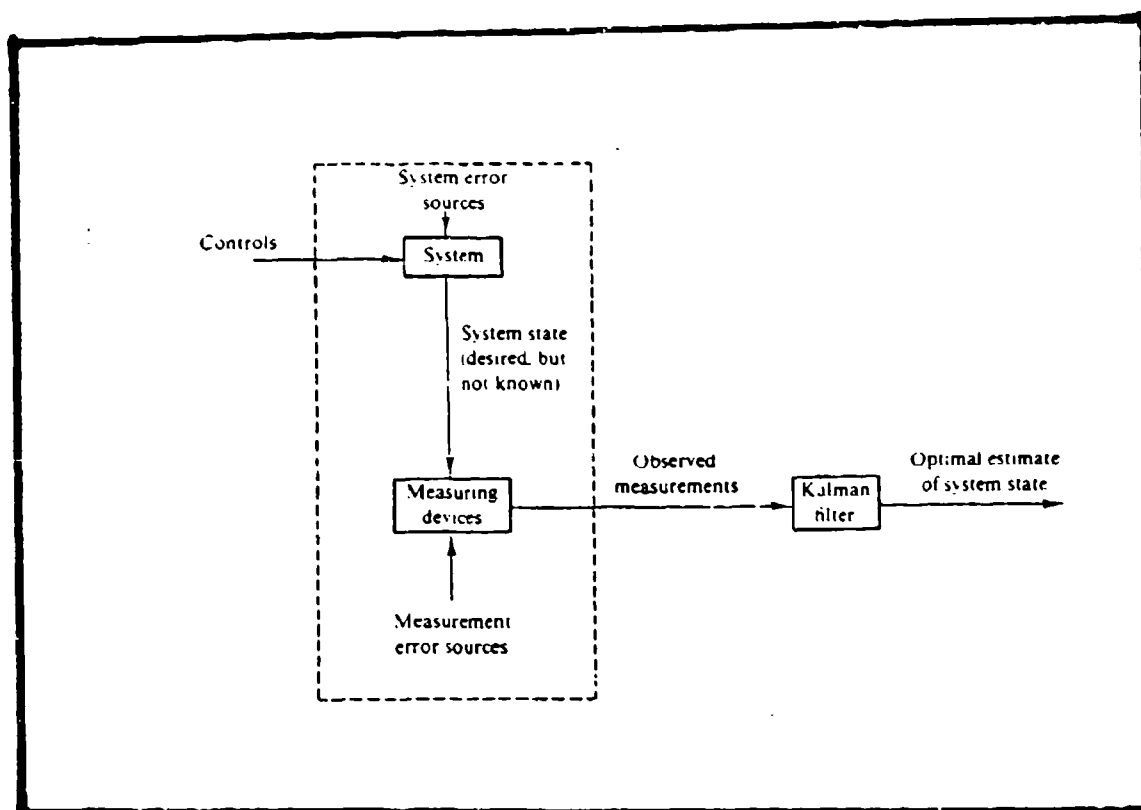


**Figure 3.1. Typical Kalman Filter Application**  
(Maybeck, 1979:5)

describe the system completely (Maybeck, 1979:7-9).

Linear system models are difficult, but not impossible, to find in nature. Therefore, it would appear that Kalman filter applications are severely limited. However, when nonlinearities exist, an engineer usually linearizes about either a predetermined or a calculated nominal point thus developing a linearized set of error or perturbation equations. The second-order statistics of the linearized perturbation states are equal to the second-order statistics of the original system states. However, since the nominal is removed to generate the linearized perturbation equations, the mean of the error states becomes zero (Maybeck, 1979:299-300).

The latter two assumptions, whiteness and Gaussianness, concern the noise entering the system and the noise of the measuring devices. A white noise is a noise which has a constant amount of power content across all frequencies. Furthermore, a white noise is not correlated in time. That is, the magnitude of noise signal at one instant of time does not indicate the magnitude of noise signal present at any other instant of time. Obviously, such a noise does not exist in nature. However, if the power content of a noise remains relatively constant over the bandpass of the system, then it can be represented as white as far as the system is concerned. Often times, system noises are time-correlated or do not have constant power content

within the system bandpass which violates properties of white noise. These limitations can be corrected by driving a small linear system, called a shaping filter, by a white noise and augmenting this model to the overall system model (Maybeck, 1979:7-9,180).

Two such shaping filters are used in this study: the random constant, or bias, and the exponentially time-correlated process. Figure 3.2 shows the random constant shaping filter as an undriven integrator (white noise power equal to zero) with some Gaussian distributed initial condition. The defining relationship of this shaping filter is  $\dot{x}(t)=0$ . The autocorrelation indicates that the value of the bias is not known precisely, but, whatever value it takes, remains constant for all time. This results in a spectral density which contains only a zero frequency component.

The exponentially time-correlated noise, as shown in Figure 3.3, is generated by passing a white noise through a first-order system. The describing equation of this system is  $\dot{x}(t) = -(1/T)x(t) + w(t)$  where  $T$  is the time constant of the time-correlated noise,  $n(t)$ , and  $w(t)$  is the white driving noise. The power of the white noise is  $2\sigma^2/T$  where  $\sigma^2$  is the mean-squared value of the time-correlated noise. By augmenting these noise process models to the linear system model, the system becomes one which is driven only by white noise processes.

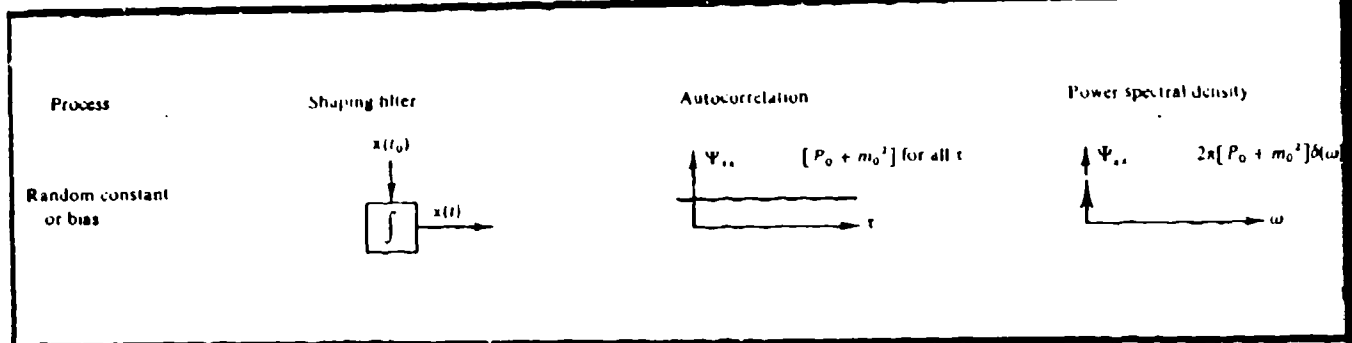


Figure 3.2. Random Constant Process  
(Maybeck, 1979:183)

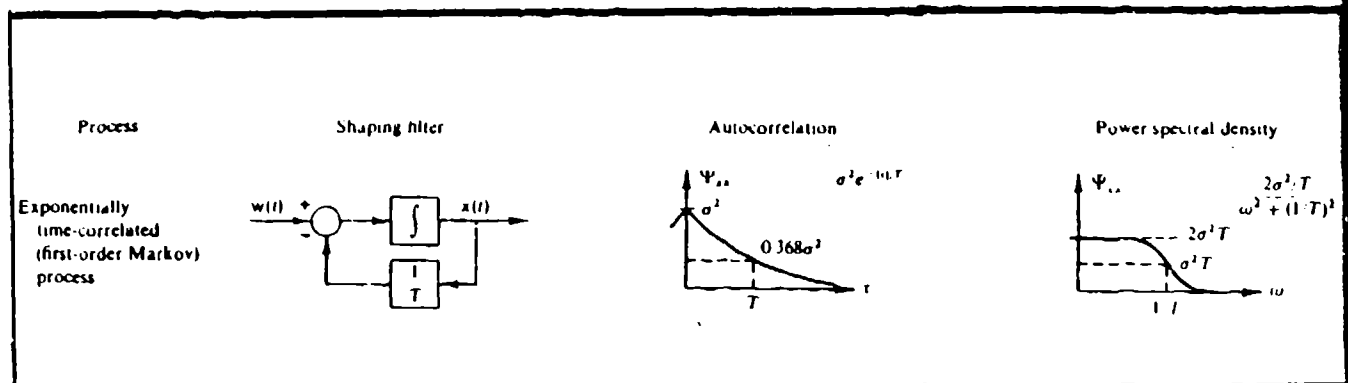


Figure 3.3. Exponentially Time-Correlated Process  
(Maybeck, 1979:183)

Gaussianness describes the amplitude of the white noise. As shown in Figure 3.4, a Gaussian distribution is bell-shaped with the peak amplitude occurring such that the actual value is equally likely to lie on either side of the mean,  $\bar{z}$ . The standard deviation,  $\sigma_z$ , indicates the mean  $\pm 1\sigma$  band where 68.3% of the probability weight is contained. The shape of the curve is completely described by its mean and variance.

If these assumptions (linear system, white and Gaussian noises) are satisfied, then the Kalman filter provides optimal estimates of the system variables.

**3.2 Estimator Equations** (Maybeck, 1979:Ch 5). The continuous-time system model is described by first-order linear differential equations with additive white driving noise:

$$\dot{\underline{x}}(t) = F(t)\underline{x}(t) + \underline{w}(t) \quad (3-1)$$

where the  $n$ -by-1 vector  $\underline{x}(t)$  represents the system states,  $F(t)$  is an  $n$ -by- $n$  matrix which models the linearized dynamic relationships between the states, and the  $n$ -by-1 dimensional zero-mean white Gaussian noise vector,  $\underline{w}(t)$ , which is independent of  $\underline{x}(t)$ , has an associated strength of

$$Q(t)\delta(\tau) = E\{\underline{w}(t)\underline{w}^T(t+\tau)\} \quad (3-2)$$

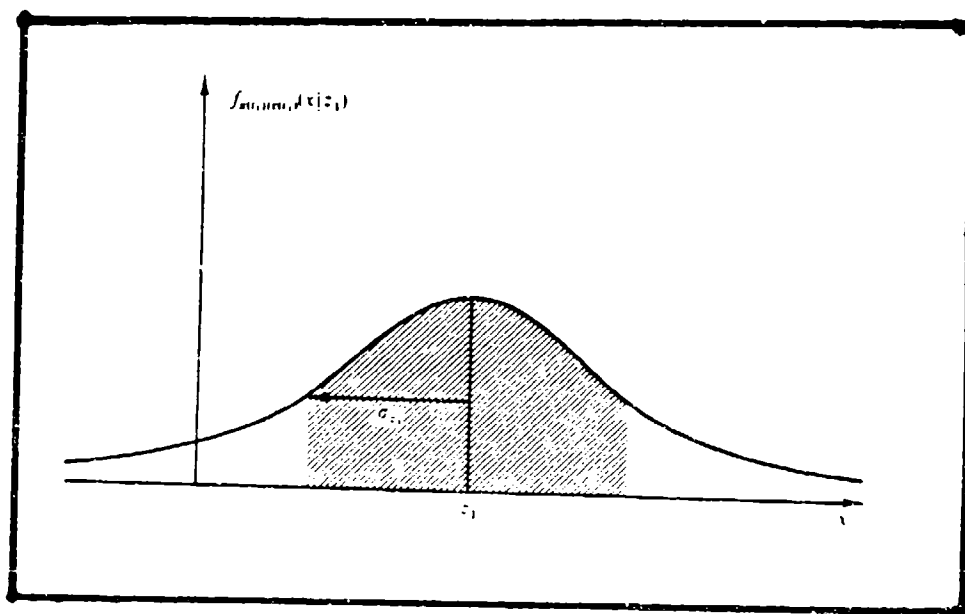


Figure 3.4. Gaussian-Shaped Distribution  
(Maybeck, 1979:10)

where  $\delta(\tau)$  is the Dirac delta function and  $E\{\cdot\}$  is the expectation operator.

For this study, it is more convenient to describe the system in the discrete-time representation. Equation (3-1) is equivalently written as a difference equation

$$\underline{x}(t_{i+1}) = \phi(t_{i+1}, t_i) \underline{x}(t_i) + \underline{w}_d(t_i) \quad (3-3)$$

where  $\phi(t_{i+1}, t_i)$  is the n-by-n state transition matrix which relates the system states in their discrete-time representation, and

$$E\{\underline{w}_d(t_i) \underline{w}_d^T(t_j)\} = Q_d(t_i) \quad i=j \quad (3-4)$$

$$E\{\underline{w}_d(t_i) \underline{w}_d^T(t_j)\} = \underline{0} \quad i \neq j \quad (3-5)$$

where

$$Q_d(t_{i+1}) = \int_{t_i}^{t_{i+1}} \phi(t_{i+1}, \tau) Q(t_i) \phi^T(t_{i+1}, \tau) d\tau$$

In this study, the time-varying F-matrix is approximated as constant for the time interval from  $t_i$  to  $t_{i+1}$ . Therefore, the state transition matrix is computed by

$$\phi(t_{i+1}, t_i) = \exp[F(t_{i+1} - t_i)] \quad (3-6)$$

$Q_d(t_i)$  of Equation (3-4) is approximated to first order by

the relationship

$$Q_d(t_i) = Q(t_{i+1})(t_{i+1} - t_i) \quad (3-7)$$

This approximation is valid for systems in which the sample time is short compared to the time constant of its fastest dynamic mode. In actuality, the noise strength matrix,  $Q_d$ , would be adjusted to match empirical test data for truth modelling. A reduced order Kalman filter would require further tuning to match the truth model characteristics properly. Therefore, using Equation (3-7) results in a crude approximation. But, for comparison purposes, it is adequate for this study.

Discrete measurements,  $\underline{z}(t_i)$ , used by the Kalman filter can be either linear or nonlinear functions of the modelled states corrupted by measurement noise vector,  $\underline{n}(t_i)$ . As with the dynamics model, the nonlinear measurement functions can be linearized about a nominal and considered constant for a given time of interest. This results in a measurement model

$$\underline{z}(t_i) = H(t_i)\underline{x}(t_i) + \underline{n}(t_i) \quad (3-8)$$

where  $H(t_i)$  is the linearized relationship between the measurements and the states. The time-correlated portion of the corruptive noise,  $\underline{n}$ , is removed in the same manner

as the driving noise described previously. That is, a linear shaping filter corresponding to the correlated properties of the noise is augmented to the system model dynamics, leaving only a white measurement uncertainty,  $\underline{v}(t_1)$ , which is independent of  $\underline{w}(\cdot)$  and  $\underline{x}(\cdot)$ . Thus, the augmented system model becomes

$$\underline{x}(t_1) = \Phi(t_1, t_{1-1})\underline{x}(t_{1-1}) + \underline{w}_d(t_1) \quad (3-9)$$

$$\underline{z}(t_1) = H(t_1)\underline{x}(t_1) + \underline{v}(t_1) \quad (3-10)$$

where the dimension of  $H(t_1)$  and  $\underline{x}(\cdot)$  are increased due to the addition of the shaping filter states, and the measurement noise strength,  $R(t_1)$  is given by

$$E\{\underline{v}(t_1)\underline{v}^T(t_j)\} = \begin{cases} R(t_1) & t_1 = t_j \\ 0 & t_1 \neq t_j \end{cases} \quad (3-11)$$

Equations (3-9) and (3-10) describe the discrete-time system driven by white system noise having noise-corrupted measurements available at discrete instants of time.

The Kalman estimator optimally combines the state dynamics model and the measurements to produce state estimates,  $\hat{\underline{x}}(t_1)$ , and their associated covariances,  $P(t_1)$  in an iterative two-step process starting from some initial conditions  $\hat{\underline{x}}(t_0)$  and  $P(t_0)$ :

a. Time propagation

$$\hat{\underline{x}}(t_1^-) = \phi(t_1, t_{1-1}) \hat{\underline{x}}(t_{1-1}^+) \quad (3-12)$$

$$\begin{aligned} P(t_1^-) = & \phi(t_1, t_{1-1}) P(t_{1-1}^+) \phi^T(t_1, t_{1-1}) \\ & + Q_d(t_{1-1}) \end{aligned} \quad (3-13)$$

b. Measurement update

$$\begin{aligned} K(t_1) = & P(t_1^-) H^T(t_1) \{ H(t_1) P(t_1^-) H^T(t_1) \\ & + R(t_1) \}^{-1} \end{aligned} \quad (3-14)$$

$$\begin{aligned} \hat{\underline{x}}(t_1^+) = & \{ I - K(t_1) H(t_1) \} \hat{\underline{x}}(t_1^-) \\ & + K(t_1) \underline{z}(t_1) \end{aligned} \quad (3-15)$$

$$\begin{aligned} P(t_1^+) = & \{ I - K(t_1) H(t_1) \} P(t_1^-) \\ & \times \{ I - K(t_1) H(t_1) \}^T \\ & + K(t_1) R(t_1) K^T(t_1) \end{aligned} \quad (3-16)$$

In the Equations (3-12) through (3-16), the "-" and "+" superscripts above the time arguments indicate the instant of time immediately before and after a measurement is taken, respectively.  $K(t_1)$  represents the Kalman gain which optimally weights the system dynamics model and the available measurement vector,  $\underline{z}(t_1)$ . For error state analysis, the mean is always assumed zero, but Equations

(3-12) and (3-15) are used in modelling later in this chapter. The Joseph Form of the measurement update was chosen because it is less sensitive to arithmetic truncation than other, nonsymmetric, forms.

### 3.3 INS Error Model

This section presents the INS error model which is linearized from the nonlinear relationships of Chapter II. First, the basic linearized equations describing the relationship between platform tilts, position errors, and velocity errors are listed. This system is augmented to include errors due to the barometric altimeter measurement, and INS instrumentation errors.

3.3.1 Basic Equations. The basic INS error model consists of nine states and is taken directly from Britting's model of a NSLL INS (Britting, 1971:122). Britting used  $\alpha$  and  $\kappa$  as altitude aiding for illustrative purposes to stabilize the vertical channel of the INS. Therefore, the simplification  $\alpha = \kappa = 0$  is made because the Kalman filter used in this study optimally combines the altimeter measurement with the dynamics model rather than performing the weighting nonoptimally within the dynamics model as described by Britting. The perturbation equations can be written as nine linear differential equations in which the error state vector, in spherical coordinates, is defined as

$$\underline{x}_S^T = (\epsilon_N \quad \epsilon_E \quad \epsilon_D \quad \delta L \quad \delta l \quad \delta h \quad \delta \dot{L} \quad \delta \dot{l} \quad \delta \dot{h}) \quad (3-17)$$

where

$\epsilon_{(.)}$  are the platform misalignments about the north, east, and down axes,

$\delta$  represents a perturbation,

$h$  is altitude, and

$L$  and  $l$  are defined as latitude and longitude, respectively.

The dynamics equations are (with the time argument removed)

$$\dot{x}_1 = -\dot{\lambda} \sin(L)x_2 + \dot{L}x_3 - \dot{\lambda} \sin(L)x_4 + \cos(L)x_8 \quad (3-18)$$

$$\dot{x}_2 = \dot{\lambda} \sin(L)x_1 + \dot{\lambda} \cos(L)x_3 - x_7 \quad (3-19)$$

$$\dot{x}_3 = -\dot{L}x_1 - \dot{\lambda} \cos(L)x_2 - \dot{\lambda} \cos(L)x_4 - \sin(L)x_8 \quad (3-20)$$

$$\dot{x}_4 = x_7 \quad (3-21)$$

$$\dot{x}_5 = x_8 \quad (3-22)$$

$$\dot{x}_6 = x_9 \quad (3-23)$$

$$\begin{aligned} \dot{x}_7 = & -(f_D/R)x_2 + (f_E/R)x_3 - \dot{l}(\dot{l}+2w_{1e})\cos(2L)x_4 \\ & -(1/R)(\ddot{L} + (1/2)\dot{l}(\dot{l}+2w_{1e})\sin(2L))x_6 \\ & -(2\dot{h}/R)x_7 - \dot{\lambda} \sin(2L)x_8 - (2L/R)x_9 \end{aligned} \quad (3-24)$$

$$\begin{aligned} \dot{x}_8 = & (f_D/R\cos(L))x_1 - (f_N/R\cos(L))x_3 \\ & + (\ddot{l}\tan(L) + 2(\dot{h}/R)\dot{\lambda}\tan(L) + 2\dot{L}\dot{\lambda})x_4 \\ & - ((\ddot{l}/R) - (2\dot{\lambda}\dot{L}/R)\tan(L))x_6 + 2\dot{\lambda}\tan(L)x_7 \\ & - 2((\dot{h}/R) - \dot{L}\tan(L))x_8 - ((2/R)(\dot{l}+w_{1e}))x_9 \end{aligned} \quad (3-25)$$

$$\begin{aligned}\dot{x}_9 = & f_E x_1 - f_N x_2 - (R\dot{l}(\dot{l} + 2w_{1e})\sin(2L))x_4 \\ & + (2w_E^2 + \dot{l}^2 + \dot{l}(\dot{l} + 2w_{1e})\cos^2(L))x_6 + 2R\dot{L}x_7 \\ & + (2R\dot{L}\cos^2(L))x_8\end{aligned}\quad (3-26)$$

For convenience, the state vector is transformed to a form in which errors along the navigation frame coordinates, in linear dimensions, are readily available. That is,

$$\underline{x}_C^T = [\epsilon_N \quad \epsilon_E \quad \epsilon_D \quad \delta P_{IN} \quad \delta P_{IE} \quad \delta P_{ID} \quad \delta V_{IN} \quad \delta V_{IE} \quad \delta V_{ID}] \quad (3-27)$$

where  $P_{I(.)}$  and  $V_{I(.)}$  are the INS position and velocity error components along the NED navigation coordinate axes. This transformation is performed by applying the following first-order approximations (Britting, 1971:97-98):

$$\delta P_{IN} = R\delta L \qquad \delta V_{IN} = R\dot{\delta L} \quad (3-28)$$

$$\delta P_{IE} = R \cos(L) \delta l \qquad \delta V_{IE} = R \cos(L) \dot{\delta l} \quad (3-29)$$

$$\delta P_{ID} = -\delta h \qquad \delta V_{ID} = -\dot{\delta h} \quad (3-30)$$

So,

$$\underline{x}_C = T \underline{x}_S \quad (3-31)$$

and

$$\dot{\underline{x}}_C = T F_S T^{-1} \underline{x}_C \quad (3-32)$$

where

$$T = \text{diag}(1, 1, 1, R, R \cos(L), -1, R, R \cos(L), -1) \quad (3-33)$$

and  $F_g$ , shown in Figure 3.5, is the system dynamics matrix obtained from Equations (3-18) through (3-26).

This results in the basic INS error dynamics model described by

$$\dot{\underline{x}}_c(t) = F_c(t) \underline{x}_c(t) + \underline{n}_1(t) \quad (3-34)$$

The instrument uncertainties,  $\underline{n}_1(t)$ , are directly expressed along the platform axes, thus further motivating the necessity of the transformation.

### 3.3.2 Complete INS Error Model.

3.3.2.1 Barometric altimeter. The basic model of Equation (3-34) requires, as a minimum, altitude aiding for stability purposes. A first-order Markov process describing the baro-altimeter error is augmented to the basic system equation such that

$$\delta \dot{h}_b = \dot{x}_{10} = -(1/\tau_h) x_{10} + w_{alt} \quad (3-35)$$

where  $\tau_h$  relates the correlation distance of weather patterns,  $d_{alt}$ , with the aircraft speed,  $s$ . That is,

$\dot{x}_1$	$\dot{x}_2$	$\dot{x}_3$	$\dot{x}_4$	$\dot{x}_5$	$\dot{x}_6$	$\dot{x}_7$	$\dot{x}_8$	$\dot{x}_9$
	$-\dot{\lambda} \sin L$	$\dot{L}$	$-\dot{\lambda} \sin L$					
$\dot{\lambda} \sin L$		$\dot{\lambda} \cos L$						
$-\dot{L}$	$-\dot{\lambda} \cos L$		$-\dot{\lambda} \cos L$					
	$-f_D/R$	$f_E/R$	$-i(i + 2\omega_e)\cos 2L$	$*F_{76}$	$-2\dot{h}/R$	$-\dot{\lambda} \sin 2L$	$-2\dot{L}/R$	
$f_D/R \cos L$		$-f_N/R \cos L$	$*F_{84}$	$*F_{86}$	$2\dot{\lambda} \tan L$	$*F_{88}$	$2(i + \omega_e)/R$	
$f_E$	$-f_N$		$-R[i(i + 2\omega_e)\sin 2L]$	$*F_{96}$	$2R\dot{L}$	$2R\dot{\lambda} \cos^2 L$		

Figure 3.5 9-State INS Error Dynamics Model

$$\tau_h = d_{alt}/s \quad (3-36)$$

The white driving noise,  $w_{alt}$ , has a strength of

$$Q_{alt} = 2\sigma_{alt}^2/\tau_h \quad (3-37)$$

where  $\sigma_{alt}^2$  is the standard deviation of the altitude of a constant pressure surface. The values used in this study are

$d_{alt} = 1.6 \times 10^6$  feet,  
and  $\sigma_{alt} = 500$  feet  
(Widnall and Grundy, 1973:123-126).

The measurement of the error in vertical position is formed as (Maybeck, 1979:309)

$$z_h(t_1) = \delta P_{ID}(t_1) - \delta h_b(t_1) + v(t_1) \quad (3-38)$$

The 10-state INS error model developed thus far is the minimum useful configuration for three-dimensional applications and represents the baseline INS error model. This results in the system matrix  $F_B$  as shown in Figure 3.6.

**3.3.2.2 Error Sources.** The INS error dynamics, Equation (3-34), is driven additionally by gyro and accelerometer errors. The gyro errors directly drive the

$$\mathbf{F}_B =$$

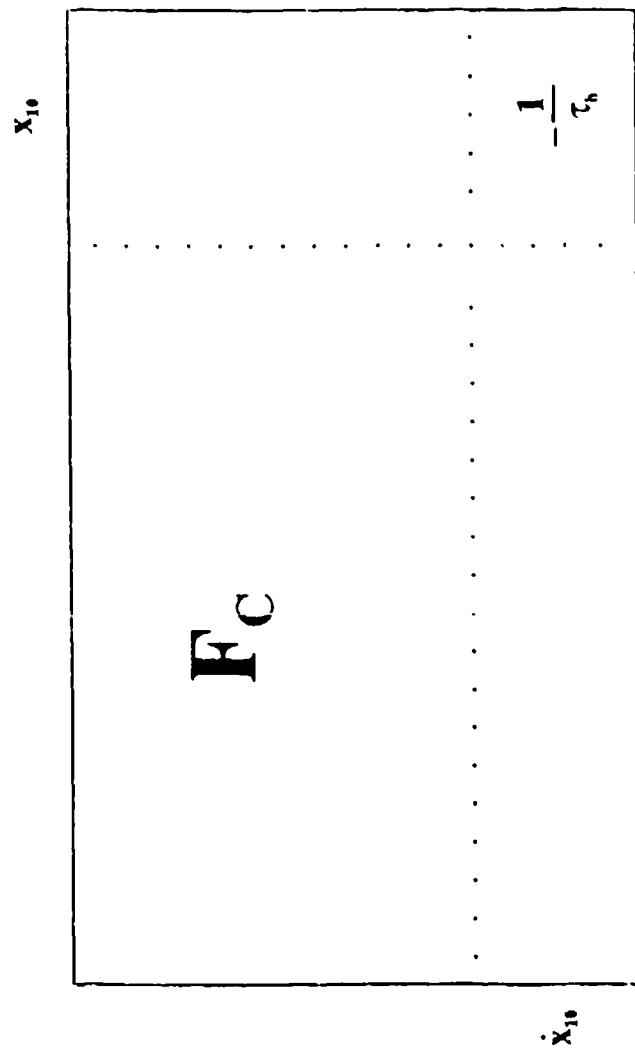


Figure 3.6 INS Error Dynamics Model with Altimeter Aiding

platform tilt equations and are modelled as a constant bias plus additional white noise. Refinements, such as slow variations of the bias, scale-factor and g-sensitivity errors, are possible but due to the slow coupling of these errors through the platform misalignments and the short duration of the aircraft maneuvers to be analyzed, are not included in the model. The bias states (gyro drifts), are augmented to the system equations as

$$\dot{D}_N = \dot{x}_{11} = 0 \quad \dot{D}_E = \dot{x}_{12} = 0 \quad \dot{D}_D = \dot{x}_{13} = 0 \quad (3-39)$$

where  $D_N$ ,  $D_E$ , and  $D_D$  represent the drift due to the north, east, and down gyros, respectively. The equations for  $\dot{x}_1$ ,  $\dot{x}_2$ , and  $\dot{x}_3$  are modified to reflect these new states. That is,

$$\begin{aligned} \dot{x}_1 &= \dot{x}_1(\text{previous}) + x_{11} \\ \dot{x}_2 &= \dot{x}_2(\text{previous}) + x_{12} \\ \dot{x}_3 &= \dot{x}_3(\text{previous}) + x_{13} \end{aligned} \quad (3-40)$$

(Widnall and Grundy, 1973:86-88)

The accelerometer errors are treated more accurately due to the direct nature in which they drive system errors during the short maneuver duration. The error model contains white noise plus two states for each accelerometer: bias,  $B$ , and scale factor,  $SF$ . Both are

modelled as random constants and augmented to the system equations

$$\begin{aligned}\dot{B}_N &= \dot{x}_{14} = 0 \\ \dot{B}_E &= \dot{x}_{15} = 0 \\ \dot{B}_D &= \dot{x}_{16} = 0 \\ \dot{SF}_N &= \dot{x}_{17} = 0 \\ \dot{SF}_E &= \dot{x}_{18} = 0 \\ \dot{SF}_D &= \dot{x}_{19} = 0\end{aligned}$$

The  $\delta\dot{V}$  equations are modified to reflect the inclusion of these new states. That is,

$$\begin{aligned}\dot{x}_7 &= \dot{x}_7(\text{previous}) + x_{14} + f_N x_{17} \\ \dot{x}_8 &= \dot{x}_8(\text{previous}) + x_{15} + f_E x_{18} \\ \dot{x}_9 &= \dot{x}_9(\text{previous}) + x_{16} + f_D x_{19}\end{aligned}\tag{3-41}$$

With the addition of the barometric altimeter error state and the 12 states associated with instrument errors, the complete INS error model is now described by

$$\dot{\underline{x}}_I(t) = F_I(t) \underline{x}_I(t) + \underline{w}_I(t)\tag{3-42}$$

where  $\underline{x}_I(t)$  is a 19-state vector. Equation (3-42) represents the complete INS error model and is shown in Figure 3.7.

$\epsilon$	$\delta P$	$\delta V$	$\delta h_b$	$D_N$	$D_E$	$D_D$	$B_N$	$B_E$	$B_D$	$SF_N$	$SF_E$	$SF_D$
$\epsilon_N$				1								
$\epsilon_E$					1							
$\epsilon_D$						1						
$\delta P_N$												
$\delta P_E$												
$\delta P_D$												
$\delta V_N$							1			$f_N$		
$\delta V_E$								1			$f_E$	
$\delta V_D$									1			$f_D$
$\delta h_b$												
$\underline{D}$												
$\underline{B}$												
$\underline{SF}$												

$F_B$

Figure 3.7 Complete (19-State) INS Error Dynamics Model

### 3.4 GPS Receiver Error Model

The basic structure of the GPS receiver error model contains 12 states defined as

$$\begin{aligned} \mathbf{x}_{BG}^T = & (\delta P_{GN} \ \delta P_{GE} \ \delta P_{GD} \ \delta V_{GN} \ \delta V_{GE} \ \delta V_{GD} \\ & \delta A_{GN} \ \delta A_{GE} \ \delta A_{GD} \ \delta h_b \ b \ d) \end{aligned} \quad (3-43)$$

where

$\delta P_{G(.)}$  is the GPS-derived position error vector component

$\delta V_{G(.)}$  is the GPS-derived velocity error vector component

$\delta A_{G(.)}$  is the GPS-derived acceleration error vector component

$\delta h_b$  is the barometric altimeter error

$b$  is the range error due to user clock bias

$d$  is the range-rate error due to user clock drift

The dynamics equations associated with these states are

$$\begin{aligned} \dot{x}_1 &= x_{1+3} & i=1,2,3,4,5,6 \\ \dot{x}_j &= 0 & j=7,8,9 \\ \dot{x}_{10} &= -(1/T_h) x_{10} + w_h \\ \dot{x}_{11} &= x_{12} \\ \dot{x}_{12} &= 0 \end{aligned} \quad (3-44)$$

Equations (3-44) represent the baseline 12-state GPS receiver error model dynamics. The dynamics matrix,  $F_{BG}$ , is shown in Figure 3.8.

**3.4.1 Measurement Model.** Five measurements are available to the GPS receiver: pseudorange measurements to four satellites, as discussed in Chapter 2, and a barometric altimeter measurement. The error in the vertical position measurement is identical to the development for the INS error model. The error vector in the pseudorange measurement,  $\delta PR$ , is composed of several error sources:

$$\delta PR = U_{LOS} \delta p + bI + \delta r_x + \delta r_c + v_{PR} \quad (3-45)$$

where  $U_{LOS}$  is a matrix of four unit line-of-sight row vectors,  $u_{LOS}$ , (one to each satellite) expressed with respect to the NED navigation coordinate frame,  $I$  is the appropriately dimensioned identity matrix,  $\delta r_x$  is the error vector due to uncompensated atmospheric path delays, and  $\delta r_c$  is the vector of errors committed by the code-tracking loop (Lewantowicz, 1986). For the purposes of this study, each  $\delta r_x$  is modelled as a constant bias and a second-order code-tracking loop is considered because it performs better than the low-pass filtering of a first-order model. These models are augmented to the basic system dynamics model such that

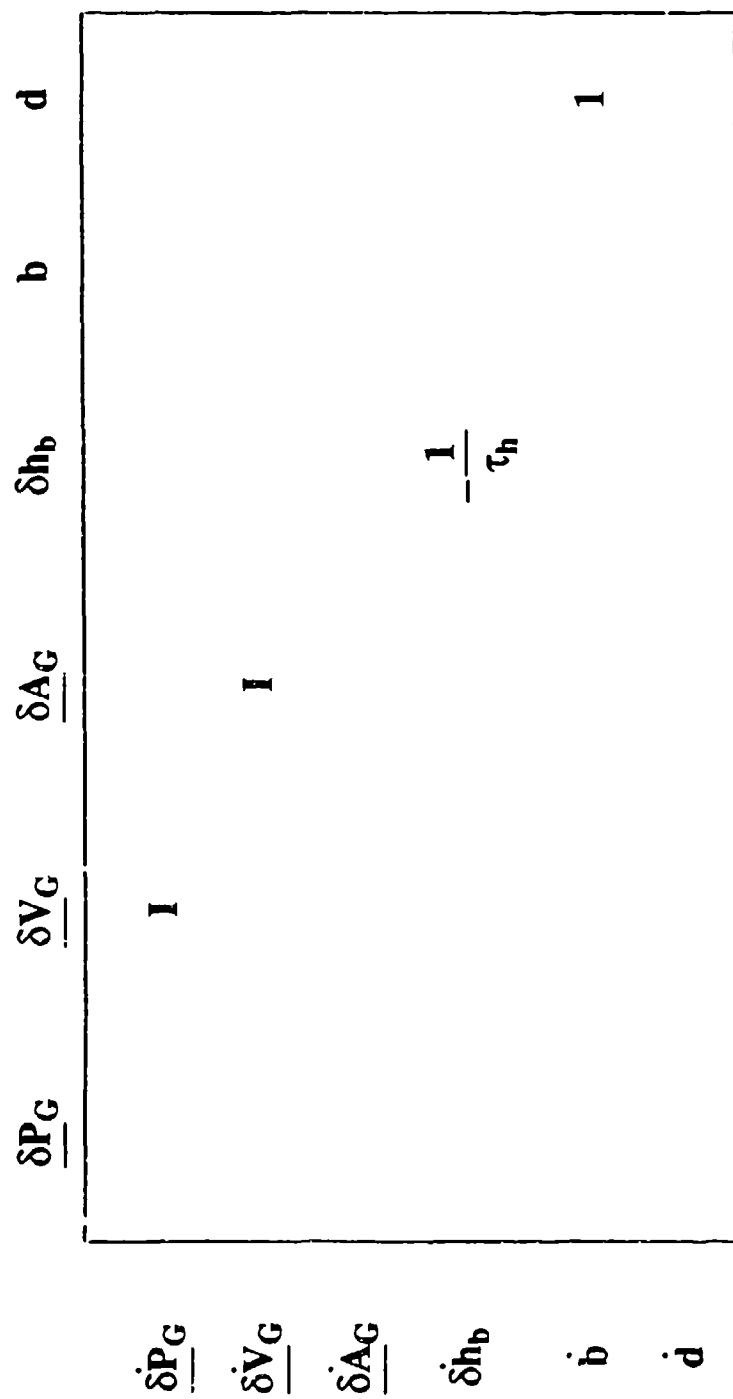


Figure 3.8 12-State GPS Receiver Error Dynamics Model

$$\delta \dot{\underline{r}}_{1x} = \dot{\underline{x}}_{(1+12)} = \underline{0} \quad i=1,2,3,4 \quad (3-46)$$

with the four second-order code-tracking loops contributing an additional eight states.

3.4.2 Code-tracking Loop. A second-order code-tracking loop error model is shown in Figure 3.9. The equations describing this loop are (Widnall, 1978:13)

$$\delta \dot{\underline{r}}_c = \underline{v}_r + \underline{a}_r(\delta \underline{r}_x + b - \delta \underline{r}_c) - \delta \underline{v}_{aid} + \underline{w}_n \quad (3-47)$$

$$\dot{\underline{v}}_r = \underline{a}_r \underline{a}_v(\delta \underline{r}_x + b - \delta \underline{r}_c) + \underline{a}_v \underline{w}_n \quad (3-48)$$

where

$\underline{v}_r$  is an internally generated variable

$\underline{a}_r$  and  $\underline{a}_v$  are constant, predetermined gains

$\delta \underline{v}_{aid}$  is the error in the externally-supplied aiding velocity, and

$\underline{w}_n$  is the white-driving noise.

For this study, a single-sided bandwidth,  $B_L$ , of 1 Hz and a damping ratio of 0.7071 is modelled. Using the relationship (Widnall, 1978:12)

$$B_L = (\underline{a}_r + \underline{a}_v)/4 \quad (3-49)$$

results in  $\underline{a}_r = 2.666 \text{ sec}^{-1}$  and  $\underline{a}_v = 1.333 \text{ sec}^{-1}$ . The poles of this system lie at  $-1.333 \pm j1.333$  in the complex s-plane. In actuality, the bandwidth of the loop varies

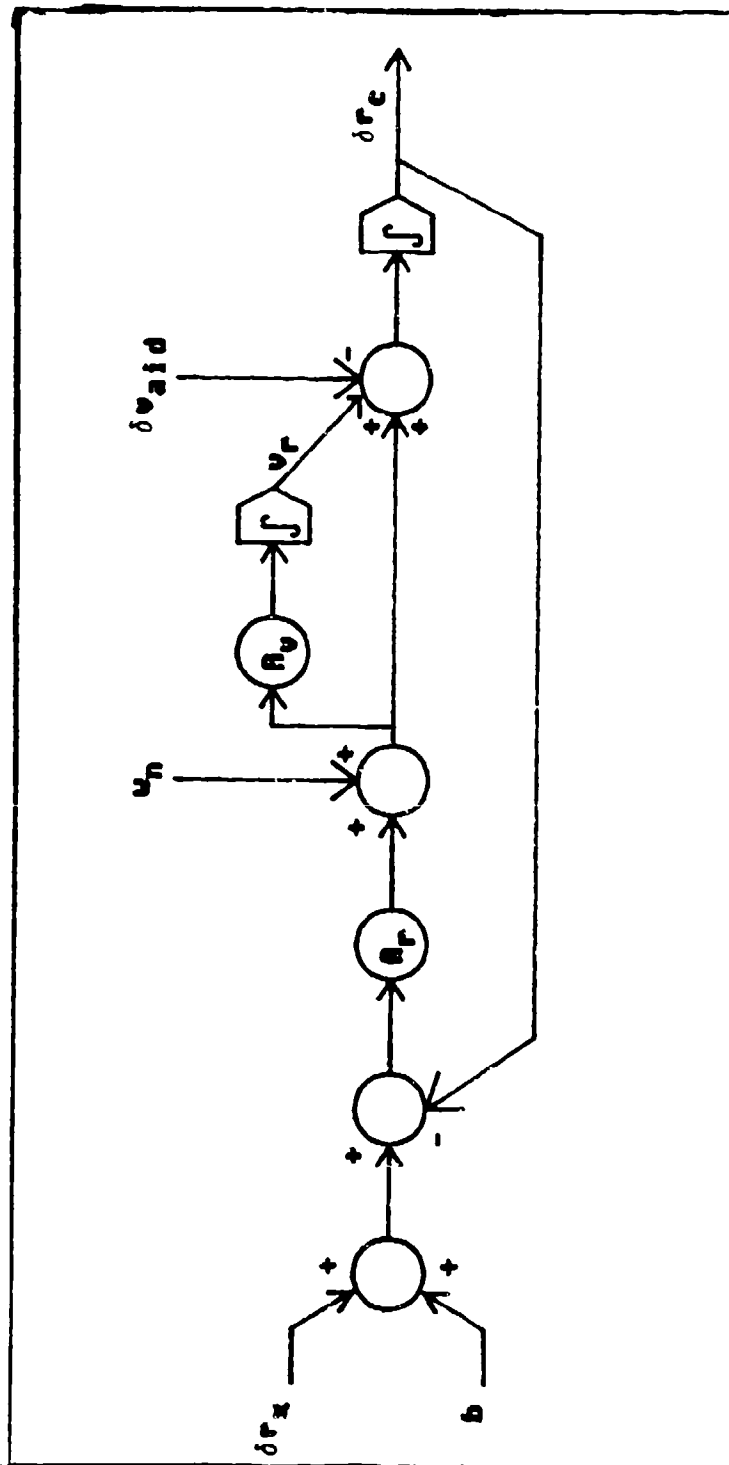


Figure 3.9. GPS Receiver Code Tracking Loop  
(Widnall, 1978:13)

with vehicle dynamics and signal-to-noise ratio of the received PRC.

These two additional states for each channel are augmented to the basic GPS receiver error dynamics model to arrive at the complete dynamic description

$$\dot{\underline{x}}_G = \underline{F}_G \underline{x}_G + \underline{w}_G \quad (3-50)$$

as shown in Figure 3.10.

### 3.5 Truth Model

The truth model is derived by combining common states in the total INS model and the total GPS receiver model, and augmenting the two systems together. Thus, only one position error vector and one velocity error vector is included in the truth model resulting in a 36-state error model described by

$$\underline{x}_t^T = [\underline{\epsilon}^T \delta \underline{p}^T \delta \underline{v}^T \delta h_b \quad \underline{d}^T \underline{B}^T \underline{S} \underline{F}^T \delta \underline{A}^T \delta \underline{x}_x^T \delta \underline{x}_c^T \underline{v}_x^T] \quad (3-51)$$

The dynamics matrix,  $\underline{F}_t$ , relating these states is formed as

$$\underline{F}_t = \begin{bmatrix} \underline{F}_I & \underline{F}_{UR} \\ \text{---} & \text{---} \\ \underline{F}_{LL} & \underline{F}_{PG} \end{bmatrix} \quad (3-52)$$

	$\underline{b}$	$\underline{d}$	$\underline{\delta r_x}$	$\underline{\delta r_c}$	$\underline{V_r}$
$\underline{\dot{\delta r_x}}$	$\mathbf{F_{BG}}$				
$\underline{\dot{\delta r_c}}$			$\mathbf{a_r I}$	$\mathbf{-a_r I}$	$\mathbf{I}$
$\underline{\dot{V}}$		$\mathbf{a_r a_v}$	$\mathbf{a_r a_v I}$	$\mathbf{-a_r a_v I}$	

Figure 3.10 Complete (24-State) GPS Receiver Error Dynamics Model

where  $F_I$  is identically the INS error dynamics matrix,  $F_{PG}$  is the portion of  $F_G$  relating the last 17 states of the truth model (excludes the duplicated position, velocity, and altimeter error states),  $F_{UR}$  adds the terms  $\delta \dot{\underline{V}} = \delta \underline{A}$  due to the acceleration error modelled within the GPS receiver, and  $F_{LL}$  adds the terms due to the error in the velocity aiding signal to the code-tracking loop. That is,

$$\delta \underline{v}_{aid} = -U_{LOS} \delta \underline{v} \quad (3-53)$$

where the four vectors of  $U_{LOS}$  and  $\delta \underline{v}$  are all expressed with respect to the NED navigation coordinate frame. The truth model is shown in Figure 3.11. Note that the truth model dynamics matrix contains the velocity aiding error signals. As will be seen in the next section, this term is not available directly to the completely modelled, but separate, GPS receiver Kalman filters, thus requiring it to be treated as an additional driving noise. Further note that when the basic GPS receiver Kalman filter is used, all code-loop tracking information is lost. This is because the code-loop is not modelled within the baseline GPS receiver error model.

### 3.6 System Integration

Examination of Figure 3.11 reveals the error in the velocity aiding provided to the GPS receiver code tracking

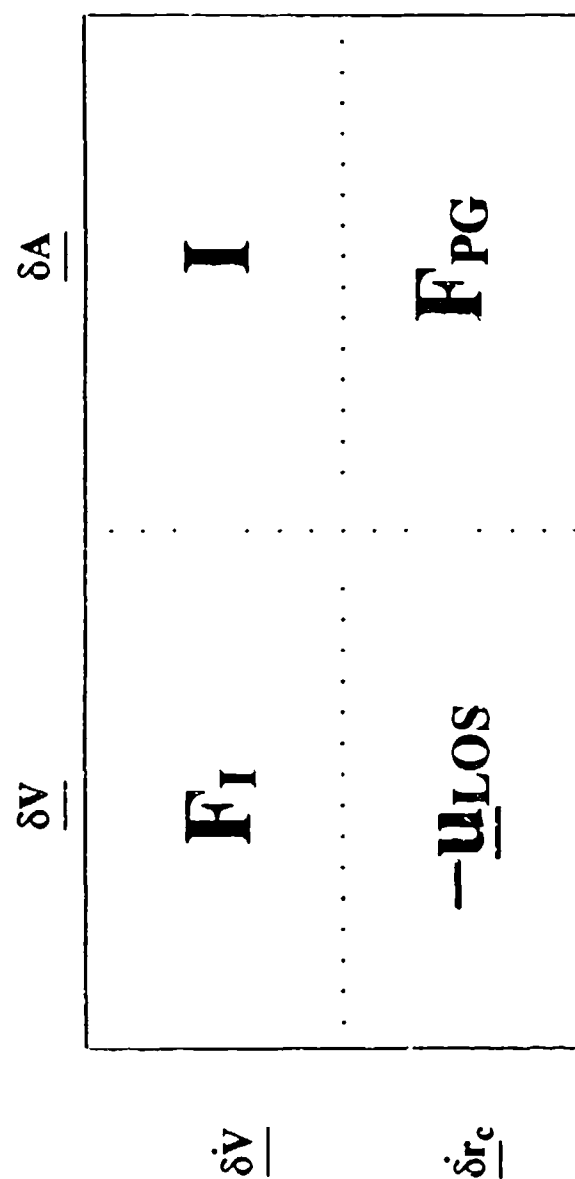


Figure 3.11 Truth Model Error Dynamics Model

loop error equations is modelled directly within the dynamics equations ( $P_{LL}$  from equation 3-48). When the INS Kalman filter and GPS receiver Kalman filter are separated, this direct relationship is no longer available.

Neglecting time correlation, the best information the GPS receiver Kalman filter has available to simulate the INS velocity aiding error is if the  $\delta v_{aid}$  of equation (3-47) is treated as additional white driving noise on the code-tracking loop. This is necessary because the GPS receiver error model does not simulate the dynamics of the INS mechanization. Therefore, it cannot estimate the time-correlated nature of the INS information. These two interacting models are referred to as the two-filter full-state system.

When the baseline Kalman filters, representative of the currently integrated system, of Figures 3.6 and 3.8 interact, the code loop error equations are not modelled within the GPS receiver error dynamics. Thus, no indication of INS aiding to the loop is possible. This represents a loss of all time and spatial correlation between the two filters in closed-loop operation.

The above situations are examined by means of performance analyses for the following systems: the 36-state (joint-solution) Kalman filter based upon the truth model; the two-filter full-state system, which models the interacting 19-state INS Kalman filter and 24-state GPS

receiver Kalman filter; and the baseline system, which includes the basic 10-state INS Kalman filter and 12-state GPS receiver Kalman filter. For the latter two suboptimal systems, the INS error Kalman filter receives position and velocity error estimates from the GPS receiver Kalman filter as measurements.

### 3.7 Performance Analysis

This section develops the thought process and algorithm considerations in order to analyze the performance of the three systems listed previously: the optimal Kalman filter, the two-filter full-state system, and the baseline system. First, a basic description of a general performance analysis is presented. Then, the specific application to each of the three systems is developed.

#### 3.7.1 General Description (Maybeck, 1979:325-337).

In general, a performance analysis is conducted as shown in Figure 3.12. First, a truth model is developed depicting all that is known about the real world. For this study, the truth model is as given in Figure 3.11. Candidate Kalman filters, based upon the truth model, are then hypothesized. Finally, within the framework of the performance analysis, the Kalman filter performance is compared against the truth model to test for adequate operation for a specific application.

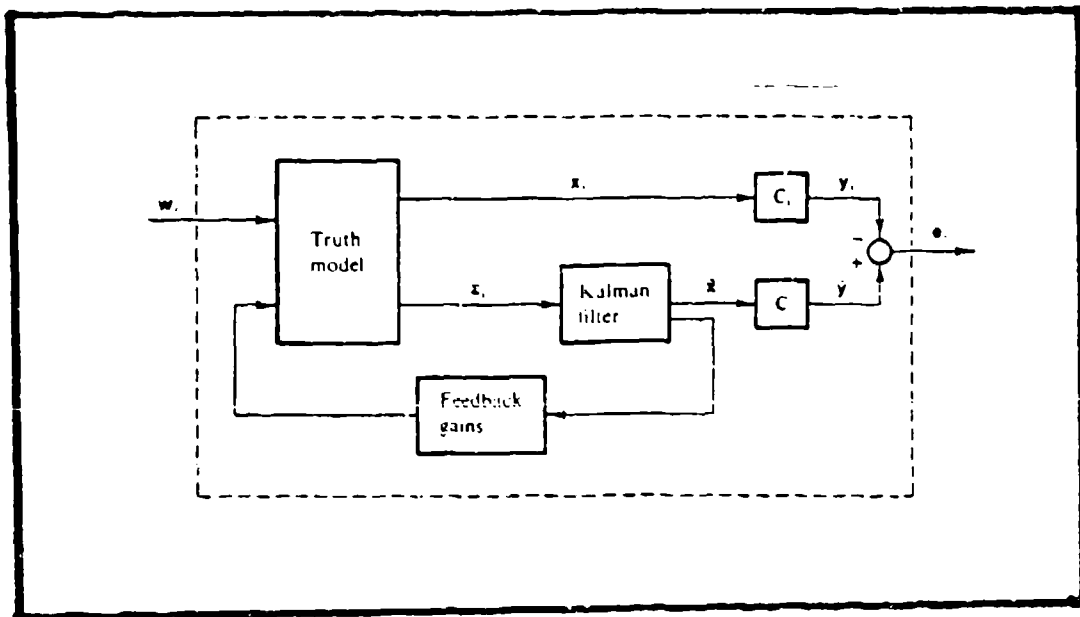


**Figure 3.12. Performance Evaluation of  
Kalman Filter Designs (Maybeck, 1979:327)**

To illustrate the method of this evaluation, consider Figure 3.12. The truth model is a mathematical description of all available modelled states. Dynamic driving noise enters the truth model, usually as a result of shaping filter augmentation. In addition, models of the measurements and white instrument noise are described within the truth model structure. From the truth model, true state values,  $\underline{x}_t$ , and measurement realizations,  $\underline{z}_t$ , are available as outputs. The Kalman filter receives the truth model measurements and, by means of the previously described estimator equations, produces its best estimate of the states,  $\hat{\underline{x}}$ , which it models. The true states of interest,  $\underline{y}_t$ , are then compared to the Kalman filter estimates of those states,  $\hat{\underline{y}}$ , to arrive at the true error committed by the Kalman filter. Finally, the feedback gains allow the truth model to account for any commanded controls being applied to the system. In many cases, as with this study, the applied control is modelled as an impulsive reset to the states which are controlled.

Consider a truth model described by

$$\dot{\underline{x}}_t(t) = F_t(t) \underline{x}_t(t) + \underline{w}_t(t) \quad (3-53)$$

$$\underline{z}_t(t_1) = H_t(t_1) \underline{x}_t(t_1) + \underline{v}_t(t_1) \quad (3-54)$$

and a Kalman filter, based upon a design model described by

$$\dot{\hat{\underline{x}}}(t) = F(t) \hat{\underline{x}}(t) + \underline{w}(t) \quad (3-55)$$

$$\underline{z}(t_1) = H(t_1) \hat{\underline{x}}(t_1) + \underline{v}(t_1) \quad (3-56)$$

where all the previous variable descriptions apply.

Since the block of Figure 3.12 is a system driven only by white noise, the models from Equations (3-53) and (3-55) can be augmented together resulting in a system described by

$$\dot{\underline{x}}_a(t) = F_a(t) \underline{x}_a(t) + \underline{w}_a(t) \quad (3-57)$$

or, in its equivalent discrete-time representation

$$\underline{x}_a(t_1^-) = \phi_a(t_1, t_{1-1}) \underline{x}_a(t_{1-1}^+) + \underline{w}_{da}(t_1) \quad (3-58)$$

where  $\underline{x}_a(\cdot)$  is the augmented state vector with partitions such that

$$\underline{x}_a = \begin{bmatrix} \underline{x}_t \\ \vdots \\ \hat{\underline{x}} \end{bmatrix} \quad (3-59)$$

$F_a(t)$  is the augmented system dynamics matrix with

partitions such that

$$F_a = \begin{bmatrix} F_t & 0 \\ 0 & F \end{bmatrix} \quad (3-60)$$

and

$$\underline{v}_a = \begin{bmatrix} \underline{v}_t \\ 0 \end{bmatrix} \quad (3-61)$$

with associated noise strength

$$Q_a = \begin{bmatrix} Q_t & 0 \\ 0 & 0 \end{bmatrix} \quad (3-62)$$

The measurement update relations are developed by considering the truth model states and the Kalman filter states separately. The truth model states do not change as a result of the Kalman filter taking a measurement. That is, the truth model states obey the dynamic description of the real world. So,

$$\underline{x}_t(t_1^+) = \underline{x}_t(t_1^-) \quad (3-63)$$

But, the Kalman filter is updated as a result of the

measurement. Similar to Equation (3-15)

$$\hat{\underline{x}}(t_1^+) = (I - K(t_1)H(t_1))\hat{\underline{x}}(t_1^-) + K(t_1)\underline{z}_t(t_1) \quad (3-64)$$

where the measurement,  $\underline{z}_t(t_1)$ , is derived from the truth model. Substituting Equation (3-54) into Equation (3-64) yields

$$\begin{aligned} \hat{\underline{x}}(t_1^+) = (I - K(t_1)H(t_1))\hat{\underline{x}}(t_1^-) + K(t_1)H_t(t_1)\underline{x}_t(t_1) \\ + K(t_1)\underline{v}_t(t_1) \end{aligned} \quad (3-65)$$

From Equations (3-63) and (3-65), an augmented description of this update is written such that

$$\underline{x}_a(t_1^+) = \Lambda_a(t_1)\underline{x}_a(t_1^-) + K_a(t_1)\underline{v}_t(t_1) \quad (3-66)$$

where

$$\Lambda_a(t_1) = \begin{bmatrix} I & 0 \\ \hline K(t_1)H_t(t_1) & I - K(t_1)H(t_1) \end{bmatrix} \quad (3-67)$$

and

$$K_a(t_1) = \begin{bmatrix} 0 \\ \hline K(t_1) \end{bmatrix} \quad (3-68)$$

$K(t_1)$  in the above equations results from the Kalman filter calculated gain as given by Equation (3-14). The second-order statistics of this augmented system are calculated, using the discrete-time representation, as

$$P_a(t_1^-) = \Phi_a(t_1, t_{1-1}) P_a(t_1^+) \Phi_a^T(t_1, t_{1-1}) + Q_{da}(t_{1-1}) \quad (3-69)$$

$$P_a(t_1^+) = A_a(t_1) P_a(t_1^-) A_a^T(t_1) + K_a(t_1) R_t(t_1) K_a^T(t_1) \quad (3-70)$$

Impulsive controls applied to the system are treated as follows

$$\underline{x}_a(t_1^{+C}) = D_a(t_1) \underline{x}_a(t_1^+) \quad (3-71)$$

$$P_a(t_1^{+C}) = D_a(t_1) P_a(t_1^+) D_a(t_1) \quad (3-72)$$

where

$$D_a(t_1) = \begin{bmatrix} I & -D_t(t_1) \\ 0 & I - D(t_1) \end{bmatrix} \quad (3-73)$$

$D_t(t_1)$  informs the truth model about impulsive resets applied to the system at discrete times, and  $D(t_1)$  similarly informs the Kalman filter of such resets. The

"+c" superscript indicates the time immediately following the measurement update ("+") and the reset command ("c").

The states of interest are obtained from the truth model and Kalman filter through the  $C_t$  and  $C$  matrices of Figure 3.12, respectively. The variance of these states of interest are calculated as

$$P_e(t) = C_a P_a(t) C_a^T \quad (3-74)$$

where

$$C_a = [-C_t \quad C] \quad (3-75)$$

The presented algorithm forms the basis of the performance analysis comparing the optimal Kalman filter, the two-filter full-state system, and the baseline system.

**3.7.2 Joint-solution Kalman Filter.** The development of the performance analysis for the joint-solution Kalman filter directly follows the development of the previous section. In this case, the truth model and the joint-solution Kalman filter possess the same state dynamics. For gain calculations, the joint-solution Kalman filter starts at the same initial conditions as the truth model. In addition, the modelled dynamics noise within the Kalman filter structure are identical to those driving the truth model. The performance of the joint-solution Kalman filter represents the best possible estimator solution.

3.7.3 Two-Filter Systems. Analysis of the two-filter full-state system and baseline system requires an extension to the performance algorithm since three models are represented simultaneously: the truth model, the GPS receiver Kalman filter, and the INS Kalman filter. In addition, the INS now has position and velocity estimates available as measurements from the GPS receiver Kalman filter. Finally, the INS Kalman filter provides velocity estimates to the GPS receiver to command the code-tracking loop in an attempt to remove doppler-induced tracking errors. This velocity aiding signal drives the GPS code loop and the INS estimation errors of the velocity become the driving noise to the GPS code loop dynamics. The full-state system is first developed. Then, the modification necessary when considering the baseline system is explained.

3.7.3.1 Full-State System. In the development of the performance analysis for the two-filter full-state system, recognize that the INS Kalman filter solution is available at a much higher rate than the GPS receiver Kalman filter solution. In typical applications, the INS Kalman filter produces a propagated state estimate at a 40 Hz rate, while the GPS receiver and INS Kalman filters perform measurement updates at a 1 Hz rate (Lewantowicz, 1987). Therefore, it is assumed the GPS receiver Kalman filter has processed its updated solution prior to

correcting for INS position and velocity errors so that the INS receives full benefit of the GPS aiding. For analysis purposes, this processing is assumed to occur instantaneously, whereas, typically, proper time tags of the information are necessary.

Consider an augmented system composed of the truth model states, the GPS receiver Kalman filter states and the INS Kalman filter states partitioned as

$$\underline{x}_a = \begin{bmatrix} \underline{x}_t \\ \underline{x}_G \\ \underline{x}_I \end{bmatrix} \quad (3-76)$$

The propagation relation of the augmented system is

$$\underline{x}_a(t_1^-) = \phi_a(t_1, t_{1-1}) \underline{x}_a(t_{1-1}) + \underline{w}_{da}(t_1) \quad (3-77)$$

where

$$\phi_a(t_1, t_{1-1}) = \begin{bmatrix} \phi_t(t_1, t_{1-1}) & 0 & 0 \\ 0 & \phi_G(t_1, t_{1-1}) & 0 \\ 0 & 0 & \phi_I(t_1, t_{1-1}) \end{bmatrix} \quad (3-78)$$

and

$$\underline{w}_{da}(t_1) = \begin{bmatrix} \underline{w}_{dt}(t_1) \\ \underline{0} \\ \underline{0} \end{bmatrix} \quad (3-79)$$

At time  $t_1^+$ , the GPS receiver Kalman filter processes its pseudorange and altimeter measurements, resulting in an updated state estimate. Thus,

$$\begin{aligned} \underline{x}_t(t_1^+) &= \underline{x}_t(t_1^-) \\ \hat{\underline{x}}_G(t_1^+) &= (I - K_G H_G) \hat{\underline{x}}_G(t_1^-) + K_G H_t \underline{x}_t(t_1^-) + K_G \underline{v}_t(t_1) \\ \hat{\underline{x}}_I(t_1^+) &= \hat{\underline{x}}_I(t_1^-) \end{aligned} \quad (3-80)$$

where the  $t$ ,  $G$ , and  $I$  subscripts refer to the truth model, the GPS receiver Kalman filter, and the INS Kalman filter, respectively. Rewriting Equations (3-80) in matrix form yields

$$\underline{x}_a(t_1^+) = \underline{A}_{a1}(t_1) \underline{x}_a(t_1^-) + \underline{K}_{a1}(t_1) \underline{v}_t(t_1) \quad (3-81)$$

where

$$\underline{A}_{a1}(t_1) = \begin{bmatrix} I & 0 & 0 \\ K_G H_t & I - K_G H_G & 0 \\ 0 & 0 & I \end{bmatrix} \quad (3-82)$$

and

$$K_{al}(t_i) = \begin{bmatrix} 0 \\ K_G \\ 0 \end{bmatrix} \quad (3-83)$$

After the GPS receiver Kalman filter solution is available, the INS Kalman filter is updated using the altimeter measurement and the GPS Kalman filter position and velocity error estimates. But, the additional position and velocity error measurements are not available from the truth model, only the altimeter measurement. However, referring to Figure 3.13, the error committed by the GPS receiver Kalman filter,  $e_G$ , is the true error and represents the true measurement. Therefore, these values are input to the INS Kalman filter as the true measurements which are processed. Defining this update time as  $t_1^{++}$ , yields

$$\begin{aligned} \underline{x}_t(t_1^{++}) &= \underline{x}_t(t_1^+) \\ \hat{\underline{x}}_G(t_1^{++}) &= \hat{\underline{x}}_G(t_1^+) \\ \hat{\underline{x}}_I(t_1^{++}) &= (I - K_I H_I) \hat{\underline{x}}_I(t_1^+) + K_I \underline{z}_{tI} \end{aligned} \quad (3-84)$$

The vector of measurements,  $\underline{z}_{tI}$ , contains partitions of the altimeter measurement and  $e_G$ . The altimeter measurement must come from the truth model such that

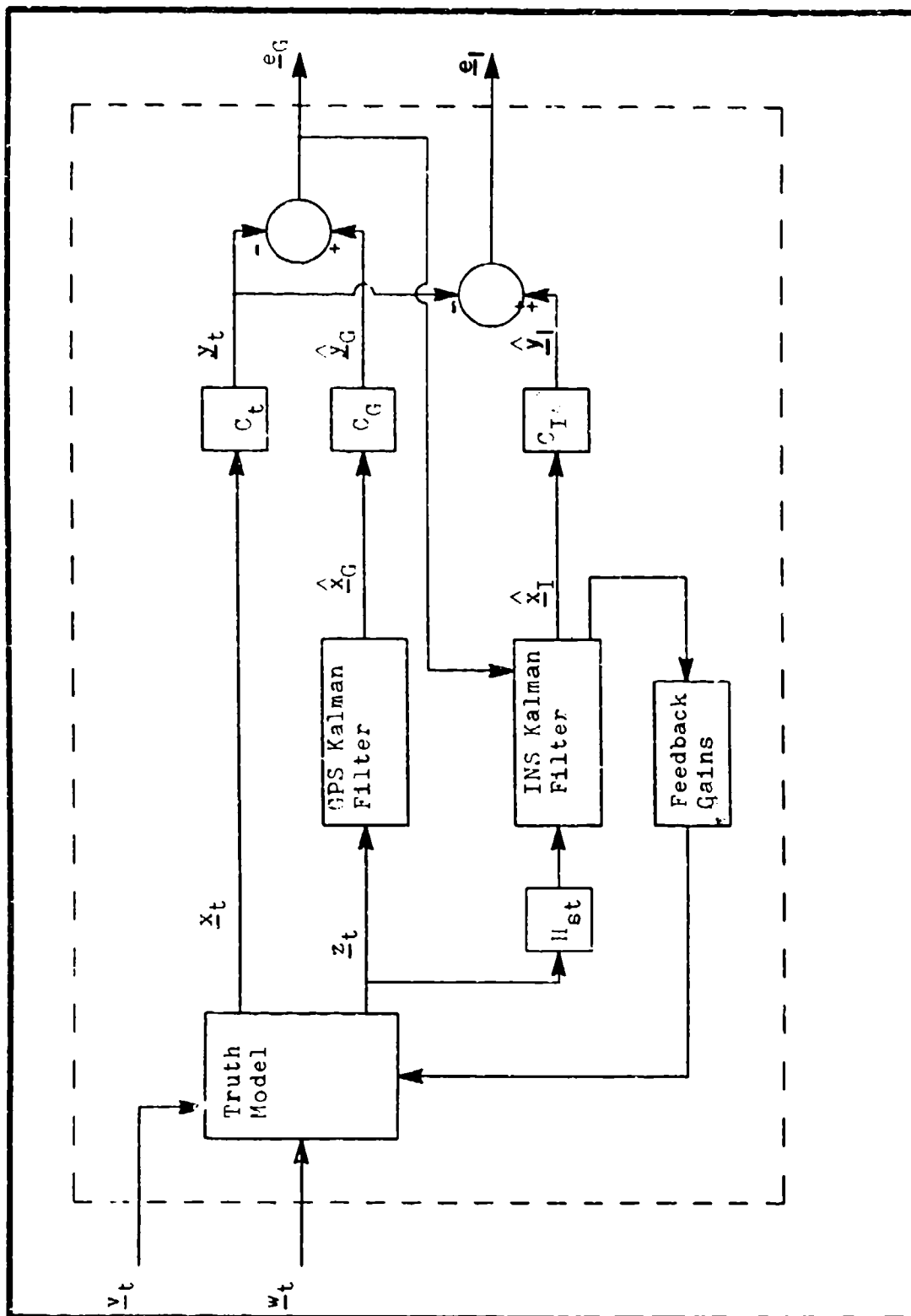


Figure 3.13. Performance Evaluation  
of the Two-Filter Systems

$$z_h = H_{st} z_t = H_{st} [H_t x_t(t_1^+) + v_t]$$

and, as seen from Figure 3.13,

$$e_G = \hat{y}_G - y_t = C_G \hat{x}_G(t_1^+) - C_t x_t(t_1^+)$$

Using these expressions, the INS update of Equation (3-84) is rewritten

$$\hat{x}_I(t_1^{++}) = [I - K_I H_I] \hat{x}_I(t_1^+) + K_I H_{st} \begin{bmatrix} H_t x_t(t_1^+) + v_t \\ C_G \hat{x}_G(t_1^+) - C_t x_t(t_1^+) \end{bmatrix}$$

This is equivalently written as

$$\begin{aligned} \hat{x}_I(t_1^{++}) = & K_I (H_{It} H_{st} H_t - H_{IG} C_t) x_t(t_1^+) + K_I H_{IG} C_G \hat{x}_G(t_1^+) \\ & + [I - K_I H_I] \hat{x}_I(t_1^+) + K_I H_{It} H_{st} v_t \end{aligned}$$

where

$C_t$  and  $C_G$  extract the position and velocity error vectors from the truth model and GPS receiver Kalman filter, respectively

$H_{st}$  extracts the altimeter measurement from the set of measurements output by the truth model, and

$H_{It}$  and  $H_{IG}$  applies the appropriate subset of the INS Kalman filter gain matrix,  $K_I$ , to the measurements.

From the relations in Equations (3-80) and (3-84), the complete update cycle is defined

$$\underline{x}_a(t_1^{++}) = A_{a2}A_{a1}\underline{x}_a(t_1^-) + (A_{a2}K_{a1} + K_{a2})\underline{v}_t(t_1) \quad (3-85)$$

where  $A_{a2}$  and  $K_{a2}$ , taken from Equations (3-84), are defined as

$$A_{a2} = \begin{bmatrix} I & 0 & 0 \\ 0 & I & 0 \\ K_I(H_{It}H_{st}H_t & K_IH_{IG}C_G & I - K_IH_I \\ -H_{IG}C_t) \end{bmatrix} \quad (3-86)$$

and

$$K_{a2} = \begin{bmatrix} 0 \\ 0 \\ K_IH_{It}H_{st} \end{bmatrix} \quad (3-87)$$

If  $A_a$  is defined as  $A_{a2}A_{a1}$  and  $K_a$  is defined as  $(A_{a2}K_{a1} + K_{a2})$ , then the covariance matrix update is calculated using Equation (3-70).

Still to be considered is the velocity aiding to the GPS receiver code-tracking loop. As an approximation to the 40 Hz rate of the INS Kalman filter propagated estimate, the time interval between  $t_1$  and  $t_{1+1}$  is divided

into  $k$  subintervals,  $\Delta t_k$ , where  $\Delta t_k = (t_{i+1} - t_i)/k$ . The control is applied impulsively each  $\Delta t_k$  using the propagated INS Kalman filter velocity error estimate available at that time. From this relationship, the reset commands are

$$\begin{aligned}\underline{x}_t(t_k^{-c}) &= \underline{x}_t(t_k^{+c}) = \underline{x}_t(t_k^-) - D_t \hat{\underline{x}}_I(t_k^-) \\ \underline{x}_G(t_k^{-c}) &= \underline{x}_G(t_k^{+c}) = \underline{\ddot{x}}_G(t_k^-) - D \hat{\underline{x}}_I(t_k^-) \\ \hat{\underline{x}}_I(t_k^{-c}) &= \hat{\underline{x}}_I(t_k^{+c}) = \hat{\underline{x}}_I(t_k^-)\end{aligned}\tag{3-88}$$

where

$$\underline{x}_a(t_k^-) = \phi_a(t_k, t_{k-1}) \underline{x}_a(t_{k-1}^{+c}) + \underline{w}_{da}(t_k)\tag{3-89}$$

and  $D_t$  and  $D$  transform the velocity errors expressed in the NED navigation coordinate frame to velocity errors along each line-of-sight vector in order to simulate the control applied to the code-tracking loop within the truth model and the GPS receiver Kalman filter, respectively. At time  $t_{i+1}$ , after  $k$  reset commands, the GPS receiver Kalman filter processes its measurements before the INS errors are corrected.

The GPS receiver Kalman filter should be told that the velocity aiding signal is not perfect. Within the truth model, the relationship between the code-loop tracking error and the velocity aiding error is modelled directly.

The GPS receiver Kalman filter, on the other hand, does not model the INS velocity error. Therefore, this direct relationship is not possible. But, it can be told that its code-loop tracking model is degraded due to the error in the INS velocity estimate. One way to help the GPS receiver Kalman filter is to add pseudonoise to the code-loop channels. Neglecting time-correlatedness, this is accomplished by transforming the INS velocity covariance to velocity covariance along the line-of-sight vectors and adding it as driving noise on the code-loop dynamics. Thus,  $\delta \underline{v}_{aid}$  is treated, within the GPS receiver Kalman filter, as a white noise with associated strength

$$(\underline{Q}_{aid})_c = \underline{U}_{LOS} \delta \underline{v}_{aid} \delta \underline{v}_{aid}^T \underline{U}_{LOS} \quad (3-90)$$

where  $(\underline{Q}_{aid})_c$  is the noise strength added to the code-loop model.

**3.7.3.2 Baseline System.** The baseline system, which contains the interacting 10-state INS Kalman filter and 12-state GPS receiver Kalman filter, is treated identically as the full-order system, conceptually. However, a major shortcoming exists: the 12-state GPS receiver Kalman filter does not contain a model of the code-loop dynamics. Therefore, in the context of the previous section, the D matrix of Equation (3-88) is a matrix of zeros and  $(\underline{Q}_{aid})_c$  cannot be incorporated to benefit the GPS receiver Kalman filter at all.

### 3.8 Closing Remarks

Chapter III presents the fundamental concepts which lead to a performance analysis. The truth model, as well as the joint-solution system, the full-state system, and the baseline system are presented. The next chapter applies these concepts to obtain covariance analysis results for a given system model and trajectory.

#### IV. Results

Analysis of the GPS-aided INS systems, described previously, requires a simulated trajectory about which the INS portion of the truth model is linearized. Four trajectories are explored as possible candidates, and are described in this chapter. The results of several performance analysis simulations are presented. The analysis is performed for static conditions, that is, the vehicle is motionless with respect to earth; for constant east velocity; and for a constant 9g acceleration turn. The systems compared include the complete (19-state) INS Kalman filter, the complete (24-state) GPS Kalman filter, the INS and GPS joint-solution Kalman filter, the two-filter full-state GPS and full-state INS system, and the baseline two-filter system (10 INS states and 12 GPS receiver states.)

##### 4.1 Trajectory Candidates

The truth model and INS Kalman filter require dynamics relinearization so the linear system assumptions of the estimator equations and performance analysis, as presented, are not violated. Examination of Equations (3-18), (3-19), (3-20), and (3-41) reveals the following parameters require relinearization:  $L$ ,  $R$ ,  $\dot{\lambda}$ ,  $\dot{L}$ ,  $\dot{i}$ ,  $\dot{h}$ ,  $\ddot{L}$ ,  $\ddot{i}$ ,  $f_N$ ,  $f_E$ , and  $f_D$ .

These values are calculated each  $\Delta t$  seconds from an assumed disturbance-free trajectory, and inserted into the equations referenced above. As an approximation, the computed elements of the dynamics matrices are held constant until the next set of parameters is available. A Kalman filter which is relinearized in this manner is commonly called an extended Kalman filter.

Four constant acceleration turns are examined. In all cases, the latitude is chosen at  $45^\circ\text{N}$  and an altitude,  $h$ , of 20,000 feet. Thus, using the earth's radius,  $R_e$ , of 20,926,435.2 feet,  $R$  is calculated as

$$R = R_e + h = 20,946,435.2 \text{ ft}$$

The value of earth's rotation rate is approximately  $7.2722 \times 10^{-5} \text{ rad/s}$ . The remaining values are calculated from the trajectories.

**4.1.1 Horizontal Turn Trajectory.** In order to maintain a horizontal constant acceleration turn, the aircraft banks such that a vertical  $1g$  component of the total acceleration exactly offsets the acceleration due to gravity in the vertical direction. The remaining component of acceleration in the horizontal plane is resolved along the north and east directions. Therefore, the parameters are calculated from the following relationships for an initial east heading turning counter-clockwise, as observed from above:

$$\begin{aligned}
v_N &= s \sin(\alpha) \\
v_E &= s \cos(\alpha) \\
v_D &= 0 \\
A_N &= f_N = A_h \cos(\alpha) \\
A_E &= f_E = A_h \sin(\alpha) \\
f_D &= 1g = 32.1726 \text{ ft/s}^2
\end{aligned}
\tag{4-1}$$

where the forward speed of the aircraft,  $s$ , is chosen to be 975 ft/s,  $\alpha$  describes the angular position through the turn, and  $A_h$  is the magnitude of the horizontal component of acceleration. These variables are shown graphically in Figure 4.1. Sign changes on the north velocity and acceleration equation describe the variables for a clockwise turn.

The velocity and acceleration terms of Equations (4-1) are transformed to spherical coordinates by the following relationships and inserted into the INS-related dynamics matrix:

$$\begin{aligned}
\dot{L} &= v_N/R & \ddot{L} &= A_N/R \\
\dot{l} &= v_E/[R \cos(L)] & \ddot{l} &= A_E/[R \cos(L)] \\
\dot{h} &= -v_D & \dot{\lambda} &= \dot{l} + w_{le}
\end{aligned}
\tag{4-2}$$

The path described from this trajectory is circular.

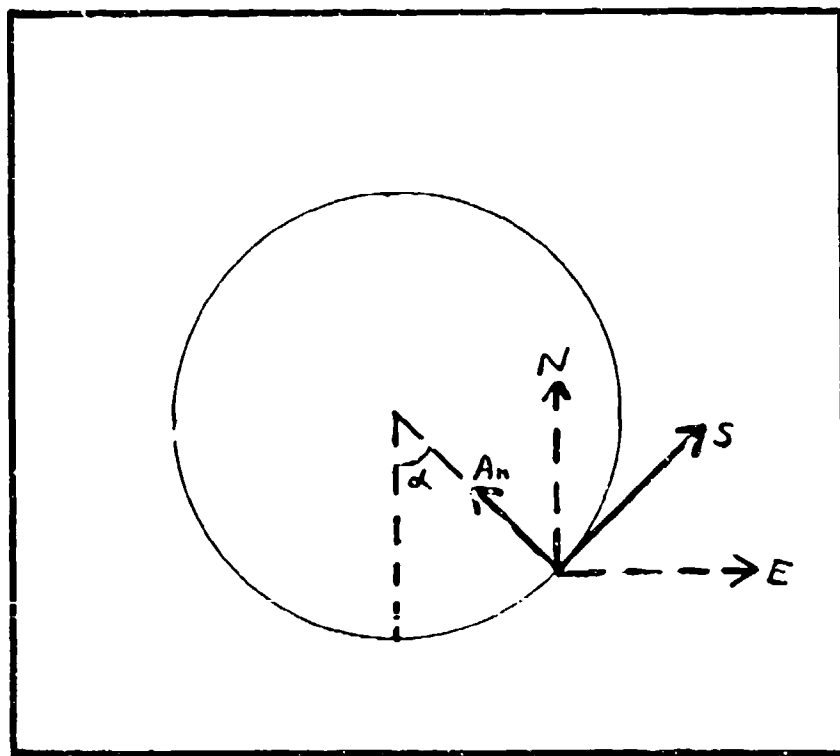


Figure 4.1. Horizontal Turn Variables

4.1.2 Vertical Turn Trajectory. The vertical trajectory, such as at an acrobatic loop maneuver, cannot be circular if a constant velocity, constant acceleration turn is performed. For an initial eastward path, the relationships as represented in Figure 4.2 result:

$$\begin{aligned}
 V_N &= 0 \\
 V_E &= s \cos(\gamma) \\
 V_D &= -s \sin(\gamma) \\
 A_N &= f_N = 0 & (4-3) \\
 A_E &= f_E = (\cos(\gamma) - T) g \sin(\gamma) \\
 f_D &= (\cos(\gamma) - T) g \cos(\gamma) - g
 \end{aligned}$$

where

$\gamma$  is the angle between the acceleration vector and the negative gravity direction, and

$T$  is the constant magnitude of acceleration commanded by the pilot and exerted on the aircraft. It includes the actual acceleration, as well as the component of gravity along the acceleration vector.

A vertical turn with an initial north heading results if the "E" and "N" subscripts in Equations (4-3) are exchanged. The relationships of Equations (4-2) also apply in these two cases.

These trajectory analyses are performed to explore the nature of the eigenvalues of the INS dynamics matrix.

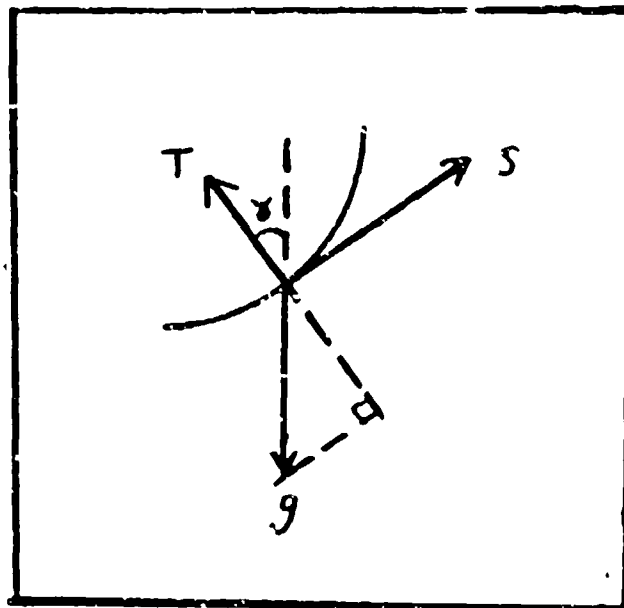


Figure 4.2. Vertical Turn Variables

## 4.2 Eigenvalue Migration

The eigenvalues of the INS dynamics matrix are explored to examine the characteristics of the INS during the four maneuvers described in the previous sections. The needed parameters are calculated at  $15^\circ$  increments of  $\alpha$  for the horizontal trajectories, and  $15^\circ$  increments of  $\gamma$  for the vertical turn trajectories. Assuming an aircraft speed of 975 ft/s and constant 9g turn, the parameters are calculated at each point through the  $360^\circ$  turns. These values of velocity, acceleration, and specific force are used to linearize the basic INS equations listed in Equations (3-18) through (3-26), and the eigenvalues of the system matrix are determined. The eigenvalue characteristics of each of the four trajectories are presented.

As shown in Figures 4.3 and 4.4, the eigenvalues of the horizontal trajectories, both clockwise and counter-clockwise, are identical. The actual migration path the eigenvalues take is not as important as the general location of the eigenvalues: a complex pair of eigenvalues always remains in the right-half s-plane throughout the maneuvers. The eigenvalue on the positive real axis is due to the vertical channel instability.

The eigenvalues generated from the vertical trajectories exhibit different characteristics. The eigenvalue plot of the east initial heading vertical turn

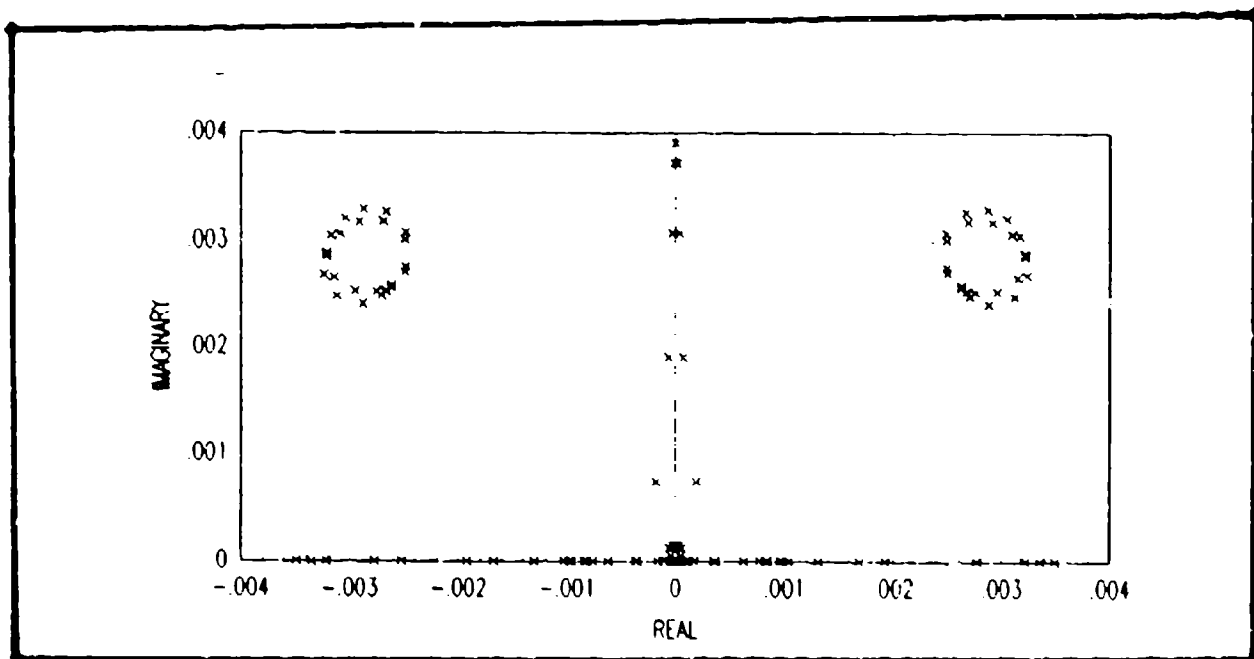


Figure 4.3. Horizontal Counter-Clockwise  
Turn Eigenvalues

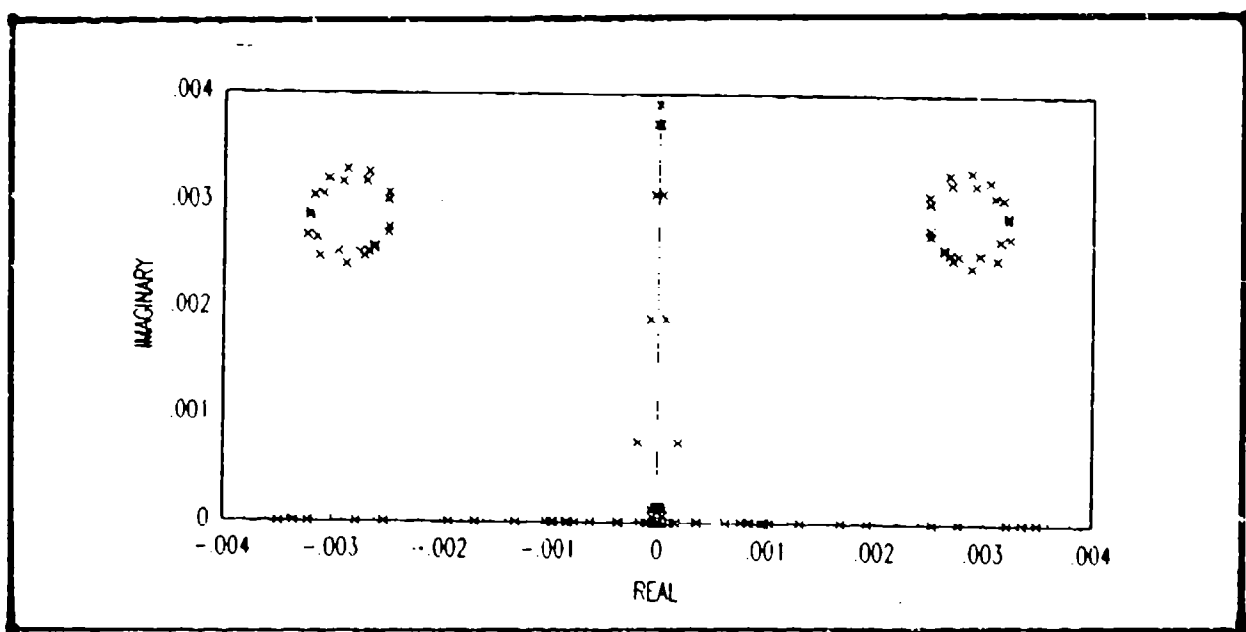


Figure 4.4. Horizontal Clockwise  
Turn Eigenvalues

trajectory, as shown in Figure 4.5, exhibits the eigenvalue due to the vertical channel instability, plus a complex pair which breaks away from the imaginary axis, migrates to the real axis, and returns to the imaginary axis.

The eigenvalues generated from the north initial heading vertical turn trajectory, shown in Figure 4.6, exhibits only a predominant vertical channel eigenvalue in the right-half s-plane. This indicates that the eastward, or longitudinal, components of motion result in an additional eigenvalue pair in the unstable region of the s-plane.

As a result of this eigenvalue migration study, only the initial east heading horizontal counter-clockwise turn maneuver is chosen for the remaining simulations. It is chosen for two reasons: it represents the most unstable nature of the four trajectories, and the angular position,  $\alpha$ , of the vehicle in the turn is linearly related to time. Additional eigenvalue plots for acceleration levels of 7g, 5g, and 3g, are also generated for this trajectory. As seen in Figures 4.3, 4.7, 4.8, and 4.9, the complex pairs of eigenvalues migrate toward the origin in these decreasing acceleration increments.

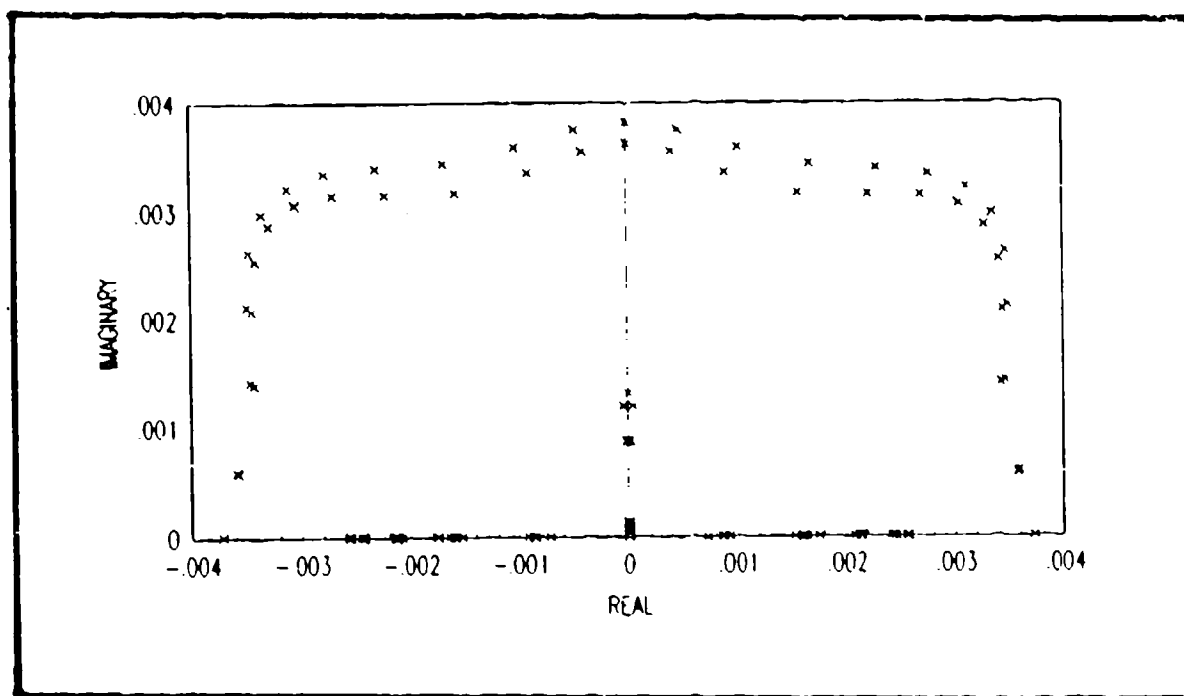


Figure 4.5. Initial East Heading  
Vertical Turn Eigenvalues

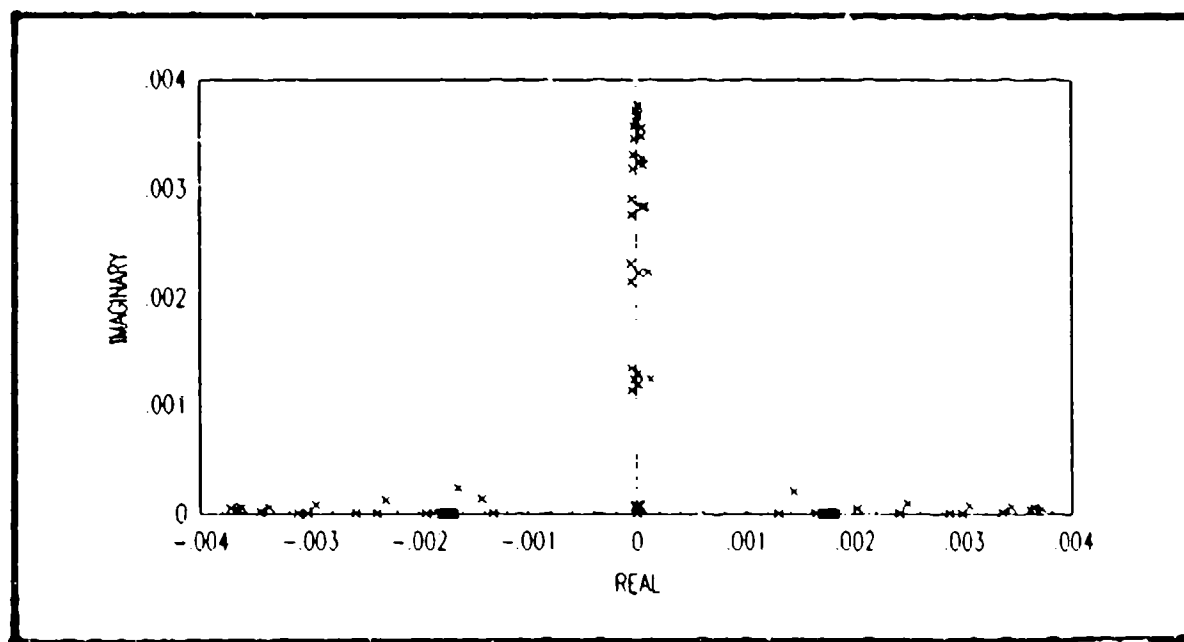


Figure 4.6. Initial North Heading  
Vertical Turn Eigenvalues

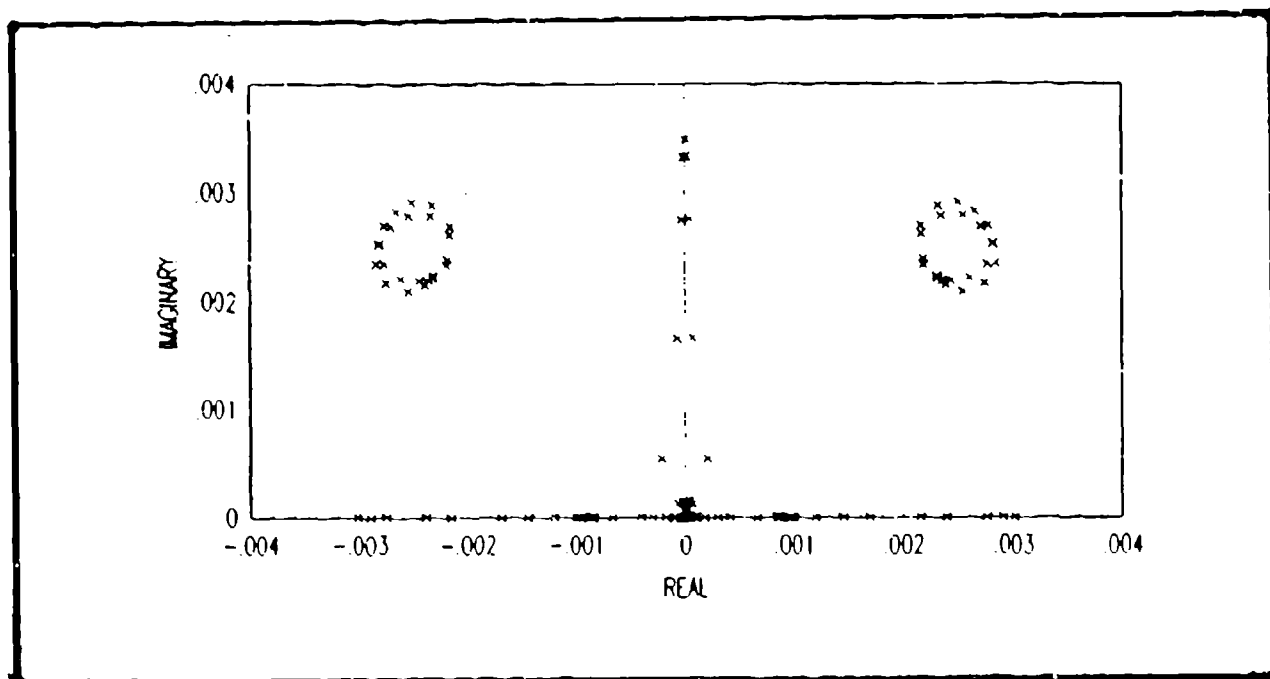


Figure 4.7. Eigenvalues  
7g Horizontal Counter-Clockwise Turn

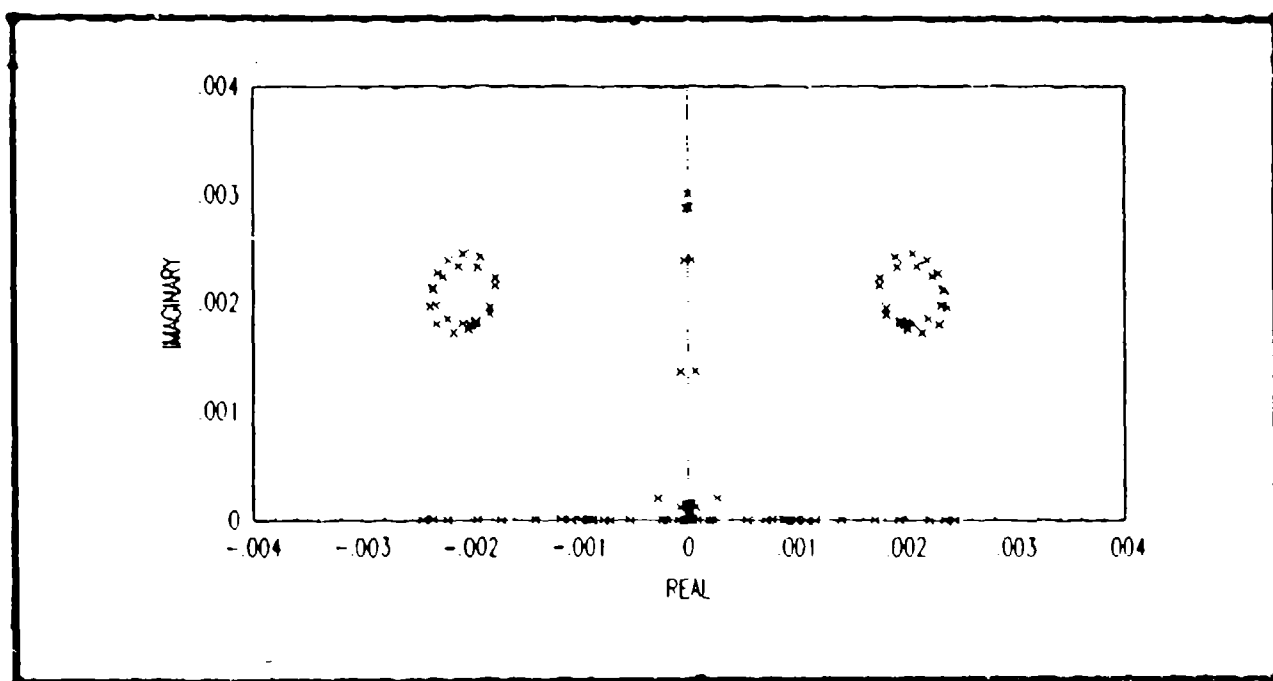


Figure 4.8. Eigenvalues  
5g Horizontal Counter-Clockwise Turn

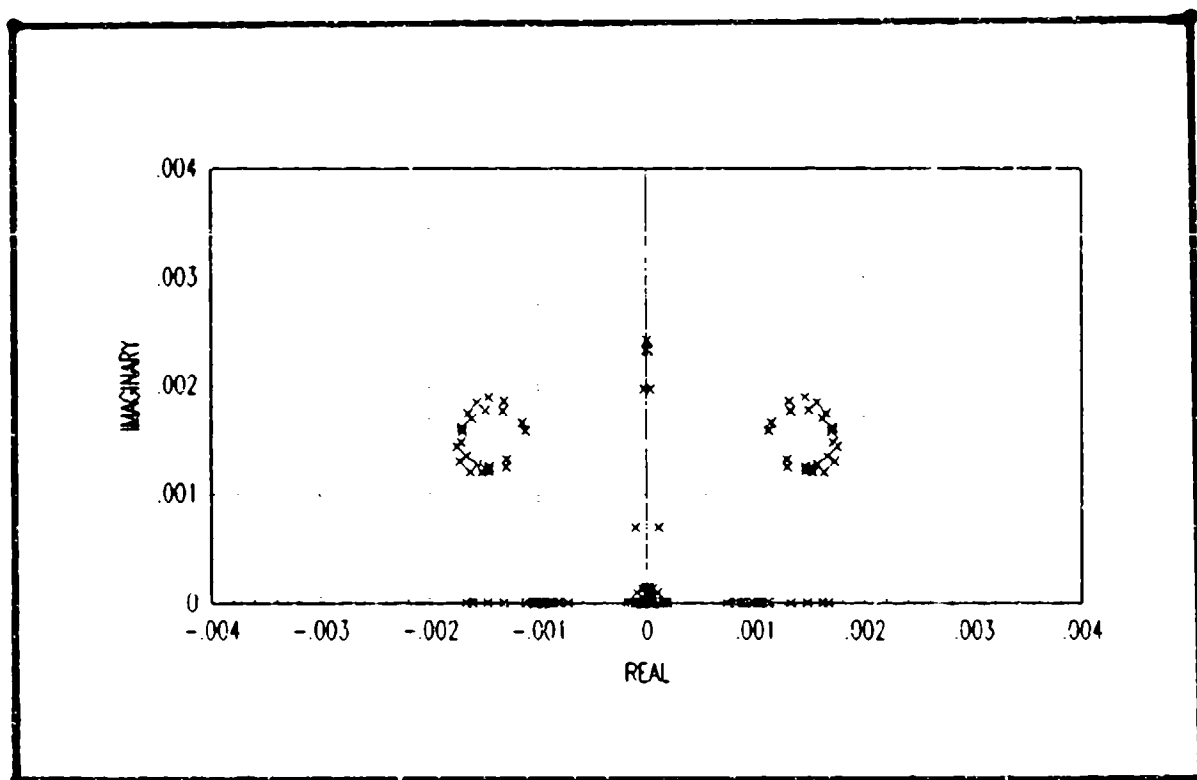


Figure 4.9. Eigenvalues  
3g Horizontal Counter-Clockwise Turn

#### 4.3 Performance Analysis Results

A performance analysis, as described in Chapter III, is conducted for the stationary, constant east velocity, and horizontal counter-clockwise turn conditions. Five systems are evaluated for each condition: the complete 19-state INS Kalman filter, the complete 24-state GPS receiver Kalman filter, the 36-state joint-solution Kalman filter, the two-filter full-state system, and the baseline system which contains the 10-state INS Kalman filter and the 12-state GPS receiver Kalman filter. For every system and the short time period of calculation, the performance achieved under the constant east velocity condition is virtually identical to the performance achieved under the stationary condition. Therefore, only constant velocity data is presented.

The main reason for the constant east velocity condition is to allow the GPS receiver portion of the Kalman filter covariance matrix to reach nearly steady-state conditions before initiating the maneuver. Because of Schuler and Foucault-induced errors present in the INS dynamics, no true steady-state condition exists. Therefore, the starting time for the turn coincides with the steady-state time of the GPS receiver Kalman filter.

In each case, measurement updates and INS dynamics relinearization occur at each  $15^\circ$  interval through the turn, starting at  $0^\circ$ . This results in  $\Delta t_1 = 0.887$  seconds.

For the two-filter systems, the GPS receiver code loop is commanded with the best available INS estimate at four times per measurement interval, resulting in  $t_k = 0.2218$  seconds.

Representative values for the discrete-time process noises are chosen to drive the system dynamics:

$$w = 6.8566 \times 10^{-8} \text{ rad/sec}$$

$$w_v = 1.5147 \times 10^{-3} \text{ ft/sec}^2$$

$$w_h = 3.9958 \text{ ft/sec}$$

$$w_n = 0.29783 \text{ ft/sec}$$

These noises are also modelled within each of the applicable Kalman filters. The truth model has initial uncertainties in order to begin the performance analysis:

$$\underline{\epsilon} = 4 \times 10^{-5} \text{ rad}$$

$$\underline{p} = 1000 \text{ ft}$$

$$\underline{v} = 1 \text{ ft/sec}$$

$$h_b = 707.1 \text{ ft}$$

$$\underline{d} = 2.648 \times 10^{-8} \text{ rad/sec}$$

$$\underline{B} = 1.515 \times 10^{-3} \text{ ft/sec}^2$$

$$\underline{SF} = 1 \times 10^{-4}$$

$$b = 3.136 \times 10^{-2} \text{ sec}$$

$$d = 3.136 \times 10^{-4}$$

$$\underline{r}_x = 10 \text{ ft}$$

The GPS receiver and INS Kalman filters are initialized, for gain calculation purposes, at the same values of uncertainty for the respective error states as the truth model states. The entire covariance matrix, which fills in with cross-covariance information during the time for the GPS receiver Kalman filter to reach steady-state, is used as initial conditions for the turn start. The measurement noises for the four pseudorange measurements are assumed to be uncorrelated and contribute  $\pm 5$  ft (1 $\sigma$ ) error. The noise associated with the vertical position measurement is chosen as  $\pm 10$  ft (1 $\sigma$ ).

Unit LOS vectors to four satellites, representative of an actual GPS satellite constellation are chosen with good relative geometry (Lewantowicz, 1987). Expressed in the NED navigation coordinate frame relative to the user, the unit LOS vectors within the DPR measurement set are

$$\begin{aligned}\underline{u}_{LOS} &= \begin{bmatrix} 0.29342 & 0.20548 & -0.93364 \end{bmatrix} \\ \underline{u}_{LOS} &= \begin{bmatrix} -0.56758 & -0.63147 & -0.52829 \end{bmatrix} \\ \underline{u}_{LOS} &= \begin{bmatrix} 0.66262 & 0.94523 & -0.31962 \end{bmatrix} \\ \underline{u}_{LOS} &= \begin{bmatrix} 0.88490 & 0.40753 & -0.21098 \end{bmatrix}\end{aligned}$$

These vectors are also used in the transformations between the LOS errors and navigation frame errors.

The values presented in this section are common to each of the systems under test. The next sections present the data obtained from each of the performance analyses.

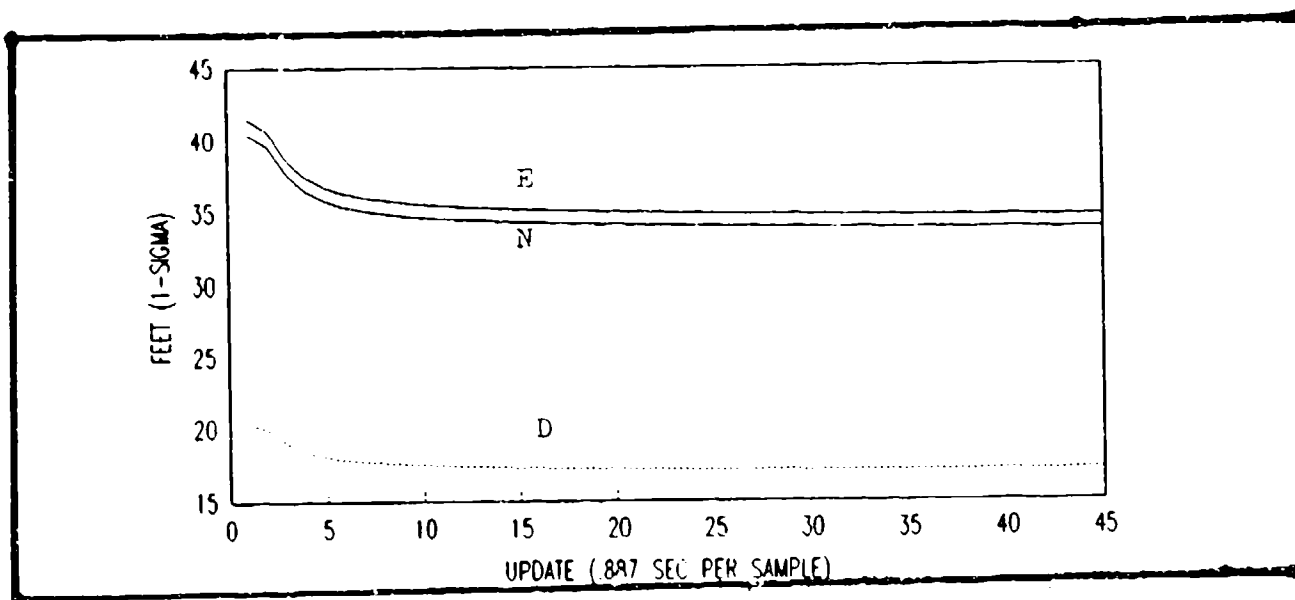


Figure 4.10. GPS Receiver Position Errors  
(Constant East Velocity)

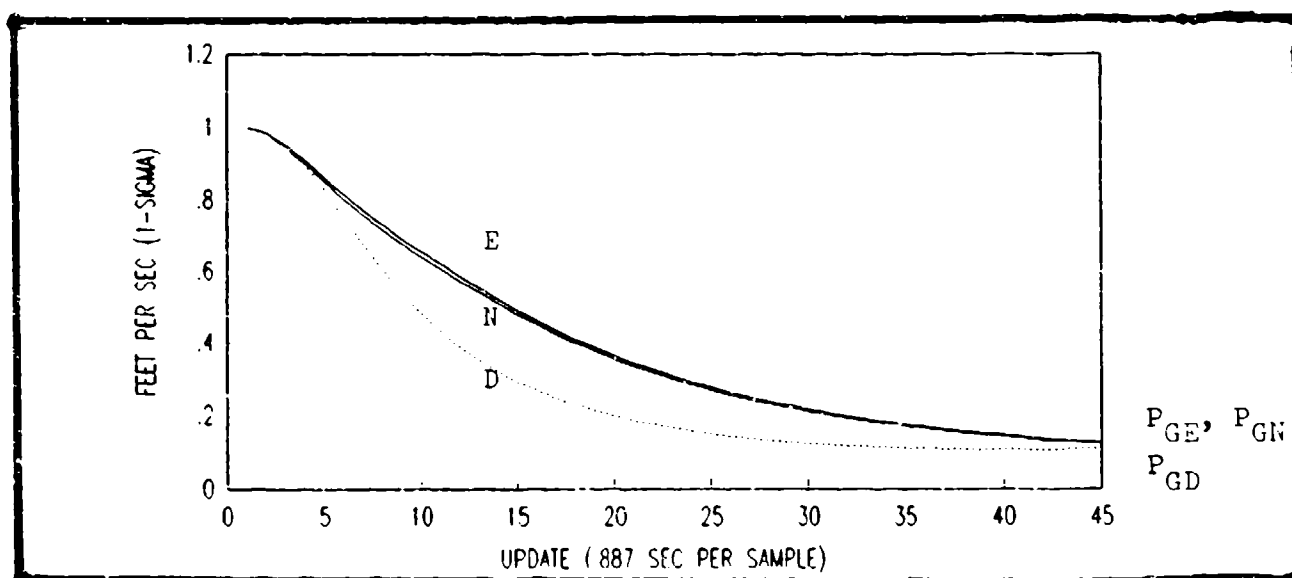


Figure 4.11. GPS Receiver Velocity Errors  
(Constant East Velocity)

4.3.1 24-State GPS Receiver Kalman Filter. The complete (24-state) GPS receiver Kalman filter performance is demonstrated. When subjected to a benign environment of stationary or constant velocity conditions, the position errors (Figure 4.10) exhibit very little change after 10 measurement updates. This rapid convergence is attributed to the high accuracy of the pseudorange measurements. The vertical position error is lower than the north and east position errors due to the additional measurement from the altimeter. The velocity errors, Figure 4.11, require 45 measurement updates before reaching essentially steady-state. This additional time is expected since no velocity measurements are available in the modelled GPS receiver Kalman filter. The  $1\sigma$  steady-state errors, for the modelled parameters, achieved are

$$\begin{array}{ll} \delta P_{GN} = 33.8 \text{ ft} & \delta V_{GN} = 0.124 \text{ ft/sec} \\ \delta P_{GE} = 34.7 \text{ ft} & \delta V_{GE} = 0.127 \text{ ft/sec} \\ \delta P_{GD} = 17.1 \text{ ft} & \delta V_{GD} = 0.110 \text{ ft/sec} \end{array}$$

The resulting covariance matrix is used as the initial conditions, corresponding to GPS receiver state uncertainties, for the horizontal turn maneuver. As shown in Figures 4.12 and 4.13 in which each update occurs in  $15^\circ$  increments about the turn, the GPS receiver tracks the position without appreciable degradation through three

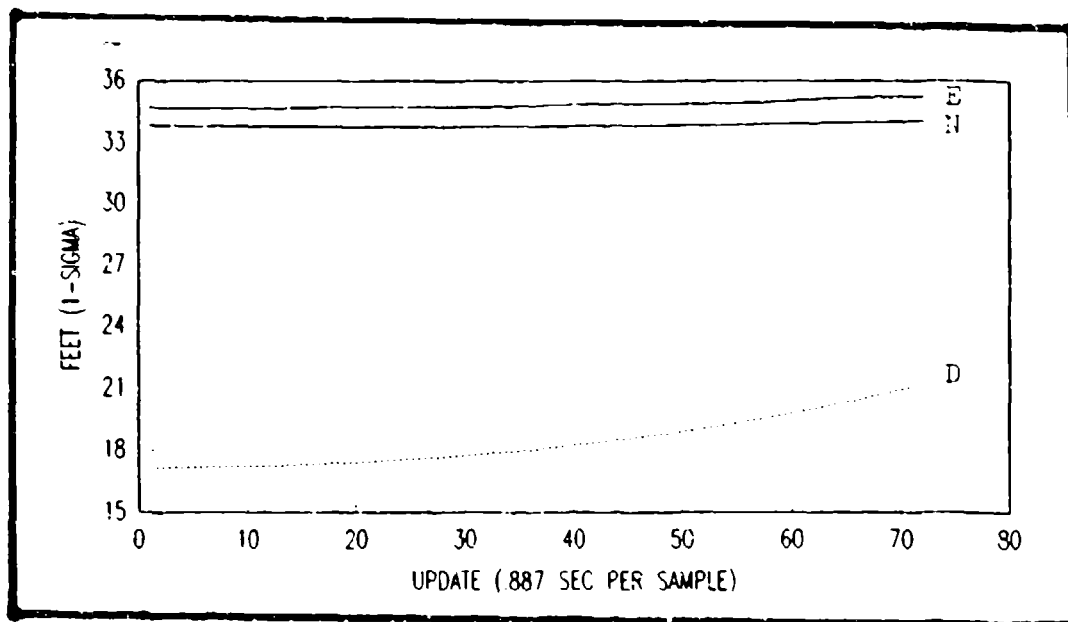


Figure 4.12. GPS Receiver Position Errors  
(9g Turn)

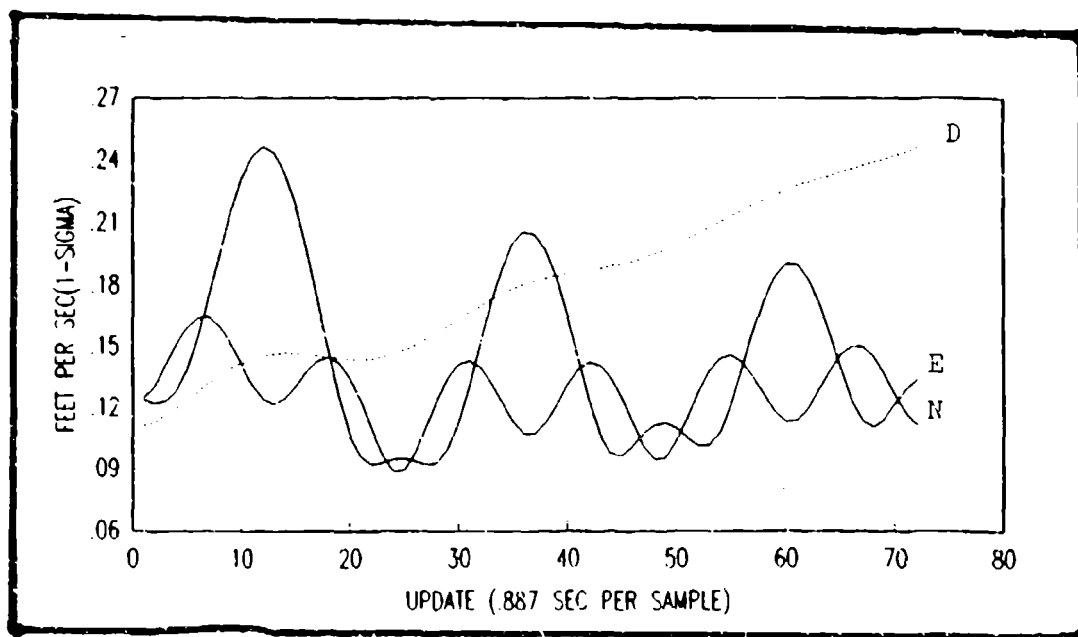


Figure 4.13. GPS Receiver Velocity Errors  
(9g Turn)

complete turns. The north and east velocity errors, after an initial transient, modulates at the turn frequency, while the vertical velocity error doubles its amplitude after three turns are completed.

The GPS receiver solution did not go catastrophically unstable as actual flight tests demonstrate. Two reasons may contribute to this observation:

- a. The GPS code loop is modelled with a 1 Hz bandwidth bandpass filter, while the frequency of the turn is approximately 0.3 Hz;
- b. The velocity errors are related to the code loop tracking errors, which is assumed linear in operation during this study. However, the dynamics of the code loop is very nonlinear outside of a small region. The errors in the code loop are related to a phase shift. If this phase shift is great enough, the system enters the nonlinear region and becomes unstable.

4.3.2 19-State INS Kalman Filter. Figures 4.14 through 4.17 exhibit the position and velocity errors committed by the 19-state INS Kalman filter during the same time period as that of the GPS receiver Kalman filter analysis. Since the INS processes only altitude measurements, the north and east errors (Figures 4.14 and 4.16) increase throughout the short time period. The north position error is related to Schuler frequency, while the east error is Schuler superimposed on a ramp. This is not

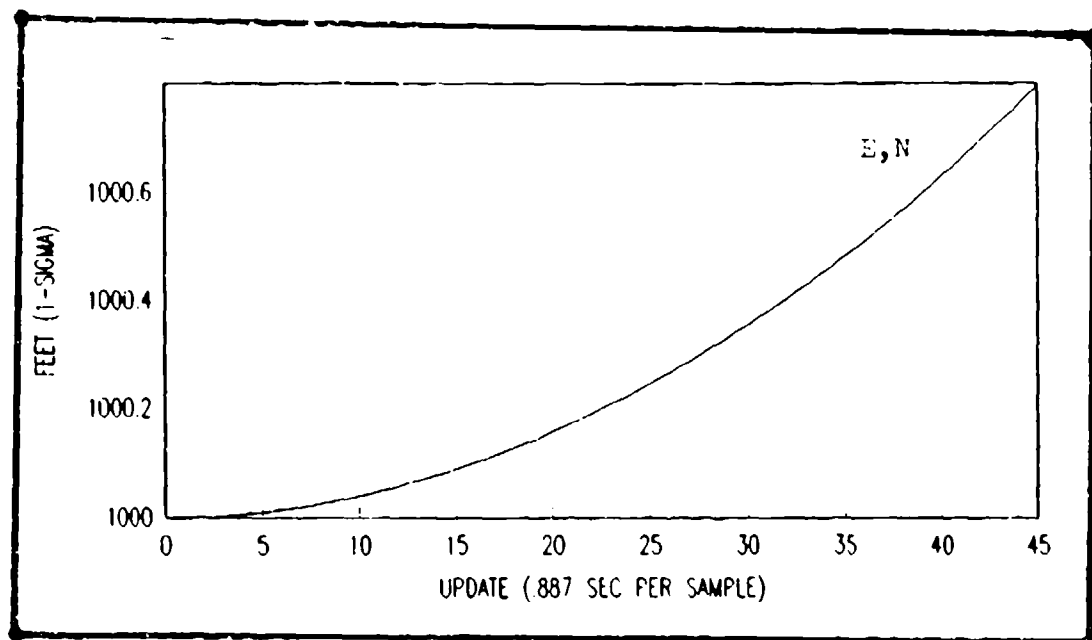


Figure 4.14. INS North and East Position Errors  
(Constant East Velocity)

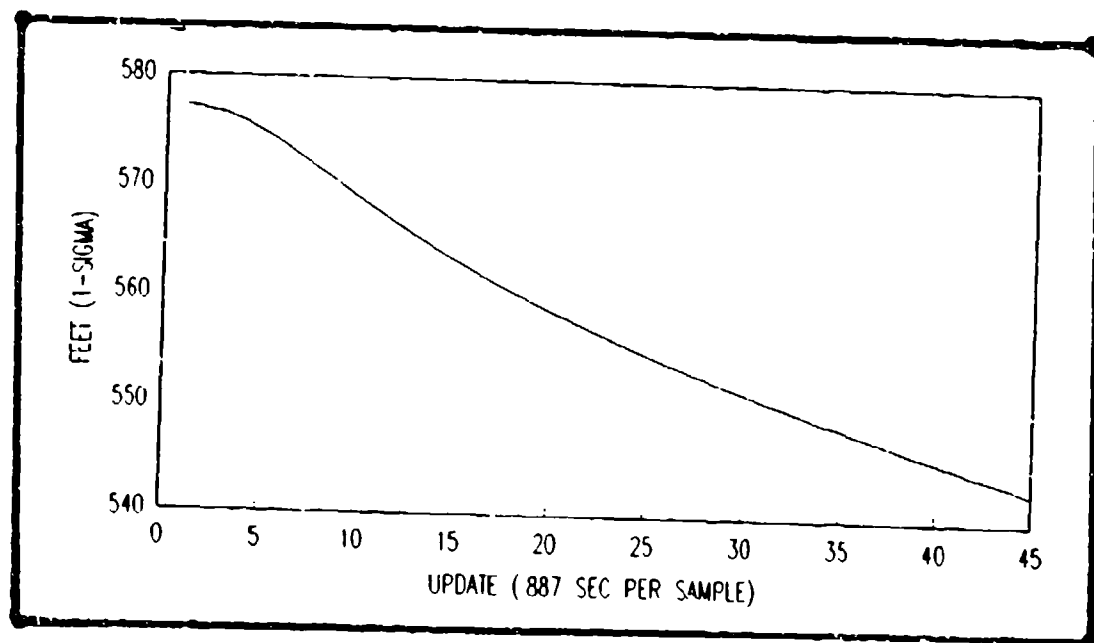


Figure 4.15. INS Vertical Position Errors  
(Constant East Velocity)

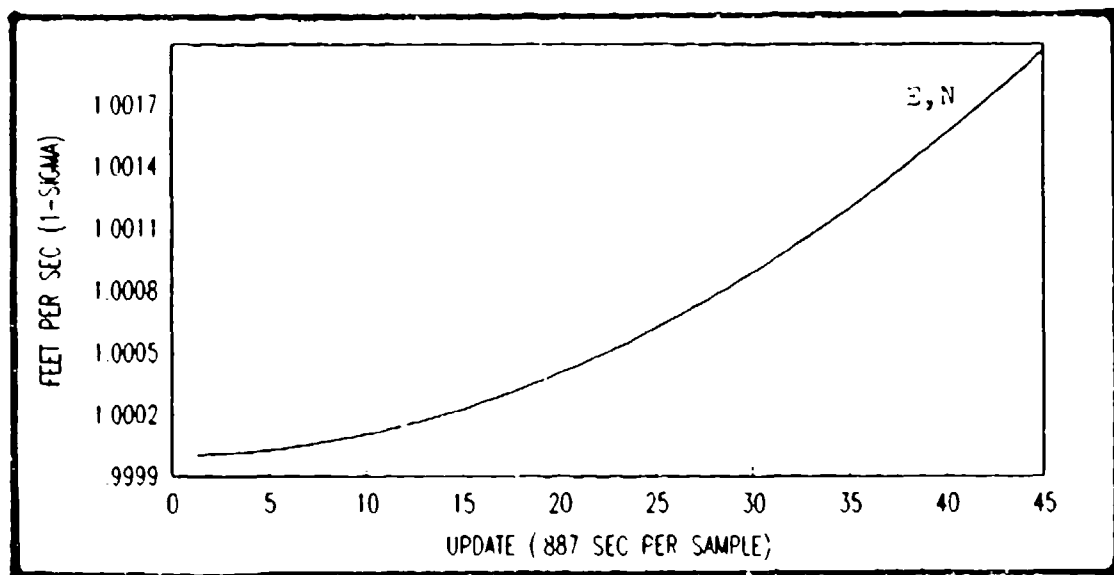


Figure 4.16. INS North and East Velocity Errors  
(Constant East Velocity)

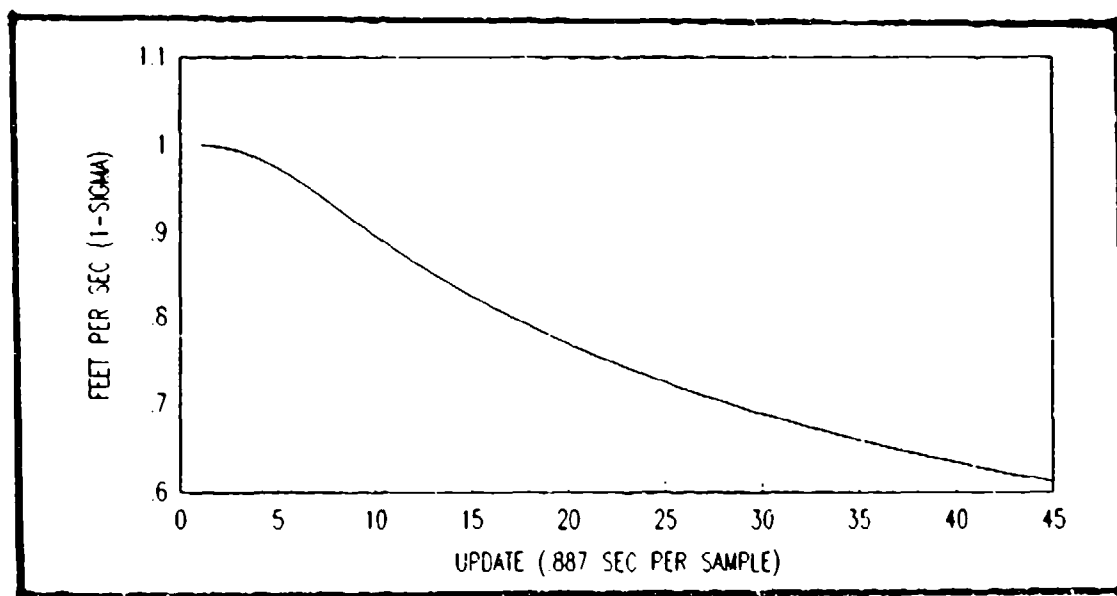


Figure 4.17. INS Vertical Velocity Errors  
(Constant East Velocity)

readily apparent for the short time of interest. The vertical errors (Figures 4.15 and 4.17) improve steadily throughout the turn due to the vertical position measurement from the altimeter. After 45 measurement updates, the 1 $\sigma$  INS Kalman filter errors are

$$\begin{array}{ll} \delta P_{IN} = 1000.8 \text{ ft} & \delta V_{IN} = 1.002 \text{ ft/sec} \\ \delta P_{IE} = 1000.8 \text{ ft} & \delta V_{IE} = 1.002 \text{ ft/sec} \\ \delta P_{ID} = 542.8 \text{ ft} & \delta V_{ID} = 0.612 \text{ ft/sec} \end{array}$$

During the turn, the high frequency accuracy of the INS is demonstrated. As seen in Figures 4.18 through 4.21, the north and east errors during the turn primarily follow the turn-induced frequency. The vertical channel continues to receive the altimeter measurement, thus exhibiting no frequency content due to the horizontal maneuver.

**4.3.3 Joint-Solution Kalman Filter.** The 36-state joint-solution Kalman filter follows closely to the highly accurate GPS receiver Kalman filter solution as shown in Figures 4.22 and 4.23 for constant east velocity. During the turn (Figures 4.24 and 4.25), the joint-solution filter exhibits the benefit of modelling the INS. After an initial overshoot, the errors reduce to below initial uncertainty levels. This is expected since the joint-solution Kalman filter appropriately weighs the accuracy of its internal model. The performance of this

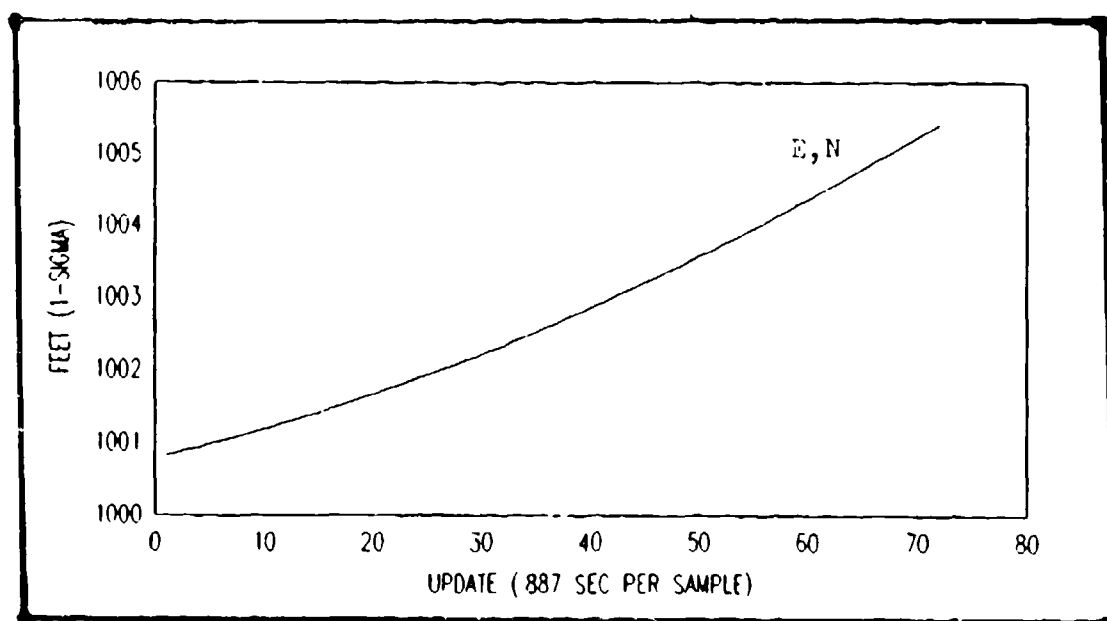


Figure 4.18. INS North and East Position Errors  
(9g Turn)

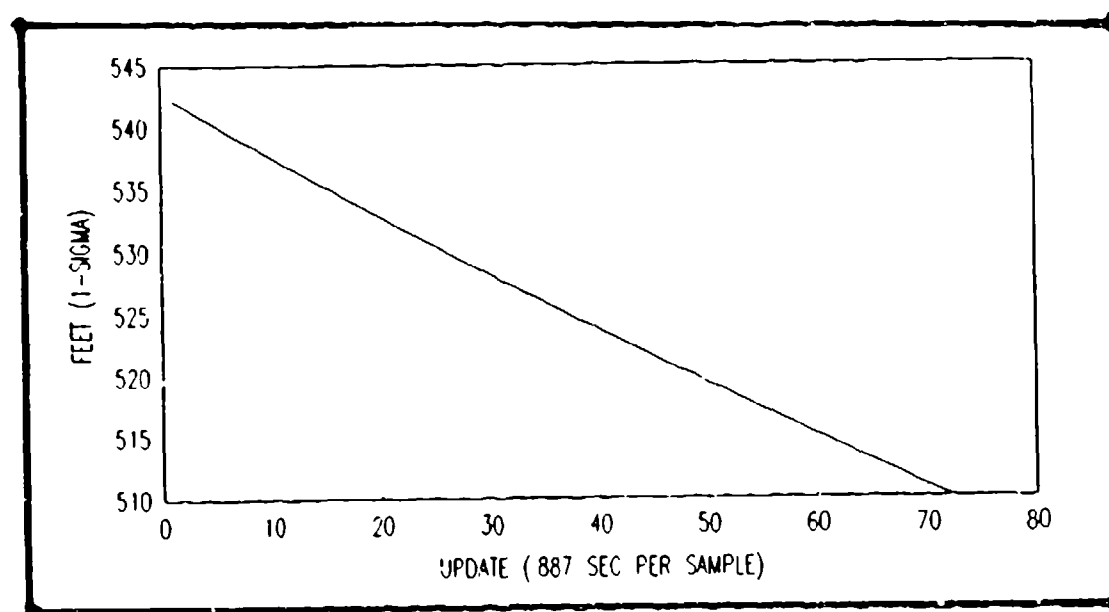


Figure 4.19. INS Vertical Position Errors  
(9g Turn)

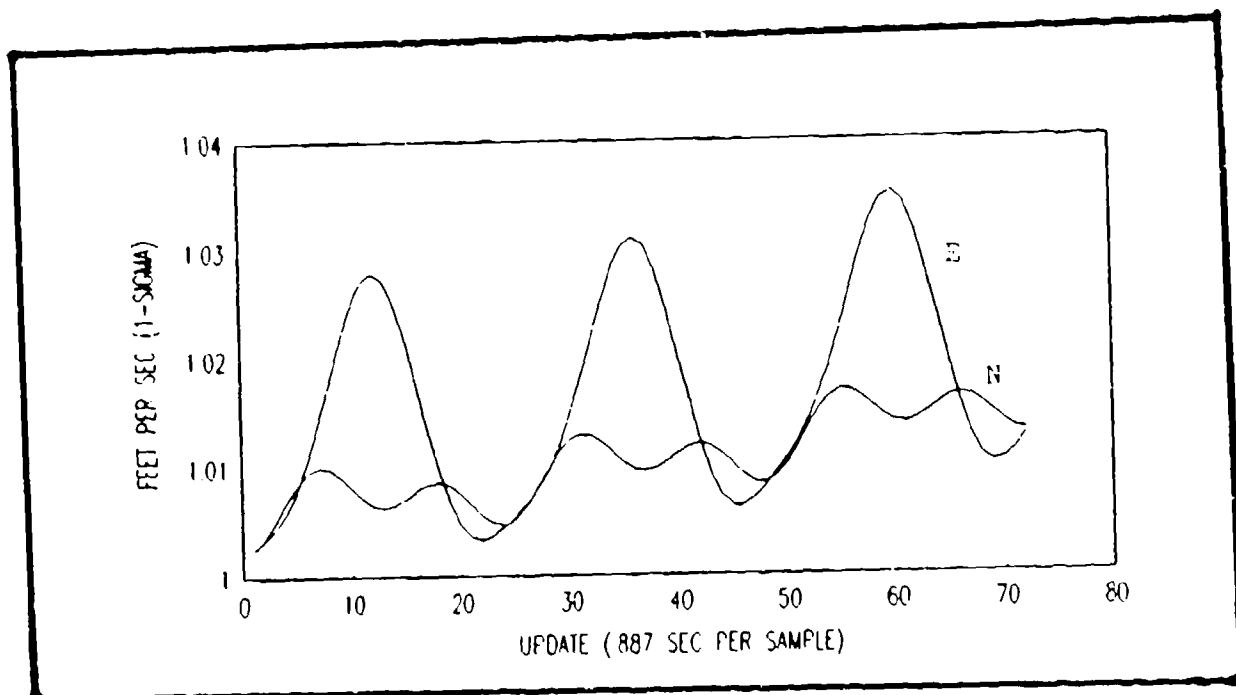


Figure 4.20. INS North and East Velocity Errors  
(9g Turn)

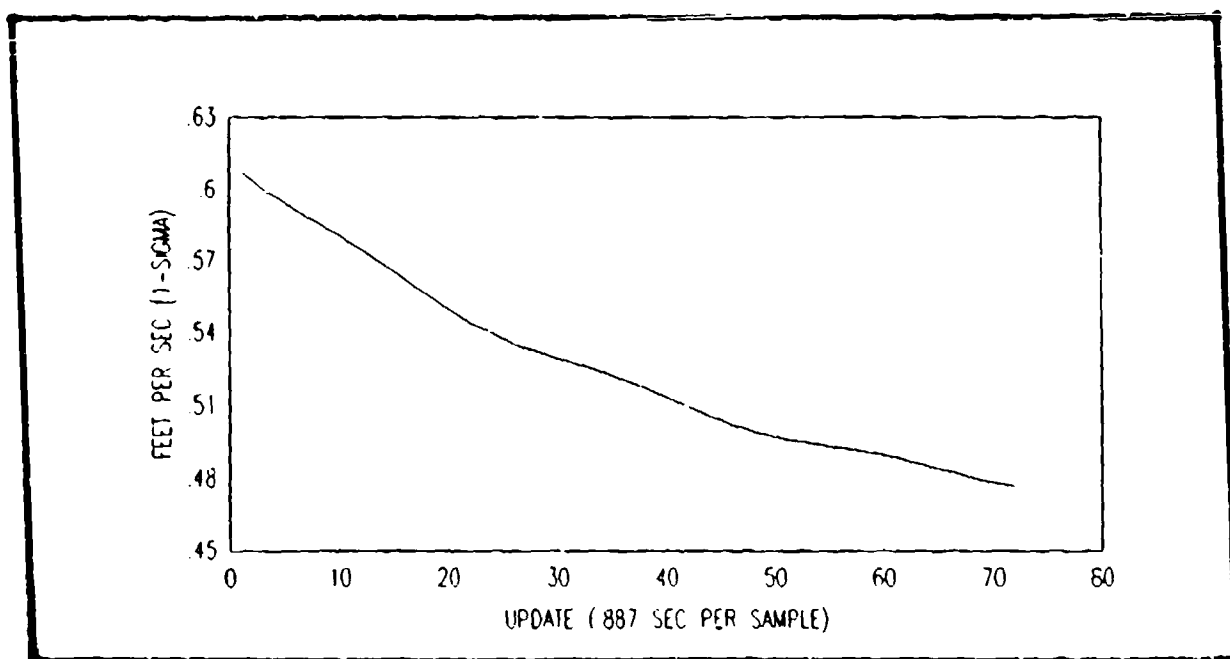


Figure 4.21. INS Vertical Velocity Errors  
(9g Turn)

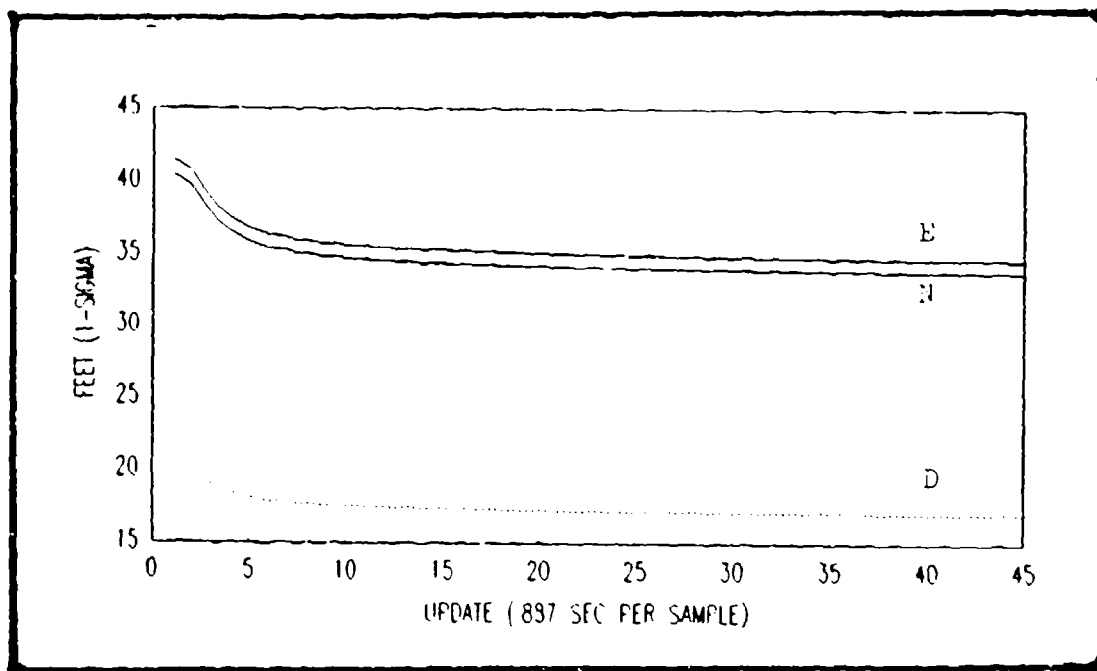


Figure 4.22. Joint-Solution Position Errors  
(Constant East Velocity)

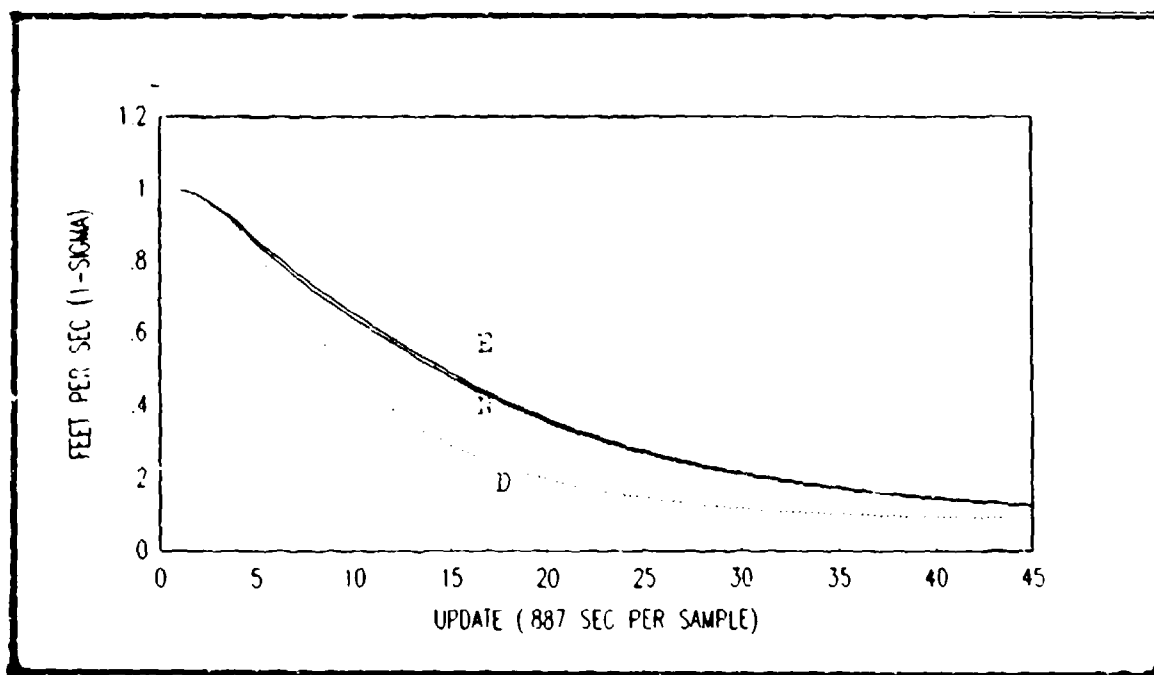


Figure 4.23. Joint-Solution Velocity Errors  
(Constant East Velocity)

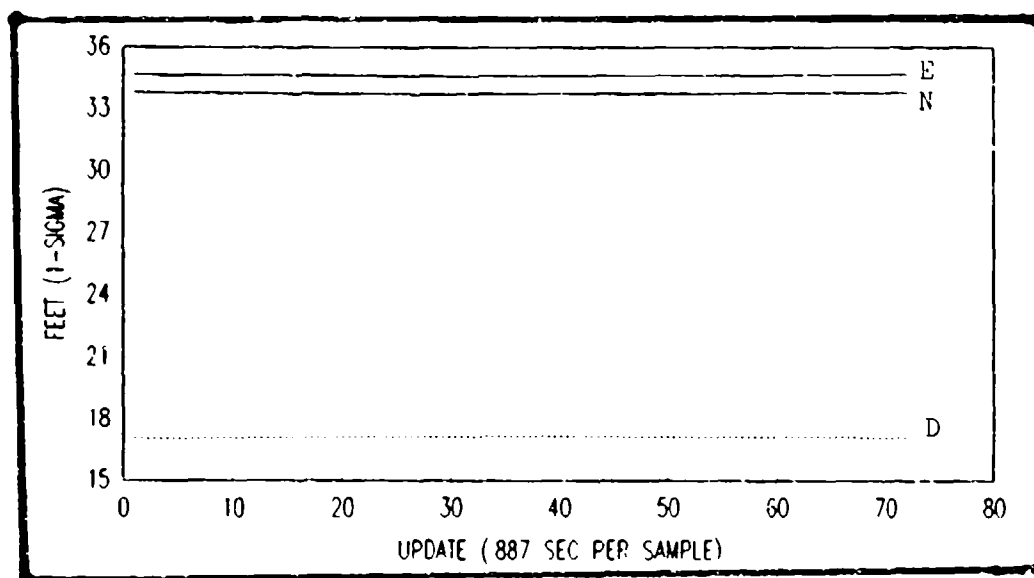


Figure 4.24. Joint-Solution Position Errors  
(9g Turn)

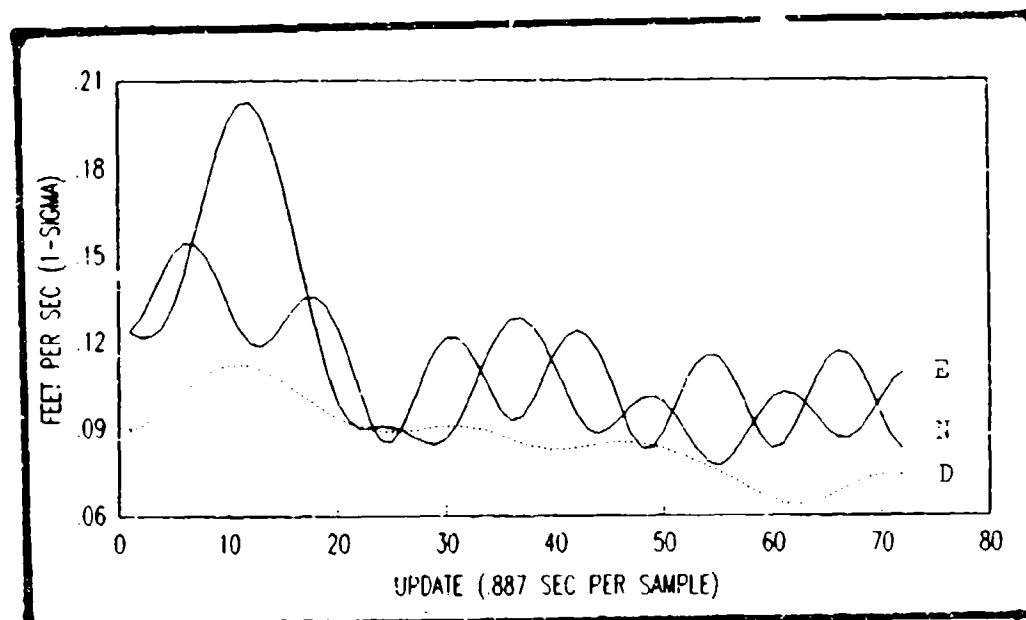


Figure 4.25. Joint-Solution Velocity Errors  
(9g Turn)

filter represents the best possible performance of all the systems modelled. However, the code loop tracking errors must be reviewed to assure linear operation is maintained throughout the transient behavior of the turn.

4.3.4 Two-Filter Systems. The two-filter system analysis is not complete and no conclusions can be drawn at this time. The expected instability of the two-filter interaction is not yet observed. In the covariance analysis algorithm the INS Kalman filter appears to be not receiving the expected GPS generated position and velocity error measurements. This deficiency is crucial to the loop closure and the expected instability. This exploration is deferred to follow-on research.

## V. Conclusions and Recommendations

The original objective of this study was to determine what minimum additional information is required to be passed between the INS Kalman filter and the GPS Kalman filter to obtain a stable, and acceptably performing, closed-loop system during high-dynamic maneuvers. This ultimate objective was not reached during this study. However, several initial steps are completed towards accomplishing this goal. The combined INS/GPS joint-solution model performance displays the characteristics of the GPS receiver during benign conditions, and weighs the INS characteristics appropriately during the selected maneuver. Work remains to be accomplished before the two-filter system analysis reaches fruition. From the significant insight gained from this study, the recommended follow-on effort should include:

- a. Model refinement is necessary such that more complex and realistic flight scenarios are explored.

These model refinements include:

1. Actual INS model parameters for a specific system application is required. The models used in this study neglected several error sources because the situation did not warrant the additional complexity. However, some of the

neglected error sources contribute significantly as flight time progresses.

ii. Exploration of the GPS receiver code loop model parameters for adequacy is required.

Models of the code loop dynamics are not readily available, particularly parameter values. Since this model is essential for a proper study to be conducted, an accurate description of the model and error sources is crucial.

iii. In addition to the code loop model, the GPS model parameters, in general, need further refinement. Again, this additional adjustment should be representative of the actual system. The values used in this study, for initial uncertainties, and system noises, were derived from articles written during the early phases of GPS development. Since much more has been accomplished in the time of these articles regarding GPS technology, it is likely modelling philosophy has changed and should be reflected.

b. The code loop errors require monitoring during the performance analysis. The linear region of these errors is modelled in this study. However, if the phase shift of the code tracking loop becomes too large, then the linear assumptions are violated, and rapid loss of lock occurs. These errors were not

observed during the course of this study, because any instability was expected to be displayed through the position and velocity errors. In retrospect, this does not appear to be true for linear assumptions.

c. The INS measurement update portion of the two-filter system requires examination. Preliminary results of this scenario displayed inadequate weighting of the GPS-derived measurement within the INS Kalman filter. This problem requires a solution to validate the algorithm.

d. GPS satellite geometry requires consideration. The geometry used in this study was very favorable: four high elevation satellites. However, if the satellites are near the horizon, it is expected that larger doppler-induced shifts of the code loop would occur under vehicle dynamics.

e. The unstable mode eigenvalues of the INS linearized dynamics model indicate that an extended period of hard maneuvers will result in increased likelihood of significant error growth, and must be examined.

## Bibliography

1. Britting, Kenneth R. Inertial Navigation Systems Analysis. New York: Wiley-Interscience, 1971.
2. Brooks, Richard A. and others. GPS Error Budgets, Accuracy and Applications Considerations for Test and Training Ranges. Contract F0470381C0101. Vandenberg AFB, CA: Federal Electric Corporation-ITT, December 1982 (AD-A128955).
3. Carrol, R.W. and W.A. Mickelson. "Velocity Aiding of Noncoherent GPS Receiver," IEEE Proceedings of the National Aerospace Electronics Conference NAECON '77. 311-318. New York: IEEE Press, 1977.
4. Cox, D. B. Jr. "Integration of GPS with Inertial Navigation Systems," Navigation, Journal of the Institute of Navigation, 25: 144-153. (Summer 1978).
5. Dosh, M.K. and M.D. Yakos. "GPS/INS Integration Using Decoupled Residual Data," Publication unknown.
6. Draper, Charles Stark. "Origins of Inertial Navigation," AIAA Journal of Guidance and Control, :449-463 (Sept-Oct 1981).
7. Eller, Donald. "GPS/IMU Navigation in a High Dynamics Environment," Publication unknown.
8. Lewantowicz, Z.H., Deputy Department Head, Electrical Engineering Department. Personal interviews. Air Force Institute of Technology, Wright-Patterson AFB, OH, 1987.
9. -----, Class handouts distributed in EENG 534, Aerospace Instrumentation for Navigation Systems. School of Engineering, Air Force Institute of Technology, Wright-Patterson AFB OH, Fall 1986.
10. Maybeck, Peter S. Stochastic Models, Estimation, and Control, Volume 1. New York: Academic Press, 1979.

11. Meyer, Lt James D. Embedded GPS Systems Test and Evaluation Program: Initial Flight Test Results. U.S. Army Yuma Proving Ground AZ, January 1987.
12. Milliken, R.J. and C.J. Zoller. "Principle of Operation of NAVSTAR and System Characteristics," Navigation, Journal of the Institute of Navigation, 25: 3-14 (Summer 1978).
13. Russell, S.S. and J.H. Schaiely, "Control Segment and User Performance," Navigation, Journal of the Institute of Navigation, 25: 74-80 (Summer 1978).
14. Spilker, J.J. Jr. "GPS Signal Structure and Performance Characteristics," Navigation, Journal of the Institute of Navigation, 25: 29-54 (Summer 1978).
15. Sturza, Mark A. "GPS Navigation Using Three Satellites and a Precise Clock," Proceedings of the National Aerospace Meeting. 117-126. Washington: The Institute of Navigation, 1983.
16. Tarabe, Toru and others. "New Integration Scheme of GPS-INS Hybrid Navigation System for Maneuvering Spacecraft," Publication unknown.
17. Upadhyay, Triveni N. and others. "Benefits of Integrating GPS and Inertial Navigation Systems," The Institute of Navigation: Proceedings of the Thirty-Eighth Annual Meeting. 120-132. Washington: The Institute of Navigation, 1982.
18. Widnall, William S. Stability of Alternate Designs for Rate Aiding of Non-coherent Mode of a GPS Receiver. Contract F3361577C1044. Cambridge MA: Intermetrics Inc, 25 September 1978.
19. Widnall, William S. and Peter A. Grundy. Inertial Navigation System Error Models. Contract F2960172C0162. Cambridge MA: Intermetrics Inc, 11 May 1973.
20. Wrigley, Walter and others. Gyroscopic Theory, Design, and Instrumentation. Cambridge MA: M.I.T. Press, 1969.

# VITA

First Lieutenant Joseph R. Cunningham [REDACTED]

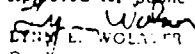
[REDACTED] attended Gannon University where he received the degree of Bachelor of Science in Electrical Engineering in 1983. Subsequent to his graduation, he attended Officers Training School (OTS) from January through March 1984. Upon completion of OTS, 1LT Cunningham was awarded a commission in the USAF and was assigned to the Aeronautical Systems Division (ASD)/Deputy for Propulsion, Air Force Systems Command at Wright-Patterson Air Force Base, Ohio. While at the Deputy of Propulsion, he was a control system engineer supporting programs for both tactical and strategic aircraft engines. In May 1986 he was assigned to the School of Engineering, Air Force Institute of Technology.

[REDACTED]

AFIT-624

# REPORT DOCUMENTATION PAGE

Form Approved  
OMB No 0704-0188

1a REPORT SECURITY CLASSIFICATION UNCLASSIFIED			1b RESTRICTIVE MARKINGS	
2a SECURITY CLASSIFICATION AUTHORITY			3 DISTRIBUTION/AVAILABILITY OF REPORT Approved for public release; distribution unlimited	
2b DECLASSIFICATION/DOWNGRADING SCHEDULE				
4 PERFORMING ORGANIZATION REPORT NUMBER(S) AFIT/GE/ENG87D-12			5 MONITORING ORGANIZATION REPORT NUMBER(S)	
6a NAME OF PERFORMING ORGANIZATION Scholl of Engineering	6b OFFICE SYMBOL (if applicable) AFIT/ENG	7a NAME OF MONITORING ORGANIZATION		
6c ADDRESS (City, State, and ZIP Code) Air Force Institute of Technology Wright-Patterson AFB, OH 45433		7b ADDRESS (City, State, and ZIP Code)		
8a NAME OF FUNDING/SPONSORING ORGANIZATION GPS Joint Program Office	8b OFFICE SYMBOL (if applicable) YEU	9 PROCUREMENT INSTRUMENT IDENTIFICATION NUMBER		
8c ADDRESS (City, State, and ZIP Code) Los Angeles AFB, CA		10 SOURCE OF FUNDING NUMBERS		
		PROGRAM ELEMENT NO	PROJECT NO	TASK NO
		WORK UNIT ACCESSION NO		
11 TITLE (Include Security Classification) See Block 19				
12 PERSONAL AUTHOR(S) Joseph R. Cunningham, B.E.E., First Lieutenant, USAF				
13a TYPE OF REPORT MS Thesis	13b TIME COVERED FROM TO	14 DATE OF REPORT (Year, Month, Day) 1987 December	15 PAGE COUNT 128	
16 SUPPLEMENTARY NOTATION				
17 COSATI CODES			18 SUBJECT TERMS (Continue on reverse if necessary and identify by block number)	
FIELD	GROUP	SUB-GROUP		
17	07	03	Global Positioning System, Inertial Navigation System, Kalman Filter, Covariance Analysis	
19 ABSTRACT (Continue on reverse if necessary and identify by block number)				
<p>Title: PERFORMANCE OF GPS-AIDED INS DURING HIGH-DYNAMIC MANEUVERS</p> <p>Thesis Chairman: Lt. Col. Z.H. Lewantowicz</p>				
<p>Approved for public release: IAW AFR 150-17.            Z.H. LEWANTOWICZ 21 May 88          Dept for Research and Professional Development          Air Force Institute of Technology (AFIT)          Wright-Patterson AFB OH 45433</p>				
20 DISTRIBUTION/AVAILABILITY OF ABSTRACT <input checked="" type="checkbox"/> UNCLASSIFIED/UNLIMITED <input type="checkbox"/> SAME AS RPT <input type="checkbox"/> DTIC USERS			21 ABSTRACT SECURITY CLASSIFICATION UNCLASSIFIED	
22a NAME OF RESPONSIBLE INDIVIDUAL Lt. Col. Z.H. Lewantowicz			22b TELEPHONE (Include Area Code) 513-255-2024	22c OFFICE SYMBOL AFIT/ENG

## Abstract

This thesis explores the unstable characteristic of an integrated inertial navigation system (INS) and Global Positioning System (GPS) receiver. During high-dynamic maneuvers, the INS Kalman filter provides velocity estimates to the GPS receiver code loop in an attempt to remove doppler-induced tracking errors. The GPS receiver Kalman filter, in turn, provides position and velocity estimates to correct INS errors. Due to the suboptimal nature of the two individual filters, this closed-loop process neglects key elements of information: time and spatial correlation. Therefore, this closed-loop system quickly becomes unstable during high-dynamic maneuvers, resulting in degraded navigational performance.

Truth models of the INS and GPS receiver are developed. Kalman filters based on these two models are combined to yield a joint-solution model Kalman filter which serves as an indication of the best structure of integration possible. The eigenvalues of the basic INS error dynamics model, when subjected to various dynamic scenarios, are examined. A candidate maneuver is selected to compare the performance of five systems: the INS truth model, the GPS receiver truth model, the joint-solution model, a two-filter system containing the INS and GPS receiver truth models, and a two-filter system containing reduced-order models of the INS and GPS receiver indicative of current system configuration. (*The GPS*)

The performance of the individual Kalman filters and the joint-solution Kalman filter are demonstrated for three selected conditions: stationary with respect to the earth, a constant east velocity, and a constant acceleration turn in the horizontal plane. Results of the two-filter systems are incomplete at this time, and require follow-on efforts.